Nitrous Oxide (N_2O) Transfer Velocity and the Effect of Ammonium on N_2O fluxes from an Agricultural Drain

---

A thesis

submitted in partial fulfilment

of the requirements for the Master of Science Degree of

Agriculture and Life Sciences

at

Lincoln University

by

Manjula Premaratne

Lincoln University

2016

To

Retired Associate Professor Rob Sherlock

who taught me how to solve the problems analytically

Abstract of a thesis submitted in partial fulfilment of the
requirements for the Master of Science Degree of Agriculture and Life Sciences

Nitrous Oxide (N_2O) Transfer Velocity and the Effect of Ammonium on N_2O fluxes from an Agricultural Drain

by

Manjula Premaratne

Indirect nitrous oxide (N_2O) emissions from rivers and drains are poorly quantified and the uncertainity surrounding the emission factor for dissolved N_2O in rivers (EF5-r) is high. Scaling the exchange of N_2O across the water – air interface is important in order to estimate the indirect N_2O emissions from rivers and drains.Therefore, this study was designed to measure the drain water N_2O emission transfer velocity (k_{N2O}) and the effect of ammonium (NH_4^+) on drain water N_2O yield. The field experiment released ^{15}N-NH_4^+, with Bromide (Br^-) as a conservative tracer, Rhodamine^{WT} as a visual tracer, and propane (C_3H_8) as a conservative tracer gas, into a drain. Visual tracer and conservative tracers allowed the drain water velocity and dilution factor to be determined, respectively. The C_3H_8 and N_2O gases were collected using headspace equilibrium and floating chamber methods. The rate of C_3H_8 escape from water to air was used to measure the N_2O transfer velocity (k_{N2O}). The gas transfer velocity model which as explained by O'Connor and Dobbins (1958), equation 2.9 as interpreted by Wilcock (1982) was also used to measure k_{N2O}. The $^{15}N_2O$ fluxes allowed the NH_4^+ contribution to the N_2O flux to be determined. The ^{15}N enrichment in biofilms and aquatic plants also allowed nitrogen assimilation to be evaluated.

The measured k_{N2O} using headspace equilibrium and the k_{N2O} estimated from Wilcock (1982) were 7.49 ± 0.72 m day^{-1} and 8.65 ± 1.23 m day^{-1}, respectively. To measure the hydro physical variations in k_{N2O}, the current study data and the data from other New Zealand studies were evaluated. The results showed that for shallow drains, water depth < 1 m, the value of k_{N2O} increased with decreasing water depth.

There was an inverse relationship between ^{15}N-NH_4^+-N enrichment and the ^{15}N enrichment of the N_2O evolved. However, there was no relationship between ^{15}N-NO_3^- enrichment with ^{15}N-N_2O enrichment indicating N_2O was produced due to nitrification of added NH_4^+-N. Following ^{15}N tracer

addition, biotic components of the drain ecosystem were highly enriched but returned to near background levels after 10 days, demonstrating that NH_4^+-N assimilation and mineralization occurred.

The calculated EF5-r values were significantly lower than the IPCC default EF5-r value; 0.0025 kg (2.5 g) N_2O-N per kg NO_3^--N. The measured EF5-r values, derived using the surface C_3H_8 flux measurements and the headspace C_3H_8 equlibrium concentrations, were 7.66E-6 (7.66 mg) and 8.20E-6 (8.20 mg) kg N_2O-N per kg NO_3^--N, respectively. However, the EF5-r values derived using floating chambers were significantly lower (3.92E-11 kg; (0.0004 mg) N_2O-N per kg NO_3^--N) and showed chamber methodology as an inefficient technique for gas flux measurements on flowing water surfaces. In contrast, the k_{N2O} measured using the Wilcock (1982) model, that used drain water speed and depth produced higher EF5-r; 9.48 E-6 kg (9.48 mg) N_2O-N per kg NO_3^--N.

Thus, this study demonstrated; (1) the tracer gas addition technique is a relaible and accurate method for N_2O flux determinations from drains, (2) in shallow drains (water depth < 1 m) the k_{N2O} value was inversely correlated with the water depths, (3) the added ^{15}N tracer permitted the role of NH_4^+ in N_2O production to be assessed and (4) the IPCC EF5-r default value overestimated N_2O emissions from agricultural drains.

Keywords: Nitrogen (N), Nitrous oxide (N_2O), N_2O flux, ammonium (NH_4^+), Nitrate (NO_3^-), propane (C_3H_8), Bromide (Br^-) Rhodamine^{WT}, N_2O transfer velocity (k_{N2O}), ^{15}N enrichment, EF5-r, Headspace equilibrium and Floating Chambers.

Acknowledgements

First of all I express my gratitude to my supervisor, Professor Tim Clough for his guidance, support, and encouragement throughout my study period and reading drafts and providing valuable comments that improved the content of the thesis enormously.

Next, I would like to thank my associate supervisor, Professor Frank Kelliher for helping me to understand the kinetic principles of the gas transfer between water and air and giving valuable comments to improve the thesis content.

Many thanks to my colleagues Teresa Symon, Rebecca D'Souza, Shiv Prasad Pokhrel, Barry Anderson, Neil Smith, Nigel Beale, Joy Jiao and Emily Huang who helped me with sampling, solution preparations, apparatus making and sample analysis. Without them, it was impossible to carry out all the tasks at once efficiently and effectively.

Special thanks to Jen Owens for providing much information about data analysis and collecting water samples. Sincerely thank Miriam Hodge and Jennifer Bufford for providing insight into how to find the effect of sampling time on data.

Many thanks to Analytical Service Manager Roger Cresswell for his support through out this study. I acknowledge and thank the Head of Soil Department, Associate Professor Peter Almond, Department Secretary, Amal Torky and Project Manger Gail Harkerss for their support for this study. Sincere thanks to Leanne Hassall and Lynne Clucas for supplying equipments and materials for the experiments.

To fellow students friends and colleagues at Soil Science Department, Soil Science Students Society and elsewhere thank you for your support, in many ways; Jason Breitmeyer, Roshean Woods, Amy Whitely, Dharini Paramachivam, Anna Carlton, Monica Giona Bucci, Veronica Penny, Tihana Vujanovic, Camilla Gardiner, Gustavo Boitt, Peter Carey, Obed Lense, Daniel Martin-Hendrie, Sally Seyedalikhani, Minakshi Mishra and Shamim Maumun.

Last, but not least, I thank my wife Aruni, daughter Malshi and son Jayavi for their support, encouragement and love.

Table of Contents

List of Tables

List of Figures

Chapter 1

Introduction

As a consequence of nitrous oxide (N_2O) being a greenhouse gas (IPCC, 2007) and impacting on stratospheric ozone depletion (Crutzen, 1981) it has received significant scientific attention. Nitrous oxide results from the microbial transformation of nitrogen (N) in soils, sediments or water bodies, (Wrage et al., 2001). When agricultural N inputs are out of balance with agroecosystem demands, the excess N may be lost. Ruminant cattle return 60 – 90% of their ingested N to the pasture as urine with loading rates of up to 1200 kg N ha^{-1} (Di & Cameron, 2002b). The pasture utilizes only a small proportion of this N and the remainder is at risk of being leached as nitrate (NO_3^-) or lost via gaseous forms. The direct gaseous loss pathways occur at the site of N deposition and include gaseous fluxes such as dinitrogen (N_2) and N_2O. The N leached from pasture soils can also, in turn, result in indirect emissions of N_2O from drains, rivers and estuaries.

New Zealand signed the Kyoto Protocol in 1998 under the auspices of the United Nations Framework Conventions on Climate change (UNFCCC). Therefore, New Zealand is legally obliged to provide annual inventories of its agricultural greenhouse gas (GHG) emissions, and must reduce its GHG emissions to 1990 levels or take responsibility for the excess emissions (Ward, 1998). Animal agriculture is responsible for 97% of the N_2O emissions in New Zealand (Ministry of Agriculture and Forestry, 2006). The established IPCC (Intergovernmental Panel on Climate Change) methodology provides default emission factors to calculate N_2O sources from anthropogenic N inputs to agroecosystems. The methododlogy also allows the use of country specific emission factors. In New Zealand, most of the research to date has focused on refining direct emission factors, not indirect emissions.

Fertilizers and animal excreta are the main sources of agricultural N_2O emissions, and they dominate global anthropogenic emissions accounting for 4.1 Tg N_2O-N yr^{-1} of a total 6.1 Tg N_2O-N yr^{-1} of direct emissions. Indirect emissions account for 0.6 Tg N_2O-N yr^{-1}, however, estimated indirect emissions are highly uncertain (0.02-1.20 Tg N_2O-N y^{-1}). The revised 1996 IPCC guidelines stated that the indirect N_2O emissions accounted for 1/3 of the global agricultural N_2O sources with 2/3 of the total uncertainty (Mosier et al., 1998). Obtaining more accurate indirect N_2O emissions data, especially for emissions resulting from leaching and runoff remains a high priority.

The N leached through soil profiles may resurface in agricultural drains. The magnitude of indirect N_2O emissions from such N contaminated water bodies may differ with agricultural ecosystem type (cropping systems, pastoral farms etc.), and over spatial and temporal scales. However, current

indirect emission factors used in NZ for leaching and run off make no distinction based on catchment use or water-body class (e.g. drain, stream, or river). Under the IPCC's 2006 guidelines, the current default emission factor for riverine N_2O production (EF5-r) has a value of 0.0025 kg N_2O-N per kg of N leached. However, data reporting N_2O emissions from agricultural drains and the N_2O exchange rate from drain water to air are scarce.

The rate of N_2O dissipation from water to air is an essential measurement for determining a loss of N_2O from waterbodies. The exchange of dissolved gasses between water and air is governed by the relative partial pressure differences of both phases. The measurement of N_2O concentrations in air and water are straightforward. However, determining the N_2O transfer coefficient (*k'* –emissions per unit time) is neither simple nor direct. Water velocity, gradient, roughness of the bottom surface, water depth and the area of the waterway exposed to air, control the value of *k*'.

1. Thus, the first objective of this study was to measure the N_2O transfer coefficient (*k'*) from water to air in an agricultural drain using a tracer gas.

Propane (C_3H_8) was used as a tracer gas in this study. Both floating chambers and headspace equilibrium methods were employed to measure the C_3H_8 emitted from the water surface and the dissolved C_3H_8 concentrations, respectively. The slope of the log of C_3H_8 concentration versus time was considered as the C_3H_8 gas transfer coefficient (k'_{C3H8}, hr^{-1} or day^{-1}). This was then normalised to a value at 20°C using the Schmidt number of 600 (Sc_{600}) and then used to estimate the N_2O fluxes from the drain water surface (Jähne et al., 1987).

No previous research has examined the effect of NH_4^+ on N_2O fluxes from drains. The N leached from farm lands into drains may be assimilated in aquatic plants and algae as organic matter. When the organic matter decomposes, biological N is released as ammonia (NH_4^+ or NH_3). Such ammonia may also undergo nitrification resulting in N_2O emissions. It is stated that 0.0025 kg N_2O-N is emitted from drains per kg of N leached (IPCC, 2006).

2. Thus, the second objective of this study was to assess the N_2O yield due to nitrification of ammonium (NH_4^+). This was achieved by adding ^{15}N tracer ($^{15}NH_4^+$) into the drain and measuring the $^{15}N_2O$ and $^{15}NO_3^-$ produced over the drain's distance.

This experiment released a tracer solution into the drain that comprised of ^{15}N enriched ammonium ($(^{15}NH_4)_2SO_4$), a conservative bromide (Br^-) tracer, a visual tracer, Rhodamine^{WT} (visual tracer) and a conservative gas tracer, C_3H_8. The Br^- and Rhodamine^{WT} tracers assisted to measure the water discharge rate and the drainage water velocity, respectively. The water samples and gas samples were collected along longitudinal transects of the drain and analysed for $^{15}NH_4^+$, $^{15}NO_3^-$ and the

tracers. Gas samples were collected to measure $^{15}N_2O$ and $^{15}N_2$ every 15 minutes using both floating chambers and headspace equilibrium methods. The drain geophysical (temperature, width, depth and velocity) and chemical (pH and DO) parameters were also measured.

This thesis is structured into six chapters. The introductory chapter is presented here. Chapter two summarises the current state of knowledge on gas transfer rate measurements, indirect emissions, EF5-r estimates and N dynamics in flowing waters. Chapter three describes objective one, the field trials that were carried out to measure N_2O transfer velocity (k_{N2O}) from water to air. Chapter four addresses the measured k_{N2O} measurements, comparison of methods used to establish k_{N2O}. Chapter five explains N_2O yield due to NH_4^+ addition. Chapter six concludes the thesis by summarising the findings with respect to N_2O yield and the effect of ^{15}N tracer on N_2O emissions and EF5-r. In addition, the recommendations for future work are also discussed with the limitations and implications of the study.

Chapter 2

Literature Review

2.1 Introduction

The purpose of this review was to evaluate and summarise literature related to the measurement of nitrous oxide (N_2O) transfer velocity measurements (k_{N2O}) and N_2O production in surface waters, published N_2O yields and fluxes from river systems, with respect to the indirect emission factor (EF5-r).

Thus, this review covers:

- Procedures and methods to measure gas exchange rates
- Data used to determine the N_2O transfer rates and the effect of hydro-physical measurements on gas exchange
- Indirect N_2O emissions
- Nitrogen transformations and pathways
- IPCC guidelines for estimating the indirect emission factor EF5 (EF5-g, EF5-r & EF5-e)
- Nitrous oxide fluxes from flowing waters (rivers, streams and drains)

2.2 Determination of N_2O exchange rates

Nitrous oxide exchange at the water-air interface is central to N_2O flux measurements, in order to establish a credible N budget. Significant effort has gone into assessing carbon dioxide (CO_2) and oxygen (O_2) transfer rates from surface waters, but very few studies have measured N_2O transfer rates. The gas transfer rates from flowing waters depend on weather conditions (temperature and wind speeds that may vary seasonally) and hydro-physical conditions (exposed water surface area to water volume ratio, speed of water and gradient and roughness of the bottom surface).

Nitrous oxide is a sparingly soluble and a non-reactive gas, and the primary mechanism of gas removal from water is atmospheric exchange. The gas transfer rate from water to air is governed by two mechanisms, identified as advection and diffusion. Advection is a transport mechanism that carries dissolved substances within the water body as a result of fluid motion, which depends on the

surface water depth and roughness of the bottom surfaces of the water body (Zappa et al., 2007). Diffusion of gas from water to air depends on the solubility of the gas which is affected by water temperature and salinity as described by the Henry's Law function (Weiss, 1974).

In addition, wind also plays a role in determining the magnitude of the gas transfer rate from water to air (Wanninkhof, 1992). As reviewed by Alin et al. (2011), many studies have investigated the interaction between water and wind speed with respect to gas exchange rates in flowing waters. If drains are sheltered from wind, the main effect on gas exchange is likely to be water turbulence. However, in open and relatively still waters such as lakes and oceans, wind is the main factor governing gas exchange (Cole & Caraco, 1998).

The loss rates of added tracer gases have been used to determine the loss rates of CO_2 and O_2. According to Graham's law the diffusion rate of gas is inversely proportional with its molar mass. Different gasses have different molecular diffusion coefficients; as a result, loss rates also differ. Thus, the rate of loss of a given gas can be related to the rate of loss of a second gas when it escapes into the atmosphere. The gas transfer rate from water to air is a first-order mechanism, thus the measurement of tracer gas loss rate allows the gas transfer rate of any gas to be determined using Schmidt number ratios (Jähne et al., 1987). The Schmidt number is a unitless ratio of the kinematic viscosity to the diffusion coefficient of the gas of interest which is sensitive to temperature. The gas loss rate is determined by plotting the log of the tracer gas concentration in the water body versus time. The slope of the graph is equivalent to the tracer gas transfer coefficient ($k'_{Tracer\ gas}$).

The $k'_{\text{Tracer gas}}$ can be employed to determine the N_2O transfer coefficient (k'_{N2O}) according to:

$$k'_{N2O} = k'_{Tracer\ gas} * (Sc_{N2O} / Sc_{Tracer\ gas})^{-n} \quad 2.1$$

where, Sc Tracer gas and Sc_{N2O} are the Schmidt numbers for the tracer gas and N_2O respectively, and n is the Schmidt number coefficient (½ for rough bottom surfaces and ⅔ for smooth bottom surfaces of the water body concerned).

Assuming the water column is well mixed, the water to air N_2O flux (F_{N2O}) is determined according to:

$$F_{N2O} = h * k'_{N2O} (X_{aq} - X_g) \quad 2.2$$

where, F_{N2O} is the N_2O flux from water to air (mol m^{-2} hr^{-1}), h is the depth of the water (m), k' is the N_2O transfer coefficient (hr^{-1}), X_{aq} is the N_2O concentration in the aqueous phase (mol m^{-3}) and X_g is the equilibrium N_2O concentration in the aqueous phase (mol m^{-3}) for a given atmospheric gas concentration and water temperature (Jähne et al., 1987; MacIntyre et al., 2001; Raymond et al., 2012).

The product of the water depth (h) and N_2O transfer coefficient (k'_{N2O}) is defined as the N_2O transfer velocity (k_{N2O}) of the source water (Equation 2.3).

$$k_{N2O} = h * k'_{N2O} \quad 2.3$$

where, k_{N2O} has units of distance per unit time (cm hr^{-1} or m day^{-1}).

Substituting k_{N2O} to 2.2, the N_2O flux from water to air can be written as:

$$F_{N2O} = k_{N2O} * (X_{aq} - X_g) \quad 2.4$$

Rearranging equation 2.4, k_{N2O} can be estimated using a flux measured with floating chambers and by knowing the equilibrium gas concentration in waters using:

$$k_{N2O} = F_{N2O} / (X_{aq} - X_g) \quad 2.5$$

The diffusive N_2O fluxes from waters can either be measured directly or calculated from the dissolved equilibrium concentrations as per equation 2.4, if the N_2O transfer velocity (k_{N2O}) is known.

2.3 Gas transfer rate measurements

2.3.1 Measurement methods

To measure water-air gas exchange rates, two methods are generally considered: either a tracer gas addition method or a natural gas dissipation method. In the tracer gas addition method, non-reactive trace gases are purposely added to the water and the gas dissipation rates are calculated by measuring changes in the gas concentration over stream distance. In natural tracer studies, naturally available dissolved gasses are used to determine the water-air gas exchange rates.

2.3.2 Tracer gases

Gases used in tracer gas addition studies include propane, hexa-fluro sulphide (SF_6), methyl chloride ($CHCl_3$) and krypton (Kr), in aquatic ecosystems such as, lakes (Cole & Caraco, 1998), oceans (Wanninkhof, 1992), estuaries (Clark et al., 1994) rivers (Caplow & Schlosser, 2004) and small streams (Wanninkhof et al., 1990); Melching and Flores (2007). Propane (C_3H_8) has been previously validated as a least-affected gas in a range of water conditions and has been used in many air-water gas exchange studies (Boumansour & Vasel, 1998).

In natural gas dissipation measurement studies, dissolved gases such as oxygen (Hall et al., 2012; Melching & Flores, 2007), carbon dioxide (Borges et al., 2004), methane (Jones Jr & Mulholland, 1998) and N_2O (Lal & Patra, 1998) have been measured to estimate the air water gas transfer coefficients.

Previously, N_2O fluxes determined flowing water studies have generally used direct measurements and have not employed N_2O transfer coefficients for their calculations. However, three studies have used tracer gasses to determine N_2O transfer coefficients in rivers. Hemond and Duran (1989) applied di-chloro-methyl-fluorine (Freon-12) as a tracer to directly measure the N_2O transfer coefficient in an N enriched river. Harrison and Matson (2003) employed a pulse of dissolved hexa fluoro sulphide (SF_6) as a volatile tracer to measure the patterns and controls on N_2O emissions from the Yaqui Valley agricultural drains of Sonora, Mexico. Wilcock and Sorrell (2008) used their previously derived methyl chloride ($CHCl_3$) transfer coefficients data to measure N_2O emissions from three agricultural drains in the North Island, New Zealand.

2.3.3 Tracer gas injection methods

Three tracer gas injection methods have been previously decribed; steady state injection (tracer gas injected as a continuous steady flow), single-slug gas injection and multi-slug gas injection (Hwa-Seong et al., 2012). The steady state injection method has been widely used and produced consistent results (Marzolf et al., 1994). However, steady injection requires significant resources in terms of consumables and labour (Hwa-Seong et al., 2012). The single slug injection is a simple method, but sample gas collections can be problematic with inconsistent results as a consequence. Multi-slug, the repeated injection of single slugs, uses less resource than the steady state injection method.

2.3.4 Tracer gas measurement methods

Both the headspace equilibrium and the floating chamber techniques may be employed to measure the dissolved tracer gas equilibrium concentrations.

The headspace equilibrium method is a separation technique where dissolved gases are extracted from the liquid phase into a headspace volume. The dissolved gas concentrations (X_{aq}) are determined following phase equilibrium at a known equilibrium temperature. Mackay et al. (1979) showed the dissolved concentration of a gas in water depends on the air-water gas distribution ratio which is approximated by the Henry's law constant (K_H). The, Henry's law constant is defined according to:

$$K_H = P_{X(g)} / X_{(aq)} \quad (2.6)$$

where, K_H is the Henry's law constant (atm m^3 mol^{-1}) which is the ratio of $P_{x(g)}$, the partial pressure of the dissolved gas X in the gaseous phase, and $X_{(aq)}$, the molar concentration of gas *X* in the aqueous phase (mol m^{-3}). The value of K_H is a function of both temperature and salinity (Wanninkhof, 1992).

Rearranging equation 2.4, the molar concentration of gas X in the aqueous phase can be estimated as,

$$X_{(aq)} = F_{(g)} / K_H \quad (2.7)$$

In the floating chamber method, a chamber floats on the water and gas accumulates in the chamber headspace. The gas flux is determined by measuring the change in the headspace gas concentration over a known time per unit area. This is performed using a best-fit regression model of the gas concentration change over time (Hutchinson and Moiser, 1981; Stolk et al., 2009).

Rearranging equation 2.6, the molar concentration of gas $X_{(aq)}$ in the aqueous phase can be estimated as,

$$X_{(aq)} = F / k \quad (2.8)$$

where, $X_{(aq)}$, is the molar concentration of gas X in the aqueous phase (mol m^{-3}), *F* is the gas flux measured in the chamber headspace (mol m^{-2} hr^{-1}) and *k* is the gas transfer velocity (m hr^{-1}).

2.3.5 Gas transfer measurement models

The predictive equations/models that are used for gas transfer coefficient estimations are mainly based on the hydrophysical characteristics of the rivers. Most of the models are mathematically complex requiring much more than general routine measurements and typically involve many assumptions. In addition, emperically derived gas transfer coefficient models are specific to the experimental river condition and are not appropriate for all waterways. An empirical model to measure the water turbulence velocity (k_{water}) was introduced by O'Connor and Dobbins (1958) as follows.

$$k_{water} = (D*U/h)^{0.5} \quad (2.9)$$

where, *U* is the river velocity (m s^{-1}), h is the average river depth (m), and D is the diffusion coefficient in water (m^2 s^{-1}) estimated by extrapolating data contained in Wise and Houghton (1968).

Equation 2.9 has been widely used to predict the gas transfer coefficient and laboratory derived data with isotropic water condition. O'Connor and Dobbins (1958) justified their model with river data. After a survey of New Zealand river aeration data and considering frequently cited predictive models, such as O'Connor and Dobbins (1958), Churchill et al., (1962), Owens et al., (1964), Langbein and Durum (1967), Isaacs and Guady (1968), Wilcock (1982) introduced a simple predictive equation for gas transfer coefficient determination. It was interpreted using equation (38) from O'Connor and Dobbins (1958) and adapted for the temperature range 10-30°C by Elmore and West (1961) as follows.

$$k = k_{(20)} * [1.0241]^{T-20} * 3.74 *[U^{0.5}/h^{1.5}] \quad 2.10$$

where, T is mean water temperature (°C), $k_{(20)}$ is k when T is 20°C, U is water velocity (m s^{-1}) and h is water depth (m). The equation has been used for reaeration measurements in streams and rivers by local government and other authorities for many years.

According to the established models, the gas transfer coefficient correlates with water velocity and inversely correlates with water depth. However, applying these models to measure the N_2O transfer coefficient in an agricultural drain could be biased due to drain characteristics, water quality and hydro-physical variations. Therefore, to understand the real time N_2O emissions from the study site, a tracer addition experiment is required.

Many studies have measured $k'_{Tracer\ gas}$ (unit of $time^{-1}$; s^{-1} or hr^{-1}) in a wide range of rivers and streams. Employing equation 2.1, k_{N2O} values were calculated from the published data for small rivers and streams (< 100 m wide) and are summarised in Table 2.1.

Table 2.1 Published gas transfer coefficient (*k'*) values in small rivers and streams (< 100 m wide) are employed to estimate the N_2O transfer-coefficient (k'_{N2O}) using equation 2.1. Adopted from Wanninkhof et al. (1990), Murphy (2003) and Alin et al. (2011).

Location	Water type	Volatile tracer/Method	Reference	Discharge volume (L s^{-1})	Water Velocity (cm s^{-1})	Water depth (cm)	*Transfer coefficient k'* at 20°C (hr^{-1}) for reference gas	Estimated N_2O transfer co-efficient at 20°C (hr^{-1})
Lakes District, UK	Stream	Disturbed Equilibrium	Owens et al. (1964)	396 ± 196 (77-612)	29 ± 15 (4 - 55)	N/A	18.5 ± 10.5 (1.1 – 46.2)	NA
Jackson river St 7 – 8 **North river**	Stream Stream	^{85}Kr Ethylene	Tsivoglou (1967)	 620	13 23	69 45	2.4 9.5	2.08 8.25
Bonner reach 1-2	Stream	Propane	Grant and Skavroneck (1980)	48	30	30	6.2	4.05
Waitoa, NZ	Stream	Methyl chloride	Wilcock, (1984)	700	19	40	16.4	15.5
Waipa, NZ	Small river	Methyl chloride	Wilcock, (1984)	36000	24	410	0.4	3.8
Waiotapu, NZ	Large stream	Methyl chloride	Wilcock (1984)	3500	38-40 40-46 33-46	79 77 70	7.7 8.0 3.9	7.31 7.60 3.70
Walker Branch, Tennessee, USA	1st order stream	SF6	Wanninkhof et al. (1990)	20	6	10	NA	NA
Walker Branch, Tennessee, USA	1st order stream	Propane	(Roberts, 2007)	5-57	NA	6-9	102 - 67	66.8–43.8
Grand Teton National Park, Wyoming	Stream	SF6	Hall & Tank, 2013	78 ± 74 (4-231)	18 ± 9 (5-33)	10 ± 4 (4-15)	81 -35.5 (41.4 – 135.2)	51.2 ± 22.4 (26.16 -85.4)
Amazon and Mekong rivers	Small rivers	Floating chambers	Alin et al. (2011)	9015 ± 13117 (70-38017)	39 ± 28 (5 - 100)	120 ± 90 (10 - 300)	10.9 ± 14.4 (1.4 - 60.2)	9.3 ± 12.3 (1.0 - 51.1)
River Lagan UK	Stream	^{85}Kr	(Murphy, 2003)	28800	36	50	28.4	24.2

2.4 Indirect N_2O emissions

2.4.1 Measurement methods

The loss of N from farmlands leads to a loss of soil fertility and potential productivity, but also poses a considerable threat to the environment (Cameron et al., 2013). New Zealand's pastoral agriculture has undergone rapid intensification since 1990 with increased stocking rates, N fertilizer usage, excreta N inputs and the use of imported N feed (Parfitt et al., 2012). Excess inputs of N followed by irrigation and rain events, may lead to large losses of N from agricultaral lands (Riley et al., 2001). Accumulation of N in ground and surface waters increases eutrophication of streams, lakes and estuaries, and emissions of N_2O from surface waters (Sutton et al., 2011).

The established IPCC (Intergovernmental Panel on Climate Change) methodology provides default emission factors to calculate N_2O sources from anthropogenic N inputs to agro ecosystems under three categories: direct emissions from agricultural lands, animal waste systems and indirect (Wilcock, 1984) emissions that are associated with volatilized, leached or exported N from farmlands (Mosier, 1998). Many of these default emission factors have been updated and replaced with New Zealand specific factors. However, most of the research to date to refine these emission factors has been performed to assess direct emissions, not indirect emissions.

Globally, anthropogenic and natural sources are responsible for total N_2O emissions of 17.9 Tg N_2O-N yr^{-1}, with a range of 8.1 – 30.7 Tg N_2O-N yr^{-1}, accumulating in the atmosphere at a rate of 3.6 Tg N_2O-N yr^{-1} (Ciais et al., 2013). The main anthropogenic sources for N_2O emissions are synthetic N fertilizers and animal excreta which account for 4.1 Tg N_2O-N yr^{-1} of direct emissons. Indirect emissions partially result from N leaching and runoff from agricultural inputs of N and account for 0.9 Tg N_2O-N yr^{-1} with a high uncertainty (0.02 – 0.12 Tg N_2O-N yr^{-1}). Recent studies describe riverine N_2O emissions as being the most uncertain in terms of magnitude, both spatially and temporally (Ivens et al., 2011).

According to past studies global indirect N_2O emissions are as large as the direct emissions (Mosier et al., 1998). Seitzinger and Kroeze (1998) predicted N inputs to rivers would triple N_2O production by 2050. Uncertainty surrounding indirect N sources and subsequent indirect N_2O emissions is large and ranges over 1.5 orders of magnitude. This arises because there is a lack of understanding of the off-site N transport mechanisms and the ensuing N_2O emissions (de Klein et al., 2001). Therefore, the quantification of the contribution of waterways to total annual N_2O emissions is a high priority.

2.4.2 Nitrous oxide production and pathways

Nitrous oxide is produced in the natural environment by both biological and non-biological processes. However, the biological processes are responsible for more than 95% of global N_2O production (Muller and Sherlock, 2004; Cias et al., 2013). Nitrification and denitrification are the main biological processes responsible for N_2O production in soil environments (Beaulieu et al., 2010). In addition, heterotrophic nitrification and nitrifier-denitrification are also biological processes producing N_2O emissions. While these processes are relatively well characterised in terrestrial ecosystems, there is less known with respect to aquatic ecosystems (Beaulieu et al., 2011).

2.4.2.1 Nitrification

Nitrifying organisms conserve energy via the oxidation of inorganic N compounds such as ammonia (NH_3) and derive carbon for growth from carbon dioxide (CO_2). Nitrification is generally thought to be an aerobic two-step N oxidation process, where ammonia (NH_3) is oxidised to nitrite (NO_2^-) by ammonia oxidising bacteria and/or archaea and thereafter to nitrate (NO_3^-) by nitrite oxidising bacteria (Delwiche, 1981). Both steps require several enzymes, and intermediates are formed (Figure 2.2). In the first step of nitrification, hydroxylamine (NH_2OH) is produced as an intermediate product during NH_3 to NO_2^- oxidation (Bremner, 1997). In the second step of nitrification, NH_2OH is oxidised to NO_2^- and NO_3^-. During both steps, nitrifying organisms release N_2O as a by-product. However, more recently, (Maartje et al., 2015) found two *Nitrospira* species that could encode all the enzymes for complete nitrification (comammox) and which performed both nitrification steps.

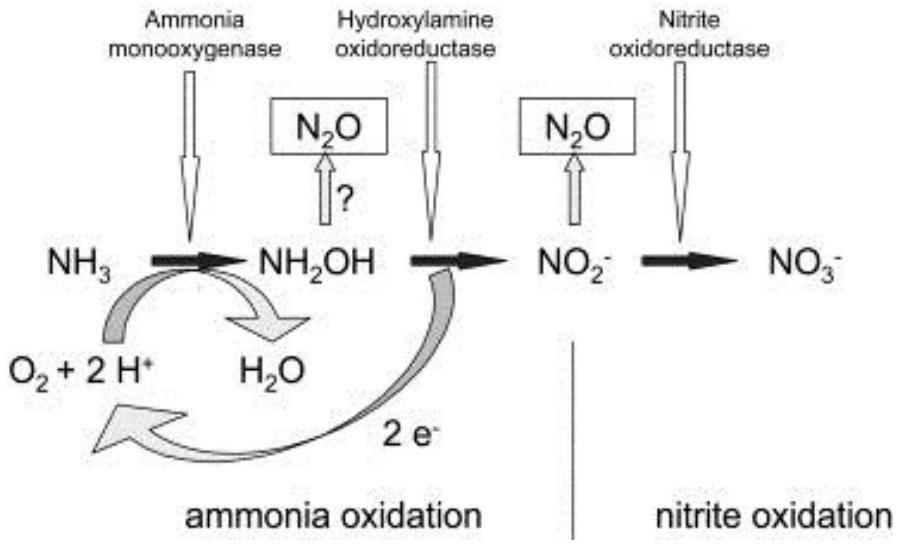

Figure 2-1 Schematic of the nitrification pathway showing N_2O production as a result of ammonia oxidation which occurs under aerobic conditions (Wrage, 2001).

Nitrification may be a significance N_2O production mechanism in river waters where organic N mineralises, leading to NH_4^+ production. There appear to be no studies that have examined the effect of NH_4^+ on river N_2O emissions, and this process remains to be investigated (Beaulieu, 2010).

2.4.2.2 Heterotrophic- nitrification

Nitrification is not limited to being an autotrophic process. In heterotrophic nitrification, organisms use carbon from organic matter for growth. Although the process of heterotrophic nitrification is similar to nitrification, different enzymes are responsible for NH_3 oxidation to hydroxylamine, and then NO_2^- and NO_3^- (Wrage et al., 2001). Heterotrophic nitrification is considered a relatively minor N_2O production process when compared to autotrophic nitrification (Wrage et al., 2001). Low pH, high amounts of oxygen and availability of organic matter favour heterotrophic nitrification (Wrage et al., 2001). Beaulieu et al. (2015) doubted heterotrophic nitrification is dominant in well oxygenated waterways.

2.4.2.3 Denitrification

Denitrification is an anerobic process where NO_3^- is reduced to dinitrogen (N_2) under anoxic conditions and N_2O is produced as an intermediate product (Wrage et al., 2001). During the denitrification process, the activity of the denitrification enzymes is repressed by O_2 (Figure 2.3). As a result, an environment lower in O_2 tends to increase the role of the denitrification process. Zhu et al. (2013) found that denitrification increased from 34% to 66% as the O_2 concentration decreased from 21% to 0% in soil. Availability of carbon, NO_3^-, high pH and temperature are also recognized as factors influencing denitrification (Seitzinger et al., 2006).

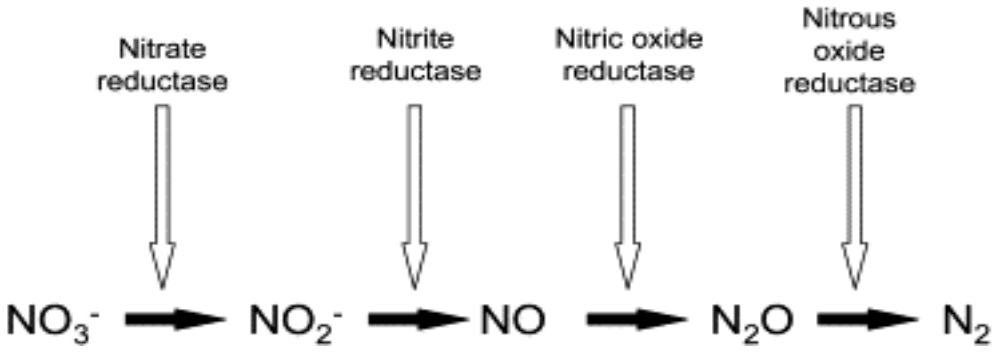

Figure 2-2 Schematic diagram of the denitrification pathway showing N_2O production as a result of nitrate respiration which occurs under anaerobic conditions (Wrage et al., 2001).

2.4.2.4 Denitrification

The nitrifier- denitrification process occurs when the O_2 status declines in the environment but when it is not totally anaerobic (Wrage et al., 2001; Zhu et al., 2013). Webster and Hopkins (1996) revealed that nitrifier-denitrification was responsible for about 30% of N_2O emissions from soils.

Considering all of the N_2O emissions pathways, denitrification and NO_3^- have been recognized as the main process and the primary source for N_2O emissions in aquatic systems respectively (Baulch et al., 2011).

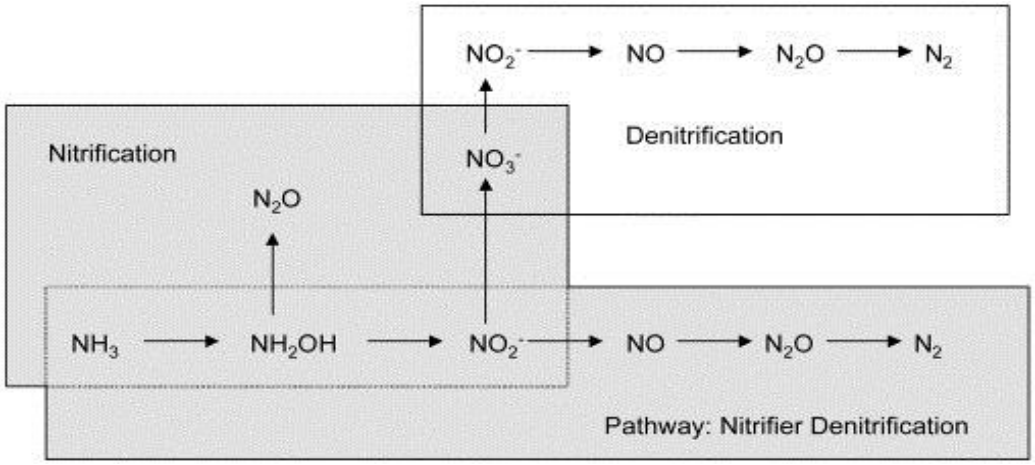

Figure 2-3 Schematic of the nitrifier-denitrification pathway where N_2O production occurs as a result of nitrate respiration by nitrifiers, when the oxygen status is declining but not totally anaerobic (Wrage, 2001).

2.4.3 Nitrous oxide production in river systems

Nitrous oxide emissions from ground and surface waters occurs either via N_2O leaching from the soil into ground or surface waters being released, or as a result of in-situ production (Reay et al., 2003).

The N input to river catchments is a consequence of leaching and runoff. As a main N component of these N inputs, NO_3^- plays an important role in N_2O emissions. However, the leached NO_3-N may also be assimilated in aquatic plants and algae as organic matter, a process known as biota assimilation. When the organic matter decomposes, biological N is released as ammonia (NH_4^+ or NH_3) and nitrified (Mosier, 1998). Such NH_4^+ or NH_3 may also undergo nitrification resulting in N_2O emissions.

Mullholand et al. (2004) explained stream denitrification and total N uptake using a schematic model. In terms of N_2O production, that model is modified for N_2O production in streams as follows.

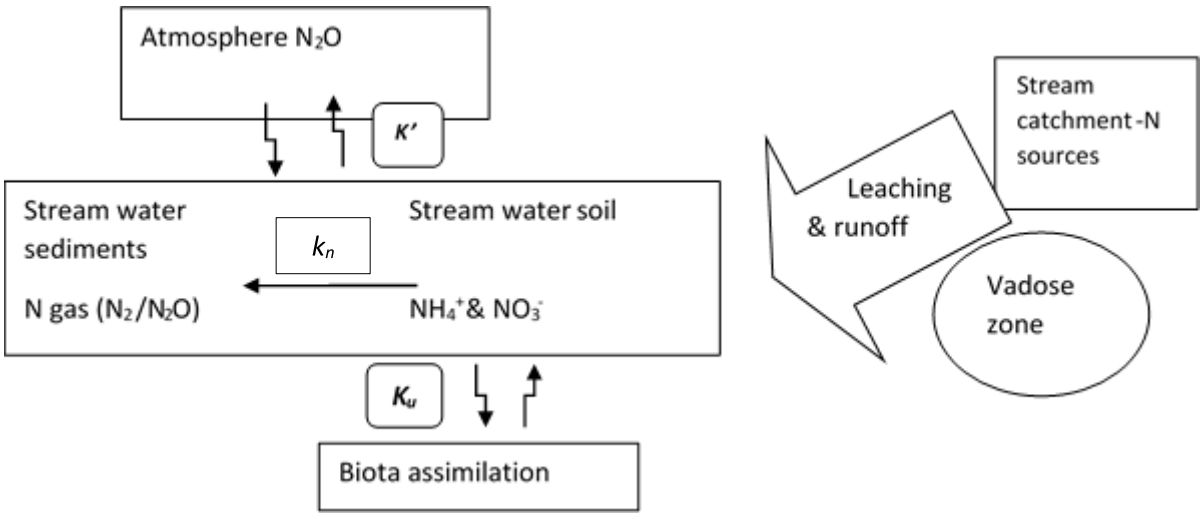

Figure 2-4 A model of N_2O production in streams (modified from Mulholland et al., 2004) (*k'*= water to air N_2O exchange rate, K_n= N_2O production rate from nitrification/denitrification and K_u= assimilative N uptake and release rate).

The in-situ production of N_2O in surface waters may vary with dissolved O_2 concentration (Clough et al., 2007; Harrison et al., 2005). During the day, due to photosynthesis, dissolved O_2 may increase and inhibit denitrification resulting in less N_2O emissions. However, at night where respiration continues in the absence of O_2 inputs via photosynthesis, the dissolved O_2 may decrease, increasing N_2O emissions.

Organic carbon may also increase the denitrification rate in waters, with high N_2O emissions recorded in the presence of both carbon and NO_3^-, an order of magnitude more than NO_3^- alone (Harrison and Matson, 2003). Algae blooms also have the potential to create favourable conditions for rapid denitrification and N_2O emissions in waterways by increasing organic carbon loads (An & Joye, 2001).

Nitrification and denitrification rates may be controlled by the surface water pH. For example, Watson et al. (1994) observed ammonium oxidisers were highly active when the pH ranged from 5.8 -8.5 with an optimum of 7.8. Knowles (1982) described denitrification as being positively related to water pH. Harrison and Matson (2003) also showed a positive correlation between N_2O emissions and pH of drainage canals.

2.4.4 Nitrous oxide from leaching and runoff

The IPCC revised Guidelines were introduced In 1996 and 1998, in order to improve the methodology for estimating annual national N_2O emission inventories. According to the IPCC Guidelines, the

national inventories use a default emission factor (EF5) for N_2O emissions from N leaching and runoff. However, further developments were required to overcome deficiencies in national inventory calculations, especially the quantification of the anthropogenic N_2O production following N leaching and runoff (Mosier et al., 1998). The second phase approach determined the direct emissions from agricultural fields, direct emissions from animal production systems and indirect emissions. The Guidelines were revised in 2006 and stated that a country has to follow the revised 1996 Guidelines and the 2000 IPCC Good Practice Guidance to measure the default emission factors, unless a country can fully justify why they have changed emission factors.

Indirect emissions partially result from N leaching and runoff (NLEACH) from agricultural systems. Agricultural inputs of N include fertiliser N (NFERT; kg N yr^{-1}) and N derived from animal excretion (NEX; kg N yr^{-1}). The fraction of N, from fertiliser and excreta that is leached (FRACLEACH), was estimated by Mosier et al., (1998) to range from 0.1- 0.8. In New Zealand a country specific value for FRACLEACH has been derived and equates to 0.07 kg (70 g) N leached from 1 kg of N input (Thomas et al., 2005).

Thus, the flux of N leached (NLEACH, kg N yr^{-1}) is:

$$NLEACH = [NFERT+NEX]*FRACLEACH \quad (2.11)$$

Production of N_2O occurs when leached N moves into the aquatic environments; ground water and surface drainage, rivers, and estuaries. Emission factors for these three zones are designated as EF5-g, EF5-r and EF5-e, respectively (Mosier, 1998). The total indirect emissions are accounted for in the IPCC methodology using three separare emission factors based on dissolved NO_3^- concentrations. The sum of these three components equates to the default value of EF5.

The N_2O emissions due to agricultural N loss through leaching and runoff N_2O (L) are calculated by multiplying NLEACH by the emission factor (EF5) for leaching and runoff,

$$N_2O\ (L) = NLEACH* EF5 \quad (2.12)$$

The previously estimated default values used to derive the N losses from designated zones in the 1996 guidelines were;

1. EF5-g = Ground water and surface drainage (0.015 kg N_2O-N per kg NLEACH)

2. EF5-r = River and flowing waters (0.0075 kg N_2O-N per kg NLEACH)

3. EF5-e = Coastal and estuary surfaces (0.0025 kg N_2O-N per kg NLEACH)

As a result, the EF5 value is assigned by taking the sum of the above default values and equates to 0.025 kg (25g) N_2O-N per kg NLEACH.

In 2006, the estimated EF5 values were revised. Dong et al., 2004 and Clough et al., 2006 examined N_2O emissions in rivers in Wales and England and lowland braided streams rivers in South Island New Zealand, respectively. These studies estimated EF5-r to equal between 0.0003 (0.3 g) and 0.0005 (0.5 g) kg N_2O-N per kg NLEACH. As a result, in 2006, the EF5 was revised downwards from 0.025 to 0.0075 kg N_2O-N/kg N leached/runoff reducing all EF5-g, EF5-r and EF5-e values to 0.0025 kg (2.5 g) N_2O-N per kg NLEACH. However, the uncertainty in the revised value of EF5 remains large (de Klein, 2006).

2.4.5 EF5-g: N_2O emissions from groundwater

Reay et al. (2003) observed N_2O emissions from out gassing sites (tile drains) through soil profiles and obtained low EF5-g values of 0.0004-0.0006 with few samples reaching the IPCC default value of 0.0025. Hiscock et al. (2003) also found low N_2O-N:NO_3-N ratios of 0.0017 to 0.0019. Following these studies, Beaulieu et al. (2008) examined 12 agricultural river basins that had discharge rates ranging from 3.0 to 62.7 L s^{-1} over 18 months period and found EF5-g equalled 0.0101. Reay et al. (2008) conducted a 17 month long study and found that, the value of EF5-g was 0.003 (range 0.00008 – 0.036) from an intensively grazed pasture catchment. These studies have observed lower EF5-g values than the current IPCC predicted values and supported the EF5-r downward revision to the new value of 0.0025. According to the IPCC methodology, NO_3^- concentrations in stream water are considered as the best predictor of N_2O emission rates.

2.4.6 EF5-r: N_2O emissions from rivers

Measurements of N_2O yields in rivers are limited. The IPCC guidelines assume the N_2O yield is 0.5% for both denitrification and nitrification (Nevison, 2000). Cole and Caraco (2001) measured N_2O fluxes from the Hudson River comparing their results with six previous river N_2O flux measurement studies and found no significant effect of NO_3^- concentrations on river N_2O emissions. Many research

studies have observed lower EF5-r values than the current IPCC methodology default value. Clough et al. (2006) found N_2O-N: NO_3^--N ratios were ≤ 0.00067 and the EF5-r value well below the current EF5-r default value of 0.0025. A potential artefact identified in this study was the degassing of N_2O in the river's upper reaches originating from groundwater sources at the springs.

Wilcock and Sorrell (2008) measured N_2O fluxes from three New Zealand spring-fed streams (NO_3^--N was 0.3 to 4.0 mg L^{-1}; flow < 0.10 to 0.97 m^3 s^{-1}) in the North Island. The mean fluxes of the study (taken from Table 2, Wilcock and Sorrell, 2008) averaged between 4.5 ± 4.0 to 17.2 ± 21.2 µmol N_2O m^{-2} h^{-1} (125 ± 112 to 483 ± 594 µg N_2O-N m^{-2} h^{-1} (± stdev). Their results were similar to those found by Clough et al. (2006) in a South Island lowland stream.

Baulch et al. (2011) studied 2 to 4 sites per stream on five streams for a 29 month period in southern Ontario, Canada. The estimated N_2O fluxes, derived using a gas exchange model, ranged from 5.8 to µg m^{-2} h^{-1} to 100 µg m^{-2} h^{-1}. This study found a strong relationship between log-transformed NO_3^- concentrations and log-transformed N_2O fluxes. Clough et al. (2011) studied N_2O dynamics over a 397 day period in the braided Ashburton River, New Zealand, where NO_3^--N concentrations averaged 0.57 mg L^{-1} (range 0.02 - 1.36 mg L^{-1}) and increased as river distance increased. The N_2O saturation averaged 114% and correlated with NO_3^- concentration.

Beaulieu et al. (2011) carried out a comprehensive ^{15}N tracer study in 72 headwater streams in the U.S.A. As a result of denitrification, ^{15}N tracer was detected in N_2O evolved from 52 of the 73 streams. This is a key study of N_2O emissions from streams, and the stream NO_3^--N concentrations correlated with N_2O emission rates. Following a modelling approach, Beaulieu et al. (2011) estimated that at the global scale, 0.75% of dissolved inorganic-N inputs were converted to N_2O via direct denitrification and nitrification. This is higher than the IPCC default.

Hinshaw and Dahlgren (2013) measured N_2O-N fluxes from the San Joaquin River in California using both floating chambers and headspace methods over a 13 month period. Nitrous oxide fluxes (9.5-352 µg N_2O-N m^{-2} h^{-1}) correlated linearly with dissolved N_2O concentrations and exponentially with N_2O saturation percentages. The calculated EF5-r value averaged 0.0028 (range 0.0012-0.0069). The highest values occurred during high flow events with low dissolved NO_3^- concentrations. Hinshaw and Dahlgren (2013) concluded that 'denitrification in anoxic sediments was the main mechanism for N_2O production.

Further research also queries the IPCC methodology. A study by Mulholland et al. (2004) found a nonlinear, positive relationship between NO_3^- loading and N_2O production. In this study, a 2-fold increase in the NO_3^- concentrations from 0.023 to 0.5 mg N L^{-1} increased N_2O production 6–fold or more, per unit area. Another non-linear effect of NO_3^- vs. N_2O-N was found by Beaulieu et al. (2011).

Following ^{15}N tracer addition, N_2O production rates increased with increasing NO_3^- loading but only 1% of the denitrified N was produced as N_2O, and there was no relationship found between N_2O yield and stream NO_3^- loading rate. This study proved that NO_3^- loading stimulated the denitrification in streams producing ^{15}N-N_2O, but the N_2O yield did not increase proportionally.

2.4.7 Conditions affecting N_2O emissions

Hypoxia, low dissolved oxygen in rivers occurs when respiration exceeds the resupply of oxygen by photosynthesis and aeration. A study by Yu et al. (2013) found a correlation between higher N_2O saturation levels in the Shanghai river network that received sewage inputs. In this study, NH_4^+-N and dissolved oxygen were positively and negatively correlated to N_2O saturation respectively. A two year study on the Grand River, Canada (Rosamond et al., 2012) found that N_2O emissions were underestimated in dry seasons and overestimated in wet seasons with no relationship between N_2O emissions and dissolved NO_3^- concentrations, although there was a negative correlation with dissolved oxygen. They concluded that hypoxia was the main driver of N_2O emissions from river systems not the NO_3^- loading rate. A study on the Grand River by Venkiteswaran et al. (2014) also concluded that N_2O fluxes were higher during hypoxic conditions at low temperature conditions. Clough et al. (2007) and Wilcock and Chapra (2005) also described diel oxygen cycles and a lack of oxygen leading to an increase in N_2O emissions from New Zealand streams. It was suggested that NO_3^- was not the only limiting factor for N_2O production in rivers.

The current IPCC methodology for EF5-r calculations does not consider river geometry or water residence time. However, Peterson et al. (2001) reported the river morphology also influenced the processing of inorganic-N in streams. Turner et al. (2015) examined the N_2O emissions based on stream order and found N_2O fluxes from low order headwater streams often had higher fluxes than the higher order down-water streams (Figure 2-5). The studies of Clough et al. (2006) and Clough et al. (2007) also considered the water residence time in river systems as a factor that could influence the value of EF5-r for New Zealand where rivers have relatively short residence times, measured in hours. Beaulieu et al. (2011) hypothesised that the longer water-residence times in large rivers would result in a greater percentage of the NO_3^- being denitrified.

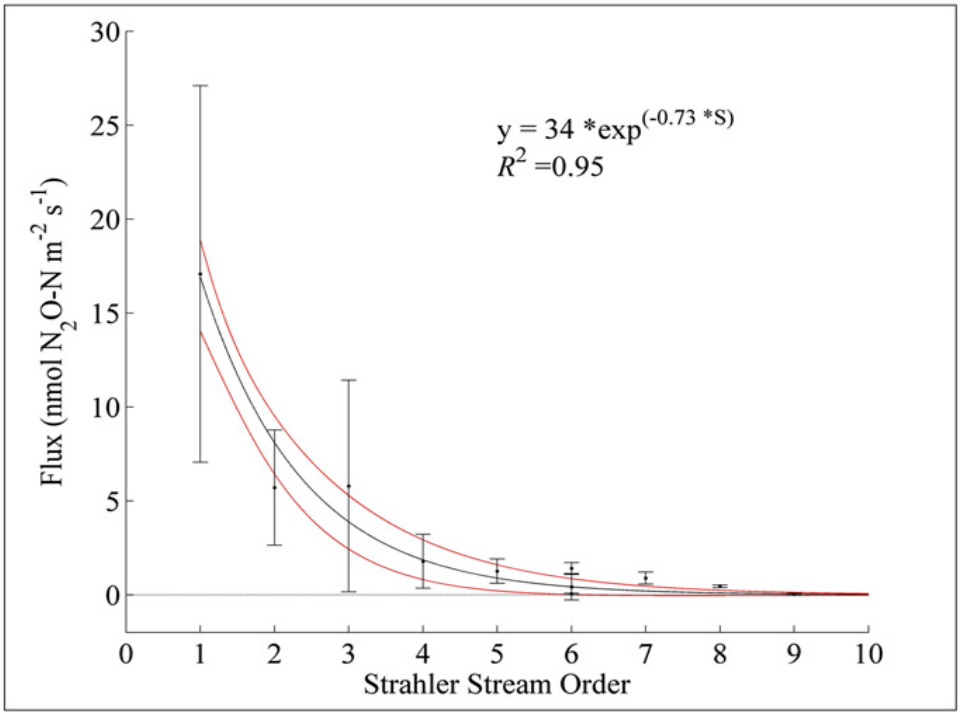

Figure 2-5 The relation between N_2O flux and the stream order in south-eastern Minnesota (Turner et al., 2015).

Current methods to estimate riverine N_2O emissions are based on the knowledge of N transformation pathways and hydrophysical conditions of waters. The effect of both nitrification and denitrification on N_2O yield from surface waters may be smaller when compared with the terrestrial ecosystems (Beaulieu et al., 2011). Seasonal variances, N residence time, water quality and hydrophysical measurements may also affect the N_2O yield from rivers. Due to variable N_2O yields and the complexity of river systems, a simple relationship between N sources and N_2O emissions from flowing waters may not exist.

2.4.8 EF5-r measurements in New Zealand

Few field studies have examined N_2O fluxes from rivers in New Zealand. Those that have include: Wilcock and Sorrell (2008), Clough et al. (2006; 2007; 2011) and a scoping study Clough and Kelliher (2012) which was performed on the longest river in New Zealand, the Waikato River (Table 2.2).

Table 2.2 Summary of EF5-r studies in New Zealand

Reference	Water body	Method	N_2O-N flux ($\mu g\ m^{-2}\ h^{-1}$)	NO_3^--N ($mg\ L^{-1}$)	EF5-r[a] range
Clough et al. 2006	LII (lowland spring-fed stream)	Floating chambers	38-501	2.5 -5.3	0.00015-0.00067
Clough et al. 2007	LII (lowland spring-fed stream)	Floating chambers	52-140	3.0	0.00042-0.00065
Clough et al. 2011	Ashburton (Braided-gravel bed)	Head-space equilibrium [b]	16-30	0.02-1.36	0.0007-0.0169
Wilcock & Sorrell 2008		Head-space equilibrium [b]			ND[b]
	Whakapipi		10-305	1.4 - 4.5	
	Toenepi		-1 – 770	0.1 – 3.4	
	Whangamaire		3 -2714	7.6 – 15.6	
Clough and Kelliher 2012	Waikato River, at 15 sites	Floating chambers	< 100	0.02 – 0.31	0.0010-0.0132

[a] Determined as the ratio of N_2O-N: NO_3^--N;[b] Not Determined in this study (Clough et al. 2012).

There remains a need to examine New Zealand's indirect N_2O emissions from headwater streams and field drains, in order to more accurately understand New Zealand's N_2O inventory. There is also a lack of measurements for the N_2O transfer rate from water to air and limited data available worldwide. Therefore, this study was performed to measure both N_2O transfer rate and the effect of NH_4^+ on N_2O emissions from an agricultural drain.

Chapter 3

Measuring the nitrous oxide transfer velocity (k_{N2O}) in an agricultural drain

3.1 Introduction

A fraction of the nitrogen nitrified within an agricultural drain may escape as N_2O, but the actual N_2O yield is unknown. One of the major reasons for this is the lack of data detailing the N_2O exchange rate between water to air. Scaling the water-air N_2O exchange in drains, streams and river systems is important when attempting to constrain indirect emissions of N_2O at temporal and spatial scales (Cole and Caraco, 2001). Knowing the N_2O transfer velocity (k_{N2O}), the diffusive N_2O fluxes from waters can either be measured directly or calculated from the dissolved equilibrium N_2O concentrations, using equation 2.4.

Two experiments were performed in the summer (January) and late winter (August) of 2015 to measure the N_2O exchange across the water- air interface in an agricultural drain. Following the continuous tracer addition method (2.3.3), the experiments were designed to measure the k_{N2O}, in a given reach, using propane (C_3H_8) as the tracer gas, while measuring the real time N_2O emissions from the drain. The experiment employed both headspace equilibrium and floating chamber methods and evaluated the consistency of the obtained values in the context of published gas transfer models and values.

3.2 Method

3.2.1 Field site

The experiments were performed at a spring-fed drain site flowing north to south alongside Raineys Road (Figure. 3-1). The drain flows into the Halswell River (43°S and 172°E), which is one of the main waterways entering Lake Ellesmere. The chemical, physical and biological measurements, described below, were collected over a 200 m length of the drain where no other inlets, that could alter the volume and its chemical composition, occurred. Adjacent farmlands were predominantly dairy pasture. The bottom of the drain was covered in fine sediments (3 – 10 cm deep) and the water was clear. Giant-meadow buttercup (*Rannunculus sp*.), sedges (*Carex sp*.) and monkey musk (*Mimulus sp.*) were abundant on the sides of the drain with a small quanity of floating duck weed (*Lemna minor*) also present.

Figure 3-1 Raineys Road drain

3.2.2 Hydrological and geophysical measurements

The drain had a gradient of 1:0.0019 (5.2 m fall over 2.7 km) which was determined using a Garmin™ GPS. Water velocity (V) was determined using the Rhodamine^{WT} dye method (Liang & Richardson, 1971). Water temperature and dissolved O_2 were measured by placing the sensor of the YSI-DO™ (USA) meter at 10 cm depth on three consecutive times at each site. Drain water geo-physical measurements were determined with a measuring tape.

The discharge rate, Q (L s^{-1}), was calculated using the bromide (Br^-) dilution data as follows (Marzolf et al., 1994).

$$Q = Solution\ [Br^-]\ X\ RR\ /\ Site\ [Br^-] \quad 3.1$$

where, *Solution [Br^-]* is the Br^- concentration of the added carboy solution (g L^{-1}), *RR* is the solution release rate (L s^{-1}) and the *Site [Br^-]* is the Br^-concentration at a given sampling site (g L^{-1}).

The mean drain depth (D), in metres, was calculated as (Alin et al., 2011);

$$D = Q\ /\ U*W \quad 3.2$$

where, Q is the water discharge rate ($m^3\ s^{-1}$), U is the water velocity at measurement site (m s^{-1}) and W is the drain width (m). Discharge rate - Q was determined from the Br^- dilutions (Equation 3.1).

Water velocity was estimated using the break-through concentration curves of the Rhodamine^{WT} dye that was injected into the drain immediately after the tracer experiment concluded. Three water samples were collected at each site; the time that maximum concentration occurred was used to estimate the drain water velocity.

Median three hourly wind speed and air temperature data were taken from the Broadfield Ews (Plant and Food Research), Lincoln metrological station (Cliflo No. 17603, - 43.62, 172.47).

3.2.3 Mixed tracer solution

Two experiments were performed: the first was a preliminary experiment (Experiment 1), performed on 20th January, 2015. Propane (C_3H_8) was added as a gas tracer with a conservative tracer (Br^-) and a visual tracer (Rhodamine^{WT} dye) to measure the gas transfer coefficient of the drain. The second experiment (Experiment 2) was performed on 12th August, 2015 with C_3H_8, Br-, Rhodamine^{WT} and the ^{15}N-NH_4^+ tracer as a nitrifiable N source, in order to measure the gas transfer coefficient and N_2O emissions due to nitrification of NH_4^+.

In experiment 1, a tracer solution was constituted on site in an 80 L carboy. The carboy solution comprised of: 0.3 kg of potassium bromide (KBr) and 10 mL of Rhodamine^{WT} dissolved in 5 L of drain water. The carboy was then filled with stream water (75 L) and mixed well before being released, while being constantly purged with 99.9% C_3H_8, into the drain using a peristaltic pump (Fondriest, CA, USA). The solution was released at a rate of 17 mL s^{-1} to increase the drain water Br^- concentration so that it was > 0.1 mg L^{-1} for 60 minutes.

In experiment 2, the tracer solution comprised of 1.0 kg of KBr and 800 g of ^{15}N enriched $(NH_4)_2SO_4$ in an 80 L carboy. When experiment 2 was performed, the drain discharge volume was estimated to be 130 L s^{-1} and the carboy solution was continuously released into the drain using a peristaltic pump at a rate of 17 mL s^{-1} while 99.9% pure C_3H_8 continued to purge the solution. The pump rate and the solution concentrations were based on needing to increase the stream water Br^- concentration by approximately 1 mg L^{-1}. Due to the potential for the visual tracer, Rhodamine^{WT}, to interfere with the NH_4^+ detection method (phenol, hypochlorite colorimetric method), Rhodamine^{WT} was added in a separate dosing experiment, immediately after the final collection of water samples as noted below, in order to determine water speed.

3.2.4 Sampling time, stations and collection

In experiment 1, water and gas sampling sites were positioned along the drain at 15, 40, 65, and 165 metres from the tracer solution injection point. The samples were collected every 15 minutes, four times for an hour (15, 30, 45 and 60 minutes) following commencement of tracer injection at time zero. At each site, sampling involved collecting triplicate water samples for dissolved C_3H_8, Br^- and Rhodamine^{WT} dye measurements.

In experiment 2, sampling sites were positioned at 15, 40, 65, 165 and 215 m from the injection point. Both water and air samples were collected every 15 minutes, five times for 1.25 hours (15, 30, 45, 60 and 75 minutes), following commencement of tracer injection at time zero. At each site, triplicate water samples were collected for dissolved C_3H_8, Br^- and Rhodamine^{WT} dye measurements.

Additionally, in experiment 2, surface C_3H_8 and N_2O gas fluxes were also determined using floating chambers at sites located at 25, 50, and 200 m. Floating chamber design, construction and gas sampling procedures were previously described in Clough et al. (2006). The total volume of the chamber headspace was 4.2 L with an area of 0.159 m^2. Fluxes of C_3H_8 were measured using three chambers at each site. Each chamber was sampled at 15 minute intervals for 75 minutes (5 times), after tracer was released, using a glass syringe, fitted with a three way stopcock and a 27 gauge needle. When sampling the needle was inserted through the septa of the chambers and flushed twice and then 10 mL gas samples were extracted and injected into pre-evacuated 6.0 mL Exetainer® (Labco Ltd, High Wycombe, UK) vials. Prior to each gas sampling, the syringe was flushed twice with ambient air to prevent any contamination between samples. Then, the sample vials were transported to the laboratory for C_3H_8 and N_2O analyses by gas chromatography (GC).

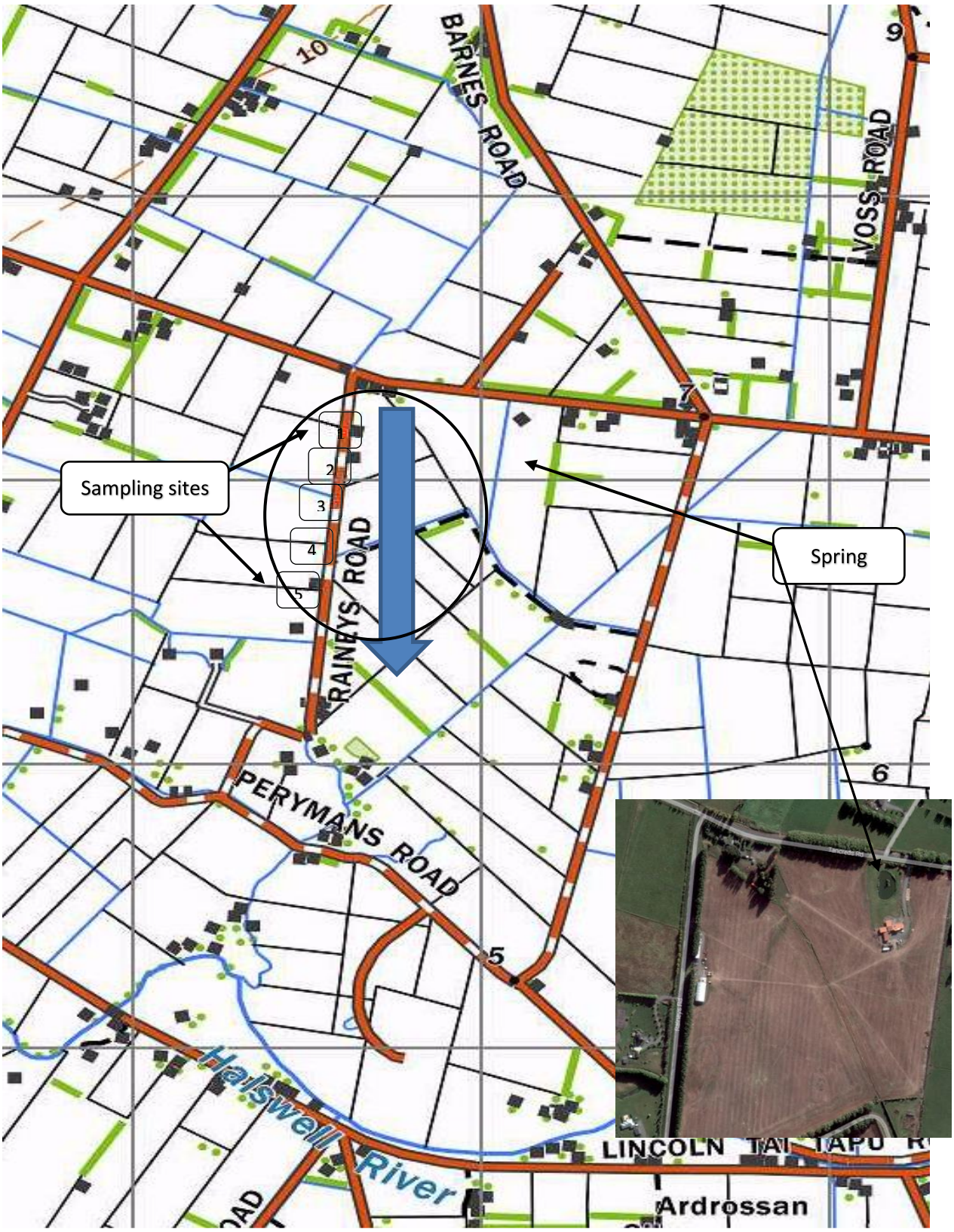

Figure 3-2 **Topographical map showing measurement sites of the Raineys road drain. Direction of the water flow is shown by the arrow. (Scale 1.0 cm: 0.25 Km)**

3.2.5 Dissolved propane measurements

In both experiments, triplicate 50 mL water samples were collected 10 cm below the water surface by slowly drawing 50 mL of water into a pre-flushed gas-tight glass syringe (Cadence science inc, Staunton, VA) fitted with a three-way stopcock (Figure 3-3).

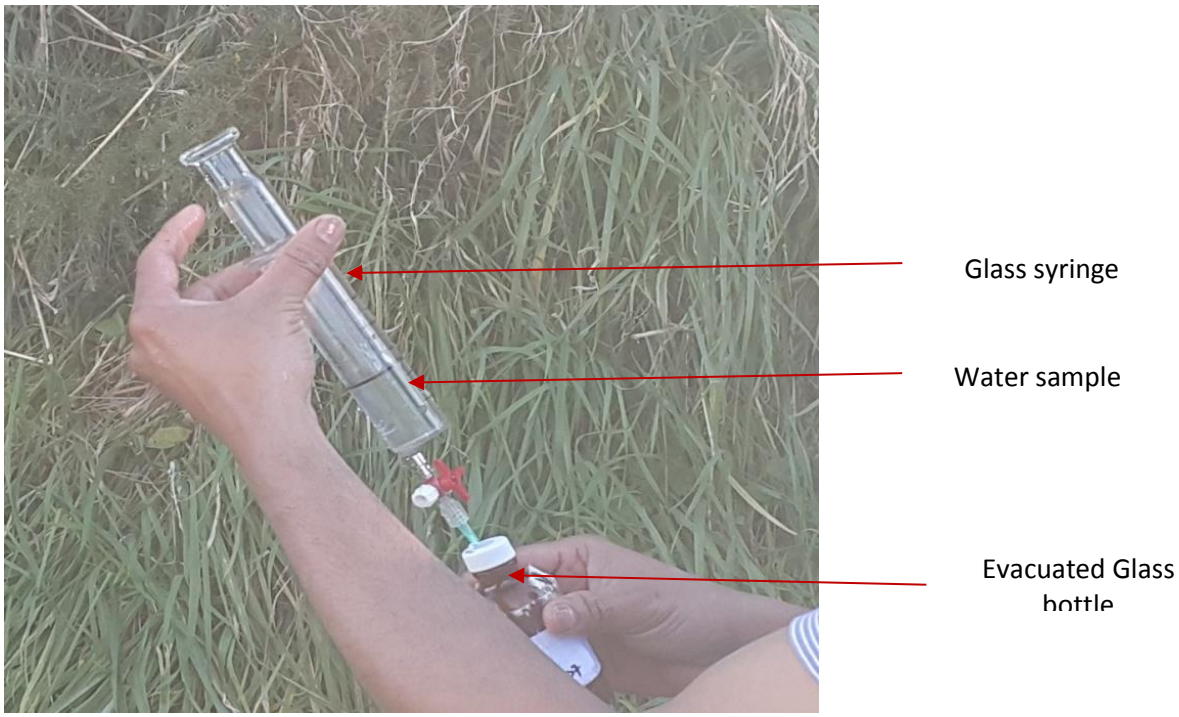

Figure 3-3 Dissolved gas extractions by headspace method

A needle was placed on the stopcock, and the dead-space within the needle was displaced with the sampled water by exerting pressure on the syringe, prior to injecting the water sample into a helium-flushed pre-evacuated glass bottle (105 ± 2 mL) fitted with a butyl rubber septum (Figure 3-3). The bottles were stored in a chilly-bin and transported to the laboratory. The bottles' headspace (55 mL) were filled with UHP helium and shaken for 5 minutes to equilibrate the dissolved gasses in the liquid and gas phases. The headspace gas was sampled using a glass syringe fitted with a three-way stopcock and then 10 mL was transferred to pre-evacuated 6.0 mL vials. Ambient air samples were also collected at each sampling site. The same sampling procedure, using 50 mL distilled water, was performed in the laboratory as a control.

3.2.6 Floating chamber gas collection and measurements

In experiment 2, gas samples were collected from floating chambers (Figure 3-4) at sites 1, 3 and 5. Five gas samples were collected from the headspace of each chamber at 15, 30, 45, 60 and 75 minutes as previously described (Clough et al., 2006).

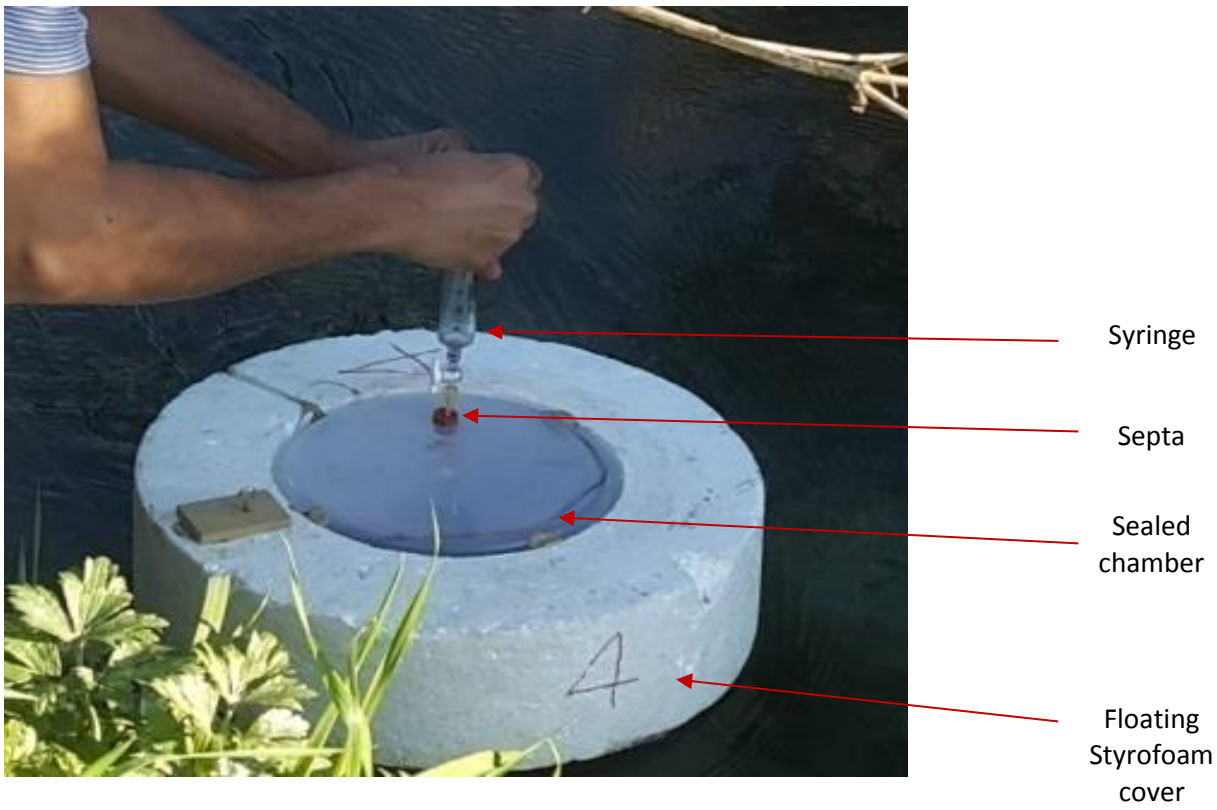

Figure 3-4 Floating chamber headspace gas sampling

3.2.7 Gas analysis

Gas samples in the 6 mL Extetainers were analysed for N_2O and C_3H_8 concentrations using an SRI 8610 CA USA, Gas Chromatograph (GC). Propane and N_2O were separated using a 2 m long Poropak Haysep B column held at 65°C, where the N_2O retention time was eight minutes and the C_3H_8 retention time was 12 minutes. Propane and N_2O concentrations were detected using a heated Flame Ionization Detector (FID) at 100°C and an Electron Capture Detector (ECD) at 310°C, respectively. A range of reference gases (0.02 to 1000 µL L^{-1}, BOC, NZ) were used to generate standard curves to determine C_3H_8 and N_2O concentrations. The configuration of the GC and sample handling procedures have been described previously (Kelliher et al., 2015).

3.2.8 Dissolved gas concentrations and gas transfer rate calculations

3.2.8.1 Headspace equilibrium method for determination of N_2O transfer coefficient (k'_{N2O})

Total dissolved C_3H_8 and N_2O concentrations were calculated using the formula of (Tiedje, 1983).

$$M = Cg\ X\ [V_g + (V_l\ x\ \beta)] \quad (3.3)$$

where, M is the total gas present in an evacuated bottle (µL), Cg is the head space gas concentration (µL L^{-1}), V_g is the volume of gas in the bottle (L), V_l is the volume of liquid (L) and β is the Bunsen coefficient (µl L^{-1}).

Since the bottles were initially evacuated all the C_3H_8 and N_2O gas derives from the 50 mL water sample initially added to the bottle. Therefore, the dissolved gas volume in a litre of water was measured by dividing M (µL) by the volume of water (L) (Davidson & Firestone, 1988).

The moles of the gas in the water sample were calculated using the ideal gas law;

$$n = PV / RT \quad (3.4)$$

where, n is the gas concentration (moles L^{-1}) , P is the atmospheric pressure (1 atm), V is the volume of gas (L) , R is the universal gas constant (0.0821 L atm K^{-1} mol^{-1}) and T is the air temperature (K).

The difference in the dissolved trace gas concentrations (dC) between time zero and travel time t (dt) is equivalent to the amount of gas lost into the atmosphere. Thus, the tracer gas dissipation rate was determined as;

$$dC/dt = k' (C_t - C_0) \quad (3.5)$$

where, dC/dt is the rate of concentration change per minute (mol L^{-1} min^{-1}), k' is the gas transfer coefficient (min^{-1}), C_t is the gas concentration (mol L^{-1}) after time t and C_0 is the gas concentration at time t_0 (mol L^{-1}).

The gas exchange from water to air is a first order kinetic process (Stolk et al., 2009). To measure the gas transfer coefficient (k'), the gas concentration at time t (C_t) was measured as;

$$C_t = C_0 - k' (t_1 - t_0) \quad (3.6)$$

Therefore,

$$ln\ C_t\ /\ C_0 \quad = \quad -k'\ (t_1 - t_0) \qquad 3.7$$

where, $(t_1 - t_0)$ is the gas travel time in minutes and ln C_t/C_0 is the natural log concentration ratio at time t and time t_0 for a given distance.

According to equation 3.7, the gas transfer coefficient (k') can be determined by plotting the logarithm of the dissolved gas concentration as a function of time (Chapra & Wilcock, 2000). The slope of the plotted linear regression is the gas transfer coefficient (k').

Generally, the gas transfer coefficient is a function of water turbulence, the kinematic viscosity and the diffusion coefficient of the water (Wanninkhof, 1992). The Schmidt number is a unitless ratio of the kinematic viscosity to the diffusion coefficient of the gas of interest (C_3H_8 and N_2O), which is sensitive to temperature. The Schmidt value (S_c) for dissolved gasses in fresh water was calculated as a function of temperature for C_3H_8 and N_2O according to equation 3.8 and 3.9 (Wanninkhof, 1992);

$$Sc_{(C3H8)} \quad = \quad 1911.1 - 118.11*T + 3.4527*T2 - 0.04132*T3 \qquad 3.8$$

$$Sc_{(N2O)} \quad = \quad 2055.6 - 137.11*T + 4.3173*T2 - 0.05435*T3 \qquad 3.9$$

where, T is the temperature in degrees Celsius.

Using the propane gas transfer coefficient (k'_{C3H8}) derived from data sets of experiment 1 and 2, the N_2O transfer coefficient (k'_{N2O}) was estimated as follows;

$$k'_{N2O} \quad = \quad (Sc_{N2O} / Sc_{C3H8})^{-n} * k'_{C3H8} \qquad 3.10$$

where, Sc is the temperature specific Schmidt number for C_3H_8 and N_2O (Wanninkhof, 1992), n is the Schmidt exponent, which is equal to 0.5 for rough bottom surfaces and 0.66 for smooth bottom surfaces (Jähne et al., 1987). Then, the estimated k'_{N2O} is standardised at 20°C as $k'_{2(N2O)}$ according to (Wanninkhof, 1992);

$$k'_{2(N2O)} \quad = \quad k'_{N2O}\ (600 / Sc_{N2O(T)})^{-n} \qquad 3.11$$

where, $k'_{2(N2O)}$ is the N_2O gas transfer coefficient standardised at 20°C and $Sc_{N2O(T)}$ is the N_2O Schmidt number at temperature T.

The water-air N_2O transfer coefficient transfers to the air-water N_2O transfer velocity that is specific for the measurement drain. As per equation 2.3, the calculated $k'_{2(N2O)}$ value was multiplied by depth

of the drain (m) to determine the air-water N_2O transfer velocity (k_{N2O}), which can be used to directly calculate the N_2O flux.

3.2.8.2 Floating chamber method for determination of N_2O transfer velocity (k_{N2O}) using propane (C_3H_8) as a tracer gas

The gas flux, F (µmol m^{-2} hr^{-1}) from the drain surface was calculated using the following equation (Beaulieu et al., 2011; Frankignoulle, 1988).

$$F = (dC/dt) * (V/A) * (P/RT) \quad 3.12$$

where, *dC/dt* is the increased rate of gas partial pressure within the chamber (µL L^{-1} hr^{-1}), *V* is the volume of chamber (L), *A* is the surface area of the drain water enclosed in the chamber (m^2), *P* is the atmospheric pressure (atm), *R* is the universal gas constant (0.0821 L atm K^{-1} mol^{-1}), and *T* is the air temperature in (K).

Then, the calculated propane flux (F_{C3H8}) from the chamber measurements and the dissolved gas concentrations at each site were substituted into equation 3.13 to determine the C_3H_8 transfer velocity (k_{C3H8}) according to (Beaulieu et al., 2008);

$$k_{C3H8} = F_{C3H8} / (X_{aq} - X_g) \quad 3.13$$

where, k_{C3H8} is the C_3H_8 transfer velocity (m hr^{-1}), *F* is the C_3H_8 flux from water to air (µmol or moles, m^{-2} hr^{-1}), X_{aq} is the C_3H_8 concentration in the aqueous phase (moles m^{-3}), X_g is the equilibrium C_3H_8 concentration in the liquid phase (mol m^{-3}).

Using the C_3H_8 gas transfer velocity (k_{C3H8}), the N_2O transfer velocity (k_{N2O}) was estimated as follows.

$$k_{N2O} = (Sc_{N2O} / Sc_{C3H8})^{-n} * k_{C3H8} \quad 3.14$$

where, *Sc* is the temperature specific Schmidt number for C_3H_8 and N_2O (Wanninkhof, 1992), *n* is the Schmidt exponent, which is equal to 0.5 for rough bottom surfaces and 0.66 for smooth bottom surfaces (Jähne et al., 1987).

Then the estimated k_{N2O} was standardised at 20°C as $k_{(N2O)}$ according to the previously described equation 3.11 as follows (Wanninkhof, 1992);

$$k_{(N2O)} = k_{N2O} (600 / Sc_{N2O(T)})^{-n} \quad 3.15$$

where, $k_{2(N2O)}$ is the N_2O gas transfer velocity standardised at 20°C and $Sc_{N2O(T)}$ is the N_2O Schmidt number at temperature T.

3.2.8.3 Determination of N_2O transfer velocity (k_{N2O}) from Wilcock (1982) model

Oxygen transfer velocity (k_{O2}) was determined for sampling site depth using equation 2.10. Using the k_{O2} derived from data sets of experiment 1 and 2, the N_2O transfer coefficient (k_{N2O}) was estimated as follows;

$$k_{N2O} = (Sc_{N2O} / Sc_{O2})^{-n} * k_{O2} \quad 3.16$$

where, *Sc* is the temperature specific Schmidt number for N_2O and O_2 (Wanninkhof, 1992), *n* is the Schmidt exponent, which is equal to 0.5 for rough bottom surfaces and 0.66 for smooth bottom surfaces (Jähne et al., 1987). Then, the estimated k_{N2O} is standardised at 20°C as $k_{(N2O)}$ as per equation 3.11.

3.2.8.3 Direct N_2O transfer velocity (k_{N2O}) using N_2O flux and dissolved N_2O concentrations

The N_2O flux from the drain surface was calculated according to equation 3.12. Then, equation 2.4 was used to estimate k_{N2O}, substituting the measured N_2O flux and the known equilibrium N_2O concentrations. The estimated k_{N2O} is standardised at 20°C as $k_{(N2O)}$ as per equation 3.11.

3.2.9 Statistical analysis

Statistical analyses were performed using Minitab® version 16 (Minitab Inc., PA, USA) and Microsoft Excel, 2010. Means, standard deviations and standard errors were calculated for data as appropriate. Analysis of variance was employed, if the means of variables differed between sampling times. When the difference occurred, the effect of time on tracer mixing was calculated by the sum of squares between groups divided by the total sum of squares (η^2). The Bonferroni post-hoc tests were performed to determine the significance of the variations between sampling times.

3.3 Results

3.3.1 Micro-metrological conditions

During the first tracer addition (Experiment 1), average atmospheric pressure, air temperature and wind speed were 1012 mbar, 17.3°C and 5.9 km hr^{-1} (Southwest), respectively. During the second tracer addition (Experiment 2), average atmospheric pressure and air temperature were 1022 mbar and 6.4°C, respectively. The wind speed was 2.2 km h^{-1} from the northeast over the 1.5 hr experimental period.

3.3.2 Drain water hydro physical measurements

Hydro physical conditions of the drain were typical in both experiment 1 (summer) and experiment 2 (late winter). The drain discharge rate (Equation 3.1) was stable over the 1 and 1.5 hr study periods of experiments 1 and 2, respectively. From December 2014 to September 2015, fortnightly recorded typical base flow rates averaged 54 ± 21 L s^{-1} in summer (December 2014 to February 2015), 78 ± 33 L s^{-1} in autumn (March to May 2015), and 135 ± 45 L s^{-1} in winter (June to August, 2015). The drain water temperature, dissolved O_2, and geo-physical measurements are summarised in Table 3.1 and 3.2.

Table 3.1 Experiment 1; the drain water chemistry and physical measurements. (Temperature and dissolved oxygen errors = ± standard deviations of three samples).

Measurement	Site 1 (15 m)	Site 2 (40 m)	Site 3 (65 m)	Site 4 (165 m)	Mean
Temperature °C (n=3)	15.1 ± 0.2	15.2 ± 0.3	15.3 ± 0.4	15.5 ± 0.3	15.3 ± 0.3
Dissolved O_2 mg L^{-1} (n=3)	11.2 ± 0.9	11.0 ± 0.6	11.1 ± 0.8	10.7 ± 0.3	11.0 ± 0.7
Width (m)	1.35	1.45	1.50	1.40	1.42 ± 0.05
Wetted width (m)	2.10	2.25	1.98	2.32	2.16 ± 0.12
Depth (m) (n=3)	0.19 ± 0.02	0.18 ± 0.02	0.19 ± 0.02	0.20 ± 0.0.03	0.19 ± 0.02

Table 3.2 Experiment 2; the drain water chemistry and physical measurements. (Temperature and dissolved oxygen errors = ± standard deviations of three samples).

Measurement	Site 1 (15 m)	Site 2 (40 m)	Site 3 (65 m)	Site 4 (165 m)	Site 5 (215 m)	Mean
Temperature °C (n=3)	11.3 ± 0.3	11.5 ± 0.2	11.9 ± 0.2	12.2 ± 0.3	12.4± 0.4	11.9 ± 0.31
Dissolved O_2 mg L^{-1} (n=3)	12.4 ± 0.9	11.4± 0.6	11.3 ± 0.8	11.2 ± 0.3	11.0 ± 0.3	11.5 ± 0.6
Width (m)	1.43	1.52	1.64	1.47	1.98	1.61 ± 0.20
Wetted width (m)	2.26	2.34	2.08	2.59	3.35	2.52 ± 0.44
Depth (m), (n=3)	0.32 ± 0.03	0.31 ± 0.02	0.30 ± 0.02	0.36 ± 0.04	0.38 ± 0.05	0.33 ± 0.03

The drain physical measurements (Table 3.1 and 3.2) show that, the drain width, wetted width and water depth during experiment 1 were smaller than during experiment 2. In experiment 1, the average drain water temperature at site 1 was 15.1 ± 0.2°C and this increased to 15.5 ± 0.3°C at 165 m downstream. In experiment 2, the average drain water temperature at site 1 was 11.3 ± 0.3°C and this increased to 12.4 ± 0.4°C at 215 m downstream (Table 3.1 and 3.2).

3.3.3 Drain water Bromide (Br^-) measurements

In experiment 1, Br^- was released into the drain at a rate of 0.017 L s^{-1} at a concentration of 3 g L^{-1}. In experiment 2, Br^- was released into the drain at the same rate, but the concentration of Br^- was increased to 10 g L^{-1} due to the larger discharge volume in the drain at this time. Before commencement of Br^- addition, there was no detectable Br^- in the water. The discharge rate, Q (L s^{-1}) was calculated using the bromide (Br^-) dilution data as per equation 3.1.

In experiment 1, at site 1, the overall mean Br^- concentration was 0.76 ± 0.02 mg L^{-1} and at site 5, it was 0.66 ± 0.10 mg L^{-1} (Figure 3-5). In experiment 2, at site 1, the overall mean Br^- concentration was 1.35 ± 0.04 mg L^{-1} and at site 5, it was 1.08 ± 0.21 mg L^{-1} for all sampling times (Figure 3-6).

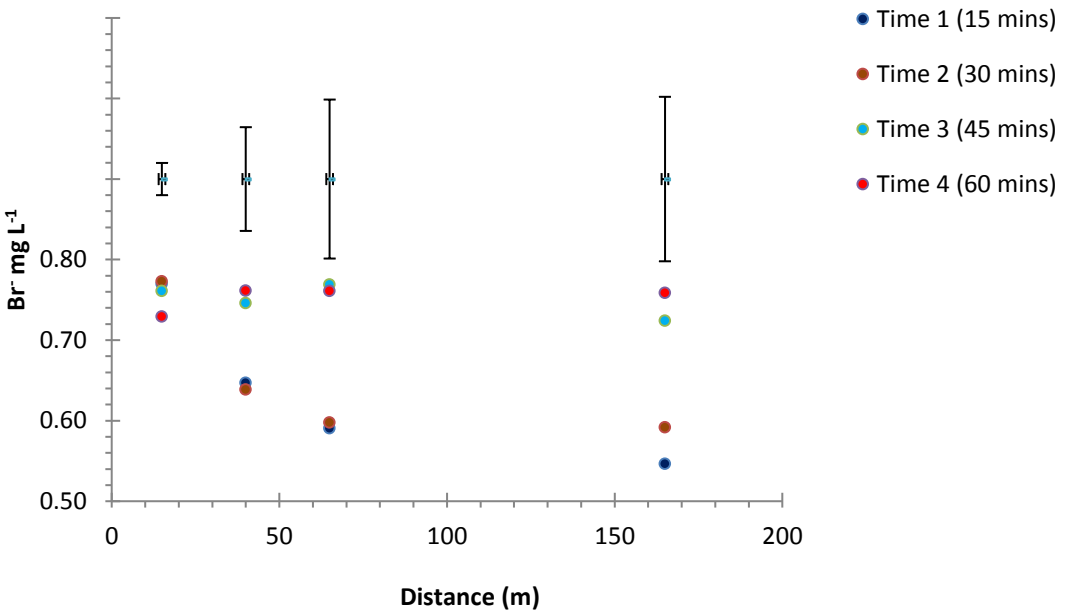

Figure 3-5 **Experiment 1: Drain water Br^- concentration over distance and sampling time following commencement of tracer solution injection at time zero. Error bars = stdev, (n = 4) of mean Br^- concentrations over all sampling times.**

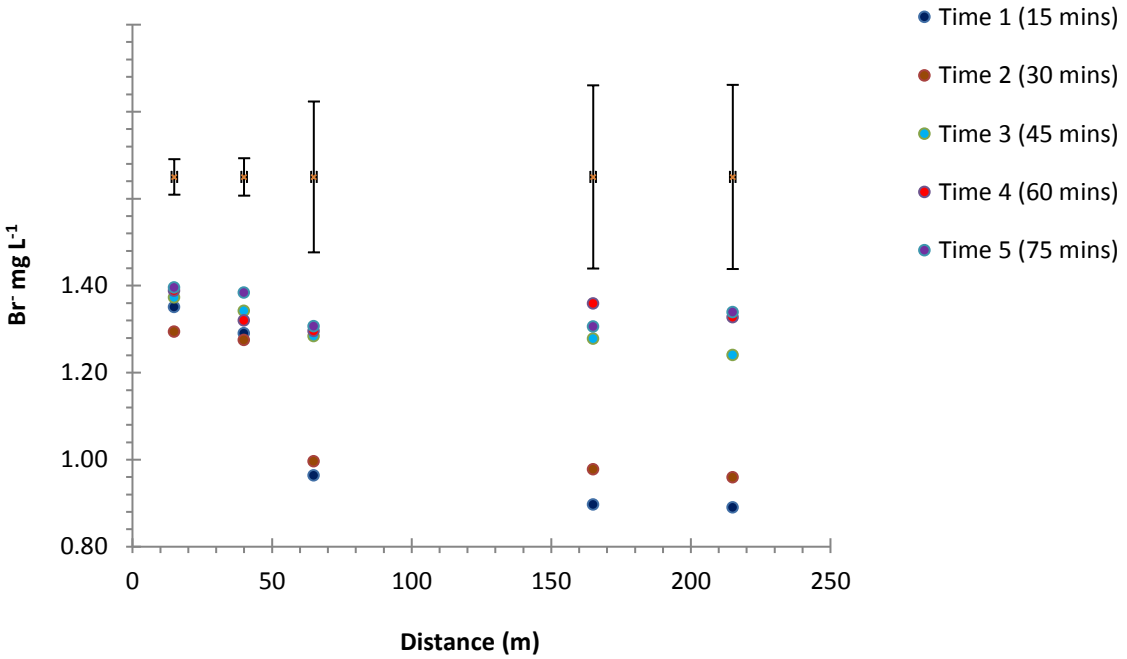

Figure 3-6 **Experiment 2: Drain water Br^- concentration over distance and sampling time following commencement of tracer solution injection at time zero. Error bars = Stdev, (n = 5) of mean Br^- concentrations over all sampling times.**

The standard deviations of the Br^- concentrations (Stdev) in both experiments increased with sampling distance (Figures 3-5 & 3-6). There was also a trend for Br^- concentrations to increase as time progressed, especially in downstream sampling sites. The variations in Br^- concentrations may occur due to insufficient mixing of tracer solution at the earlier sampling times and the impact of time on Br^- concentration is evaluated further below.

3.3.4 Drain water steady state measurements – correction from Br^- concentration

A one-way analysis of variance (ANOVA) was performed to assess the impact of time on Br^- concentrations at a given sampling site. There were statistical differences in Br^- concentration due to sampling time in both experiments 1 and 2 ($p < 0.05$). The mean Br^- concentration differences declined with later sample collections; increased sampling times (Figure 3-5 and 3-6). In experiment 1, the time effect on Br^- concentration, calculated using η^2 (Sum of squares between groups divided by the total sum of squares) for times 1, 2, 3, 4, times 2, 3, 4, and times 3 and 4 were 0.54, 0.47 and 0.07, respectively. Thus, the effect of sampling time on Br^- concentration was not significant when sampling times 3 and 4 were considered. In addition, in experiment 1, the Post hoc corrected T-test (two samples assuming equal variances between sampling times) for sampling times 3 and 4 was < 0.012 which further demonstrated that there were no significant Br^- concentration differences between sampling times 3 and 4. In experiment 2, the time effect on Br^- concentration was again estimated using η^2 for times 1, 2, 3, 4, 5, times 2, 3, 4, 5 and times 3, 4 and 5 with values of 0.58, 0.49 and 0.17, respectively. Following the same trend as in experiment 1, the time effect on Br^- concentration in experiment 2 declined with increasing sampling times. The Post hoc corrected T-test between sampling times 3, 4 and 5 of experiment 2 was < 0.1. Thus, in experiment 2, there were no significant Br^- concentration differences between sampling times 3, 4 and 5.

Therefore, it was concluded that the drain water mixed with the tracer solution to reach a steady state by sampling times 3 and 4 in experiment 1, and by sampling times 3, 4 and 5 in experiment 2.

In experiment 1, the average Br^- concentration across all sites when pooling data for times 3 and 4, was 0.76 ± 0.02 mg L^{-1}. In experiment 2, the average Br^- concentration at time 3, 4 and 5 was 1.33 ± 0.05 mg L^{-1} across all sites. Therefore, the estimated steady state drain water discharge rates (Equation 3.1) derived using these average Br^- concentrations, in experiment 1 and 2 were 67.5 ± 1 L s^{-1} and 126.7 ± 3.6 L s^{-1}, respectively.

3.3.5 Drain water velocity

Water velocity was estimated using the breakthrough concentration curves of the Rhodamine^{WT} dye that was injected into the drain immediately after experiments concluded. The injection time was taken as time zero.

In experiment 1, the Rhodamine^{WT} dye was released at site 1 (15 m) and three water samples were collected at sites 2 (40 m), 3 (65 m) and 4 (165 m). The estimated travel times from site 1 to sites 2, 3 and 4 were 127, 215 and 553 seconds respectively. The slope of the time (seconds) vs. distance (m) plot equates to the drain water velocity (Figure 3-7) which was 0.299 m s^{-1}.

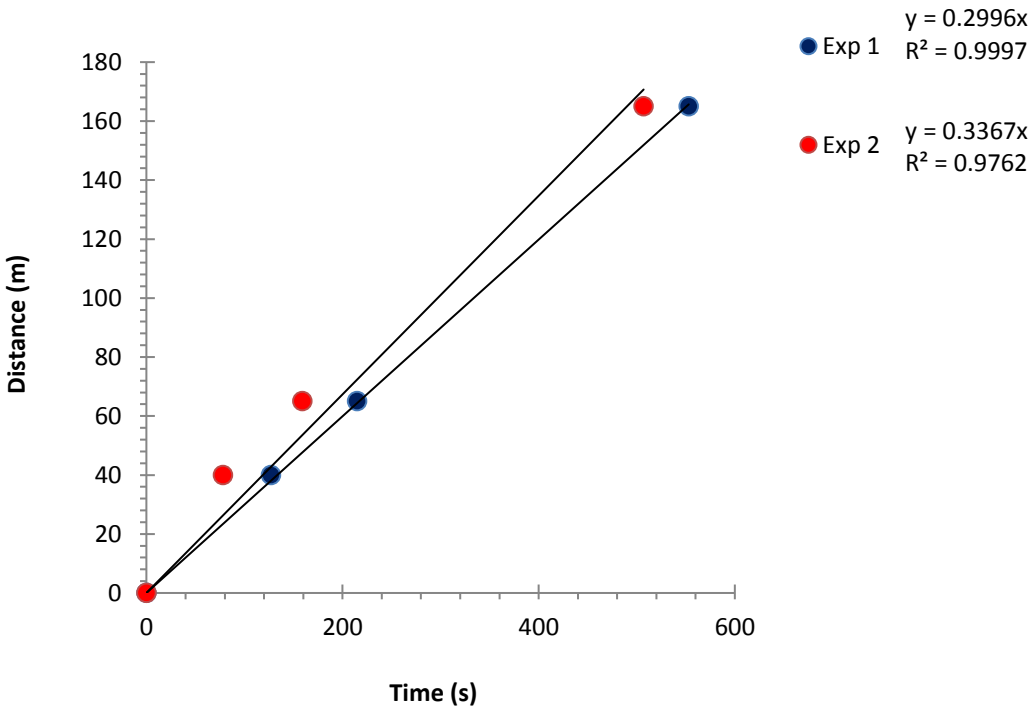

Figure 3-7 Mean water velocity obtained from the slope of graph for both experiment 1 and 2. Travel time is determined using breakthrough concentrations of Rhodamine^{WT} dye.

In experiment 2 three water samples were collected at sites 2 (40 m), 3 (65 m) and 4 (165 m) and a plot of time vs distance showed the drain water velocity was 0.337 m s^{-1} (Figure 3-7).

3.3.6 Nitrous oxide transfer velocity (k_{N2O}) measurement using propane (C_3H_8) as a tracer gas

3.3.6.1 Headspace equilibrium

Determination of k_{N2O} values are based on the Br^- analyses data. The results of 3.3.4 showed uniform mixing of the tracer solutions at times 3 and 4 for experiment 1 and at times 3, 4 and 5 for experiment 2. Thus, the natural log data of dilution corrected C_3H_8 concentrations (Ln [C_3H_8/Br^-]) were used to determine k'_{N2O} come from times 3 and 4 for experiment 1 and times 3, 4 and 5 for experiment 2.

In experiment 1, at sampling times 3 and 4, a total of 24 water samples were collected. However, six gas samples were rejected due to insufficient vacuum within the sample bottles' headspace and so 18 of the samples were used to determine the C_3H_8 transfer coefficient (k'_{C3H8}). The calculated Ln [C_3H_8/Br^-] values were plotted according to equation 3.7, and the best-fit lines determined using Minitab® version 16. The slope of the best-fit line equates to the C_3H_8 transfer coefficient (k'_{C3H8}); 0.035 min^{-1} (Figure 3-8).

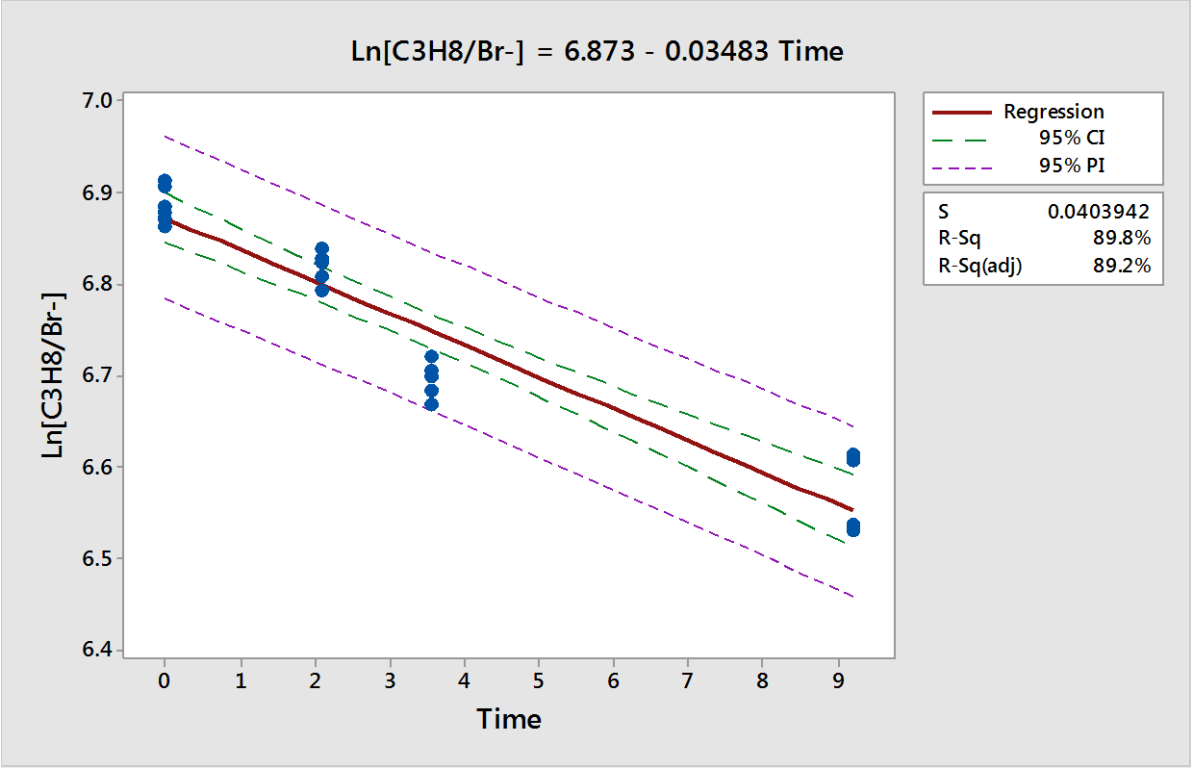

Figure 3-8 Experiment 1, results of the natural log of C_3H_8/Br^- over time. The data points are individual sample values. The area between the green lines represents the 95% confidence interval and the brown line is the best-fit line. The area between the purple lines represents the prediction interval, and the slope of the best-fit line is the propane transfer coefficient (k'_{C3H8}).

In experiment 2, at sampling times 3, 4 and 5, a total of 45 water samples were collected. However, 15 gas samples were rejected due to insufficient headspace vacuum conditions within sample bottles and 30 of the samples were used for C_3H_8 transfer coefficient (k'_{C3H8}) analysis. Following the same procedure as in experiment 1, the calculated Ln [C_3H_8 / Br^-] values were plotted according to equation 3.7, and the best-fit line was determined using Minitab® version 16. The slope of the best-fit line was 0.012 min^{-1} which equates to the C_3H_8 transfer coefficient (k'_{C3H8}) (Figure 3-9).

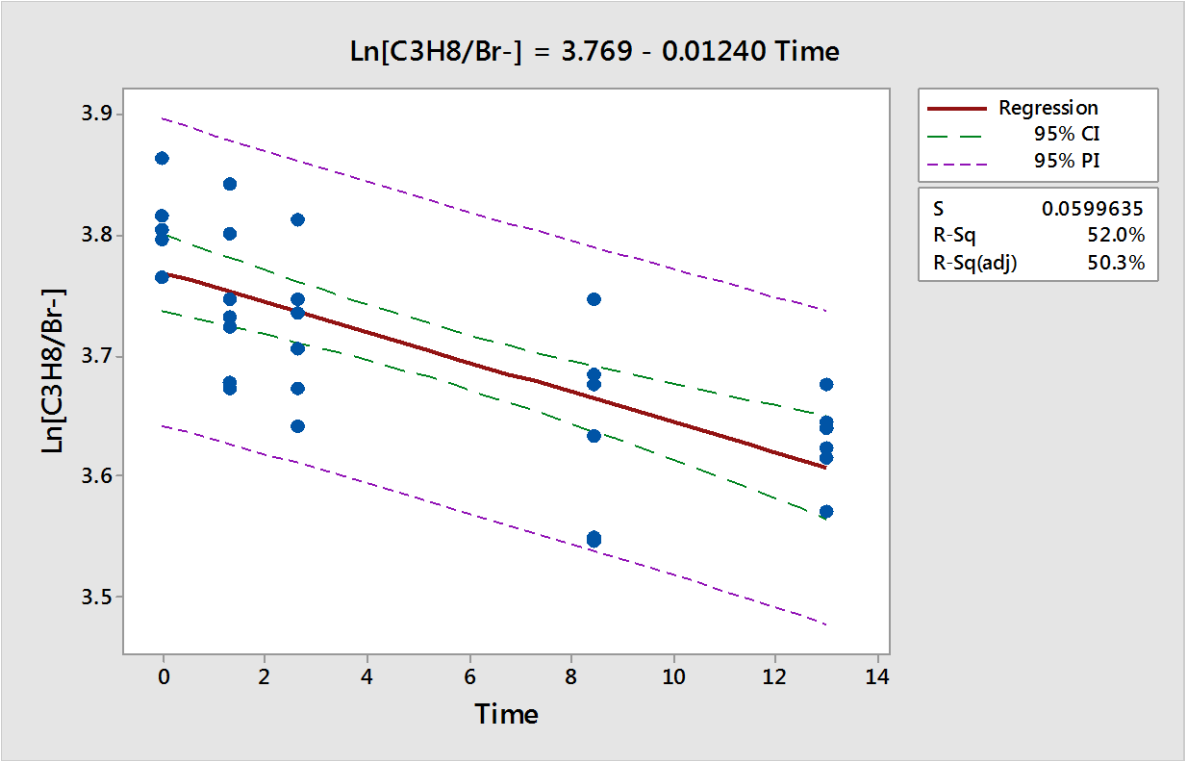

Figure 3-9 Experiment 2, results of the natural log of C_3H_8/Br^- over time. The data points are individual sample values. The area between the green lines represents the 95% confidence interval and the brown line is the best-fit line. The area between the purple lines represents the prediction interval. The slope of the best-fit line is the propane transfer coefficient (k'_{C3H8}).

The obtained C_3H_8 transfer coefficient (k'_{C3H8}) values were used to estimate the N_2O transfer coefficients (k'_{N2O}) at each sampling site (Equation, 3.10). Then, the N_2O transfer velocities (k_{N2O}) within the drain, at each sampling site, for both experiments were estimated as described in section 3.2.8.1 and results are presented in Table 3.3.

Table 3.3 Headspace N_2O transfer velocity (k_{N2O}) calculations from experiment 1 (20/01/2015) and experiment 2 (12/08/2015).

	Site	k'_{C3H8} (min^{-1})	Sc_{C3H8}	Sc_{N2O}	k'_{N2O} (min^{-1}) *Eqn 3.10*	$k_{2(N2O)}$ (min^{-1}) *Eqn 3.11*	Depth (cm)	k_{N2O} (cm hr^{-1})	$K_{(N2O)}$ (m day^{-1})
Experiment 1	1	0.035	1143	774	0.045	0.046	19.5	52.97	12.71
	2	0.035	1143	774	0.045	0.046	18.4	49.98	11.99
	3	0.035	1143	774	0.045	0.046	18.7	50.79	12.19
	4	0.035	1143	774	0.045	0.046	20.4	55.41	13.30
								Mean	**12.55**
								Stdev	**0.58**
Experiment 2	1	0.012	1399	950	0.015	0.016	32.8	30.50	7.32
	2	0.012	1399	950	0.015	0.016	31.3	29.10	6.99
	3	0.012	1399	950	0.015	0.016	29.6	27.51	6.61
	4	0.012	1399	950	0.015	0.016	35.5	33.01	7.92
	5	0.012	1399	950	0.015	0.016	37.6	34.97	8.39
								Mean	**7.44**
								Stdev	**0.72**

Stdev = Standard deviation

3.3.6.2 Floating chambers

In experiment 2, the C_3H_8 flux from the water surface was also collected using floating chambers at sample sites 1, 3 and 5. The dissolved equilibrium C_3H_8 concentration was estimated using equations 3.3 and 3.4. Then, the value of the C_3H_8 transfer velocity (k_{C3H8}) was determined using equation 3.13. The estimated k_{C3H8} was converted into k_{N2O} using equation 3.14 and the k_{N2O} values were normalized to a temperature of 20°C using equation 3.15 (Table 3.4).

Table 3.4 Nitrous oxide transfer velocity (k_{N2O}) values derived from C_3H_8 surface flux measurements

Site	C_3H_8 Flux μmol m^{-2} hr^{-1}	Equilibrated C_3H_8 (μmol m^{-3})	k_{C3H8} (m hr^{-1})	k_{N2O} (m hr^{-1})	K_{N2O} (m day^{-1})
1	10.31 ± 0.83	46. 71 ± 1.13	0.221	0.285	6.84 ± 0.94
3	8.45 ± 0.21	34.94 ± 1.70	0.217	0.281	6.83 ± 0.35
5	7.26 ± 0.22	30.52 ± 0.79	0.238	0.307	7.38 ± 0.17

The average k_{N2O} values for site 1, 3 and 5 using C_3H_8 surface flux measurements (Table 3.4) were 6.84 ± 0.94, 6.83 ± 0.35 and 7.38 ± 0.17, respectively.

3.3.7 Nitrous oxide transfer velocity (k_{N2O}) measurement using the Wilcock (1982) transfer velocity model

Using the drain water velocity and depth data for each sampling site, Wilcock (1982) modelled (Equation 2.10) the reaeration transfer velocity for oxygen (k_{O2}). This was used to determine the k_{N2O} (equation 3.16). Then, the k_{N2O} values were normalized to a temperature of 20°C using equation 3.15 (Table 3.5).

Table 3.5 N_2O transfer velocity (k_{N2O}) determined using the model of Wilcock (1982) for data from experiment 1 (20/01/2015) and experiment 2 (12/08/2015).

	Site	k_{O2} (m day^{-1})	Sc_{O2}	Sc_{N2O}	$K_{(N2O)}$ (m day^{-1})
Experiment 1	1	21.27	678	774	19.49
	2	23.20	678	774	21.26
	3	22.65	678	774	20.76
	4	19.88	678	774	18.22
Experiment 2	1	8.97	832	950	8.75
	2	9.62	832	950	9.39
	3	10.46	832	950	10.21
	4	7.97	832	950	7.77
	5	7.30	832	950	7.13

The average k_{N2O} values using the Wilcock (1982) model (Table 3.5) for experiment 1 and 2 were 19.93 ± 1.37 and 8.65 ± 1.23, respectively.

3.3.8 Direct k_{N2O} measurement from floating chambers

In experiment 2, the N_2O flux from the water surface was determined using floating chambers at sample sites 1, 3 and 5. The dissolved equilibrium N_2O concentration was estimated using 3.3 and 3.4 equations. Then, the value of the N_2O transfer velocity (k_{N2O}) was determined using equation 2.5 and the k_{N2O} values were normalized to a temperature of 20°C using equation 3.15 (Table 3.6).

Table 3.6 Nitrous oxide transfer velocity (k_{N2O}) values derived from floating chamber N_2O surface flux measurements.

Site	N_2O-N Flux (μg m^{-2} hr^{-1})	Equilibrated N_2O-N (μg m^{-3})	k_{N2O} (m hr^{-1})	K_{N2O} (m day^{-1})
1	15.37 ± 1.53	94	0.211	3.93 ± 1.32
3	29.18 ± 2.58	119	0.215	5.88 ± 2.24
5	43.99 ± 4.44	126	0.284	8.38 ± 2.41

The average k_{N2O} values for site 1, 3 and 5 using N_2O surface flux measurements (Table 3.6) were 3.93 ± 1.32, 5.88 ± 2.24 and 8.38 ± 2.41, respectively.

3.3.9 Comparisons of N_2O transfer velocity (k_{N2O}) estimations

The summary of measured k_{N2O} from headspace equilibrium method, floating chamber method, Wilcock (1982) model and the back calculated real time k_{N2O} measurements from floating chambers are summarised in Table 3.7, Figure 3-10 and Figure 3-11 as follows.

Table 3.7 Comparisons between experimentally observed k_{N2O} (m day^{-1}) using propane as a tracer gas at each site from headspace equilibrium (HS) and floating chamber (FC) methods, Wilcock (1982) model and N_2O flux measurements.

Experiment number and sampling sites		**Obtained k_{N2O} value from Headspace method (HS) Floating Chambers (FC) and surface flux measurements.**	**k_{N2O} value from Wilcock, (1982) model.**
Exp # 1	**Site 1**	12.80 (HS)*	19.49
	Site 2	12.07 (HS)*	21.26
	Site 3	12.27 (HS)*	20.76
	Site 4	13.39 (HS)*	18.22
Exp # 2	**Site 1**	7.37 (HS)*, 6.84 (FC)'	8.75
	Site 2	7.03 (HS)*	9.39
	Site 3	6.65 (HS)*, 6.83 (FC)'	10.21
	Site 4	7.97 (HS)*	7.77
	Site 5	8.44 (HS)*, 7.38 (FC)'	7.13
Experiment 1 Average ± Stdev		**12.63 ± 0.59**	**19.93 ± 1.37**
Experiment 2 Average ± Stdev		**7.49 ± 0.72 (HS)* 6.98 ± 0.34 (FC)'**	**8.65 ± 1. 23**
		6.06 ± 2.23 (SF)	

(HS)* Headspace equilibrium method, (FC)' Floating chamber method and (SF) surface flux measurements

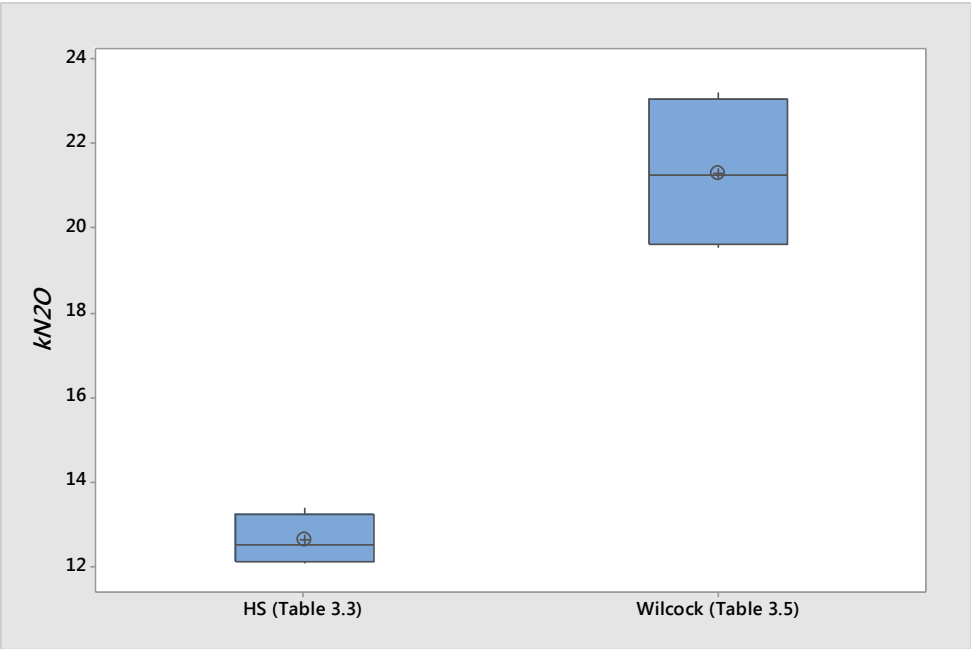

Figure 3-10 **The interquartile box plot comparisons of experiment #1 N_2O transfer velocity (k_{N2O}) determined using C_3H_8 as a tracer gas between HS (Headspace equilibrium) and Wilcock (1982) model. The box represents the interquartile range (25% to 75%) for each group, the middle line is median, the symbol is the mean value and the upper (> 75%) and lower (< 25%) whiskers are the outside values of interquartile range.**

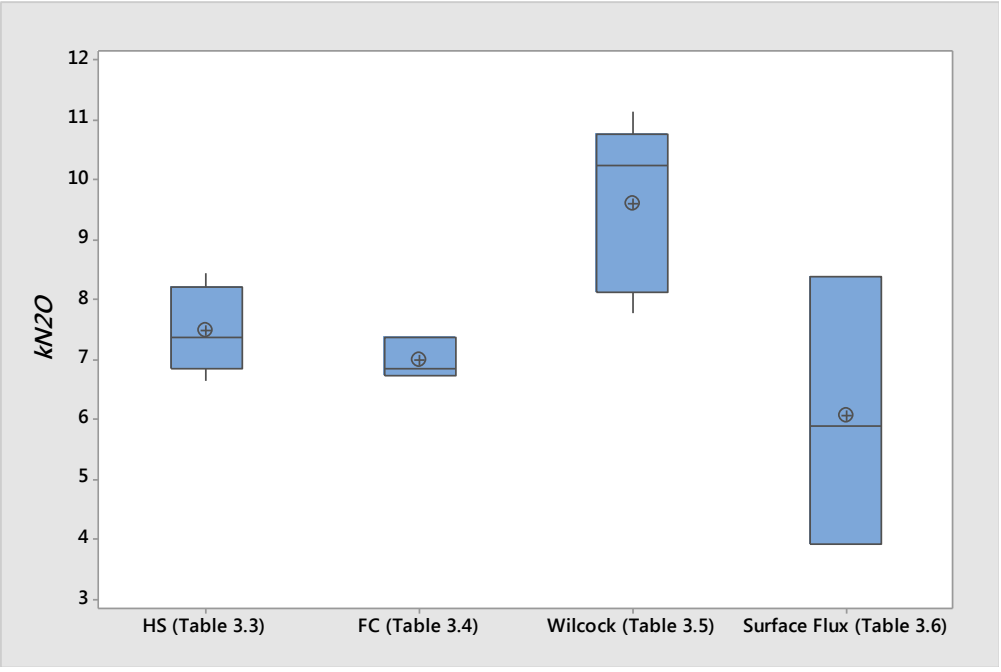

Figure 3-11 **The interquartile box plot comparisons of experiment #2 N_2O transfer velocity (k_{N2O}) determined using C_3H_8 as a tracer gas between HS (Headspace equilibrium), Floating chambers (FC) and Wilcock (1982). The determined k_{N2O} from surface flux is based on N_2O flux measured in chambers. The box represents the interquartile range (25% to 75%) for each group, the middle line is median, the symbol is the mean value of the group and the upper (> 75%) and lower whiskers (< 25%) are the outside values of the interquartile range.**

Chapter 4

Nitrous Oxide Transfer Velocity (k_{N2O})

4.1 Evaluation of methods used to establish k_{N2O}

The agreement between the N_2O transfer velocity (k_{N2O}) derived from the observed data and the predictive equation as explained by Connor and Dobbins (1958), equation 2.9 as interpreted by Wilcock (1982) was generally poor (Table 3.7).

In order to probe the cause for the difference between the values obtained using the model and direct measurements, the O'Connor and Dobbins study data were evaluated. The reaeration coefficient of the O'Connor and Dobbins model is influenced by river velocity and depth (equation 2.9). They used a two –film theory for mass transfer processes that explains the rate of dissolved particles at a surface layer being replaced by the particles arising from turbulence motion. They verified the model using a laboratory experiment and found the rate of the surface renewal proportionally increased with the water oscillation speed. However, the total turbulence motion depends on both water speed and depth. In addition, in their experiment water was isotropic (uniform), but in natural environments, the shallow drains are more likely to be anisotropic (non-uniform).

O'Connor and Dobbins study generalized their model, applying it to a wide range of river depth data. The average depth for five out of their six studies ranged between 0.57 m to 6.10 m and re-aeration coefficients ranged from 2.6 day^{-1} to 0.018 day^{-1}. However, for the study that was performed in the Elk River, the depth was only 0.27 m and the observed and computed re-aeration coefficients were 4.8 and 5.3 day^{-1}, respectively. The Elk River depth is closer to the depth of the Raineys Road drain in this study where the model computed k_{N2O} values higher than the observed values.

Few past studies have doubted the accuracy of O'Connor and Dobbins model (equation 2.9) that measured the re-aeration coefficient in low depth rivers. The summary of those studies is as follows.

1. Wilcock (1984) used $CHCl_3$ as a gas tracer to measure the re-aeration coefficient in five New Zealand (North Island) streams. Results of that study showed, the measured values were about 40% less than the estimated values.

2. Young and Huryn (1999) examined the reaeration coefficient in streams that were tributaries to the Taieri River in south east, New Zealand. They observed higher re-aeration

coefficients values than the empirically predicted values. These higher values were generally produced in small rivers/streams. Young & Huryn (1999) further stated that, removing higher values from the analysis, the O'Connor and Dobbins' model predicted values correlated with the measured values (r = 0.57).

3. Grant and Skavroneck (1980) compared the tracer addition method and predictive equations for determination of stream reaeration coefficients on three small streams in Wisconsin, USA. According to their evaluation, the O'Connor and Dobbins equation produced mean absolute error of reaeration coefficients of between 50-232% against the measured values.

4. Robert et al. (2007), added C_3H_8 with salt into the 0.06 to 0.09 m deep Walker Branch, Tennessee, as a tracer to measure the re-aeration coefficient. They found the re-aeration coefficients ranged between 5.52 - 14.42 day^{-1} and they were higher than the O'Connor and Dobbins' model predicted.

According to these previous studies and results of this current experiment, the gas transfer velocity in low depth (< 0.5 m) rivers was unable to be measured accurately using O'Connor and Dobbins model. In spite of considering discrepancies, Wilcock (1982), introduced equation 2.10 to measure oxygen transfer velocities and suggested changing the multiplier in the equation with relevant river velocity and depth data. Specifically, Wilcock (1982) increased the drain depth coefficient to a value of 1.5, which is extremely sensitive to low depths. The model was validated with six separate gas studies that were carried out in the Tarawera River, between 1983 -1986. However, the depth of five of the six study sites were between 1-3.46 m and deeper than the sites of this study.

In the current study, the C_3H_8 gas tracer enabled accurate and real time k_{N2O} measurements. According to Wilcock (1982) model, oxygen transfer velocity (k_{O2}) is proportionally sensitive to drain depth. As a result, in experiment 1, with a slightly slower speed and shallower depth, the measured k_{N2O} was 5.41 m day^{-1} higher than in experiment 2 (Table 3.5). When comparing the measured k_{N2O} using propane as a tracer gas, the Wilcock model overestimated k_{N2O} by 59.5% and 18.3% in experiments 1 and 2, respectively. According to Wilcock's (1982) suggestion, we reduced the multiplier by 28% from 3.74 to 2.7 in equation 2.10. Using the modified equation, the estimated k_{N2O} for experiment 1 was 15.1% greater than the mean measured and the estimated k_{N2O} for experiment 2 was 14.6% less than the mean measured (Table 4.1).

Table 4.1 Comparisons between k_{N2O} obtained at each site (m day^{-1}) from equation 2.10 (multiplier 3.74), and the modified model (multiplier 2.70) measured k_{N2O}.

Experiment #	k'_{N2O} (m day^{-1}) using original multiplier 3.74	k'_{N2O} (m day^{-1}) using modified multiplier 2.70	Measured Total transfer Velocity (m day^{-1})
1	19.9 ± 1.4	14.4 ± 1.0	12.63 ± 0.59 (HS)*
2	8.7 ± 1.2	6.3 ± 0.9	7.49 ± 0.72 (HS)* 6.98 ± 0.34 (FC)'

In order to find the relationship between the modified (multiplier 2.7) model predicted k_{N2O} and the water depth, each sampling sites k_{N2O} values were plotted against site depth (Figure 4-1).

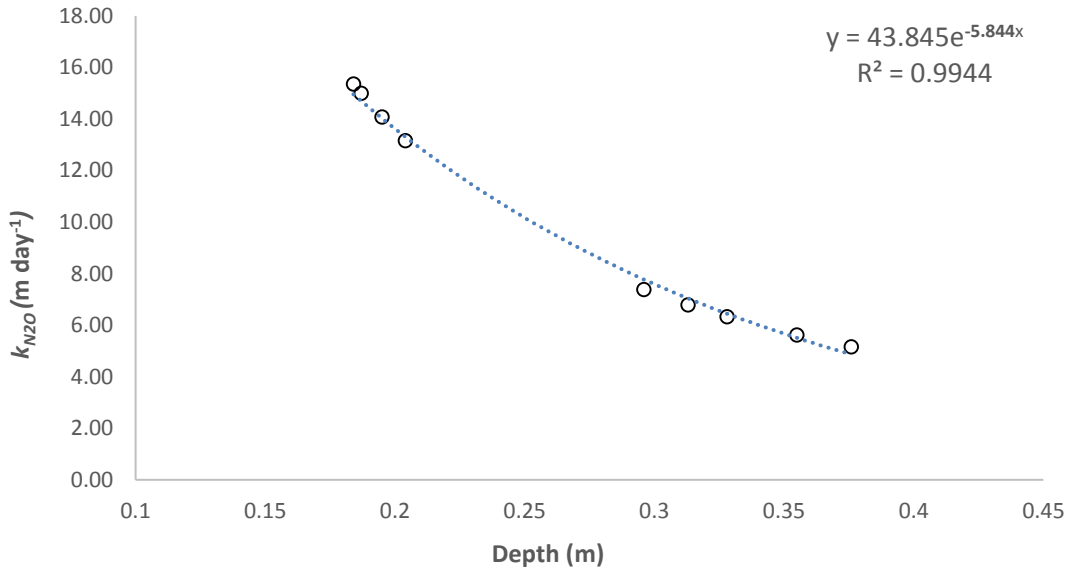

Figure 4-1 The modified model predicted k_{N2O} (m day^{-1}) in Raineys Road sites depth (m).

According to Figure 4-1, the value of k_{N2O} doubles with approximately 0.1 m of depth decrease. The modified model was applied to the low depth (<0.5 m) stream data of Wilcock (1984) and the data of Young and Huryn (1999), (Figure 4-2).

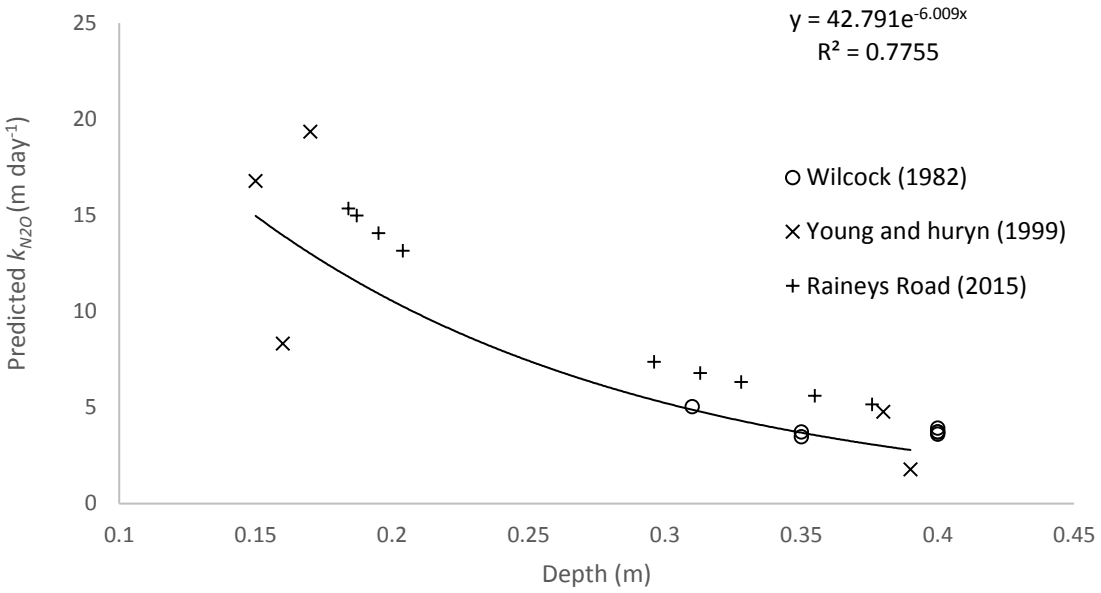

Figure 4-2 The modified model predicted k_{N2O} (m day^{-1}) vs. sampling site depth (m) of Wilcock (1984), Young, and Huryn (1999) and Raineys Road drain (2015).

The Figure 4-2 also shows k_{N2O} decreased with river depth at a similar rate; k_{N2O} halved when a drain depth increased by 0.1 m.

O'Connor and Dobbins developed their water turbulence transfer velocity model in a laboratory with a constant depth with different oscillation speeds. Their experiment was in an isotropic medium and they validated their model collecting the data from a wide range of river depths. Wilcock (1982) re-interpreted the O'Connor and Dobbins model, increasing the depth coefficient to 1.5, and suggested changing the multiplier according to the drain velocity and depth. The results of our experiments show that k_{N2O} decreases as depth increases. There is no single study that has measured k_{N2O} or k_{O2} against depth in small rivers. However, the trend with depth is incorporated into most of the energy dissipation models. Therefore, this study provides a nonlinear regression relationship between k and a gas escape coefficient as a function of the depth in shallow waters.

4.2 Gas transfer velocity in small rivers

The observed gas transfer velocities among the studies were highly variable and such variability in small rivers and streams occurred due to different hydro physical conditions. The studies have illustrated that high *k* values occur in small streams and they may be summarised as follows.

- A sensitivity analysis showed that *k* is dependent on the width to depth ratio. When water depth is shallower than 3 m, the variations in *k* are higher (Alin et al., 2011).
- Hydro-physical variations such as channel width, water velocity and depth in small streams result in highly variable *k* values (Alin et al., 2011).
- The average *k* values were 40% higher from small rivers compared to larger rivers (Wanninkhof R., 1990).
- The observed *k* values in small rivers and streams (< 100 m) have higher variability (1 to 71.1 cm h^{-1}) than in larger rivers (1.2 to 44.5 cm h^{-1}) (Alin et al., 2011).
- The wind effect on *k* values was considerably lower in small rivers. The estimated wind effect on *k* in large rivers and small rivers ranged from 0 to 5.2 cm h^{-1} and 0 to 1.3 cm h^{-1}, respectively (Rasera et al., 2008).
- Within the flowing water systems, effects of hydro physical parameters on *k* declined with stream order (Turner et al., 2015).

According to the above summary, hydro physical parameters of waters are the key drivers of *k* in small rivers and streams. In addition, exposure to the wind will also have significantly less effect in small streams with deep banks and sheltering plant canopies. The bed friction may have significant impact on *k*, but the majority of studies do not describe the drain waterbed characteristics. Roughness / bed-friction of bottom surfaces of drains is a major factor that can alter the gas transfer velocity. Drains with stony, gravel bottom surfaces break the water flow and should result in higher *k* values than drains with smooth, clay bottom surfaces. Even though the Schmidt number coefficient is assigned to address bed friction (as 0.5 for rough surfaces and 0.66 for smooth surfaces), the variations among the bottom surfaces are large. Distributions of hydrological parameters overlapped to some extent between studied data. Therefore, to develop a more refined model to measure the k_{N2O} values in drains, a broader range of hydro physical measurements is needed.

4.3 Summary and suggestion for future research

The following key aspects were observed to control k_{N2O} in two separate experiments within the drain study site.

- The tracer racer gas addition method provided more accurate and precise k_{N2O} values than the Wilcock (1982) model predicted values.
- The results show that k_{N2O} decreases as depth increases (Figure 4-1 and 4-2).
- A narrow and deeper drain system with low k_{N20} would result in lower N_2O emissions than wider and shallower drains with high k_{N2O} values.
- According to Henry's law function, water temperature is inversely correlated with the volume of the gas dissolved. Therefore, in cold winter months, drain water k_{N2O} is lower than the warmer summer months.

The following key areas have to be investigated in future studies.

- The two experiments performed are insufficient to establish clear trends in k_{N2O} against drain depth. Therefore, further tracer gas addition studies are required in variable drain depths.
- The tracer gas has to be added over a longer time scale for drain water steady state sampling.

Chapter 5

Effect of Ammonium (NH_4^+-N) on N_2O emissions from an agricultural drain

5.1 Introduction

Agricultural drains are a significance source of N_2O emissions, but relatively little is known about N_2O production and indirect emissions from waterways. River studies indicate that N_2O emissions increase with N loading (Harrisons, 2003). It has been estimated that river networks are responsible for ~ 10% of global anthropogenic N_2O emissions, but uncertainty is high (Beaulieu, 2011). Variable residence time, different N loading rates, numerous biota interactions and changes in hydro physical conditions within river systems contribute to this uncertainty.

Biological nitrification and denitrification mechanisms are the two main N_2O production pathways. Nitrification is an aerobic process in which ammonium (NH_4^+) is oxidised to nitrite (NO_2^-) and then nitrate (NO_3^-). But denitrification is an anaerobic process in which NO_3^- is reduced to N_2O and ultimately N_2. Similarly, NH_4^+ produced from organic matter decomposition in waters can be nitrified into NO_3^- and subsequently denitrified. Therefore, nitrification maybe a significance process contributing to indirect N_2O emissions from waterways. However, no studies have been performed within drains, streams or river systems to specifically examine the role of nitrification in N_2O emissions. Unlike soil systems, shallow and fast moving water within drain systems, tends to be oxygenated and well mixed. As a result, the effect of nitrification on N_2O emissions from agricultural drain systems remains to be investigated.

Experiments in this chapter tested the hypothesis that nitrification of NH_4^+-N would contribute to N_2O emissions in an agricultural drain. Similarly, the experiment provided an opportunity to both directly measure N_2O fluxes and estimate N_2O fluxes using the k_{N2O} value that was determined in chapter four.

5.2 Methods

5.2.1 Mixed tracer solution

Prior to the ^{15}N tracer addition experiment, a preliminary experiment was also performed. This evaluated NH_4^+ and NO_3^- concentration changes in the drain, following the addition of an unlabelled NH_4^+ pulse (05th June, 2015). The main ^{15}N tracer addition experiment was performed on 12th August, 2015 (previously described in chapter 3 as experiment 2).

The preliminary experiment was performed to determine, if nitrification of ammonium (NH_4^+) could be observed. A solution of NH_4^+ was made up on site in an 80 L carboy with a conservative tracer, potassium bromide (KBr). The carboy solution comprised of: 500 g of ammonium sulphate $(NH_4)_2SO_4$ and 800 g of KBr dissolved in 5 L of water inside the carboy. The carboy was then filled with stream water (75 L) and mixed well before being released into the drain using a Pegasus Alexi's peristaltic pump (Fondriest, CA, USA). The masses of added $(NH_4)_2SO_4$ and Br^- were expected to increase both NH_4^+ and Br^- concentrations in the drain by 1 mg L^{-1}, based on a solution release rate of 17 mL s^{-1}. The drain NH_4^+ and Br^- background concentrations were < 0.1 and 0 mg L^{-1}, respectively, and the estimated drain discharge volume was 67.5 L s^{-1}.

In experiment 2, the tracer solution comprised of 800 g of ^{15}N enriched $(NH_4)_2SO_4$ and 1.0 kg of KBr in an 80 L carboy. When experiment 2 was performed, the drain discharge volume was estimated at 126.7 L s^{-1}. The carboy solution was continuously released into the drain using the peristaltic pump at a rate of 17 mL s^{-1} while 99.9% pure propane (C_3H_8) continued to purge the solution. The pump rate and injected solution concentrations were chosen to result in a $^{15}NH_4^+$ enrichment of 3 atom % and a Br^- concentration of 1 mg L^{-1} approximately. Due to potential interferences of the visual tracer $Rhodamine^{WT}$ on the NH_4^+ detection method (phenol, hypochlorite colorimetric method), $Rhodamine^{WT}$ was added in a separate dosing experiment, immediately after the final collection of water samples as noted below, in order to determine water speed.

5.2.2 Sampling time, stations and collection

In the preliminary experiment, water-sampling sites were positioned along the drain at 15, 40, 65 and 165 m from the tracer injection site (Figure 3-2). At each site, triplicate water samples were collected for determination of inorganic-N (NH_4^+-N and NO_3^--N) and Br^- concentrations.

In the preliminary experiment, the sample site at 165 m had higher NO_3^- concentrations with lower C_3H_8 concentrations. Thus, another sample site was added at 215 m in experiment 2 in order to increase the potential recovery of NO_3^-. Therefore, in experiment 2 sampling sites were positioned along the drain at 15, 40, 65, 165 and 215 m. At each site, triplicate water and gas samples were collected every 15 minutes, five times for 1.25 hours (15, 30, 45, 60 and 75 minutes) following commencement of tracer injection at time zero. Samples were collected for inorganic-N concentrations and their ^{15}N enrichments (NH_4^+ and NO_3^-), dissolved N_2O (concentrations and ^{15}N enrichments), Br^- concentrations, pH, and dissolved C_3H_8 concentrations.

In experiment 2, the surface gas fluxes were also determined using floating chambers at sites located at 40, 65, and 215 m. The detailed description of floating chamber design, construction and gas sampling procedures were as previously reported in Clough et al., (2006). A 10 mL gas sample was extracted and injected into a pre-evacuated 6.0 mL Exetainer® (Labco Ltd, High Wycombe, UK). In addition, after 75 minutes, a further 15 mL gas sample was taken from each chamber and placed in a pre-evacuated 12.0 mL Exetainer for subsequent $^{15}N_2O$ analysis. Ambient air samples were also taken to measure background N_2O concentrations. Prior to each gas sampling, the syringe was flushed with ambient air to prevent cross contamination between samples. Then, the sample vials were transported to the laboratory for C_3H_8 and N_2O analysis using a GC (Section 3.2.7), and $^{15}N_2O$ analyses using a trace gas analyser (TGII) connected to a continuous isotope ratio mass-spectrophotometer (IRMS). The detailed description of IRMS analyses can be found in the section 5.2.4.

5.2.3 Dissolved N_2O measurements

The gas sampling procedures and determination of dissolved N_2O were as previously reported (Section 3.2.8). In experiment 2, the headspace gas was transferred to pre-evacuated 6.0 mL and 12.0 mL Exetainers for N_2O concentration and ^{15}N enrichment analyses, respectively. Ambient air samples were also collected at each sampling. The same procedure, using 50 mL of distilled water was performed in the laboratory to act as a control.

5.2.4 Gas sample analyses on GC and TGII-IRMS

Gas sample analysis methods for N_2O and C_3H_8 samples were as previously described in section 3.2.7.

The 12 mL gas samples collected for ^{15}N enrichment of N_2O, which were analysed using a trace gas analyser interfaced to an IRMS (TGII/IRMS; Sercon™, Crew, UK). The sample vials were placed on a Gilson auto sampler and flushed with ultra-high purity helium through a double – ended concentric needle. Since N_2O is condensable below -90°C, the N_2O was removed by cryogenic trapping in liquid nitrogen. Prior to the sample injection into the separation column, elliptical stainless steel cryo-traps were lowered into liquid nitrogen (-196°C) concentrating the N_2O. The CO_2 and water in the gas samples was scrubbed prior to this using NaOH (sodium hydroxide) and $Mg(ClO_4)_2$ (magnesium perchlorate), respectively. Then the concentrated N_2O sample was passed through a GC capillary column, (Pora PLOT- Q) 30 m long and 0.32 mm diameter (J & W Scientific, CA, USA), that separated N_2O and C_3H_8. The recorded retention times for the N_2O and C_3H_8 gasses were 540 and 585 seconds, respectively. To protect the IRMS source from C_3H_8, the analysis time was reduced to 575 seconds while the column elute was directed to exit at 570 seconds.

5.2.5 Dissolved N_2O and N_2O flux calculation

Concentrations of dissolved gasses in the drain water were estimated according to equations 3.3 and 3.4. Equilibrium N_2O concentrations (nmol L^{-1}) in the drain water were determined by taking the atmospheric N_2O partial pressure (3.29×10^{-7}atm) and the appropriate solubility coefficient for N_2O (mol L^{-1} atm^{-1}) at the temperature of the sampled water (Weiss & Price, 1980). To compare the N_2O-N emissions, due to nitrification of NH_4^+, and to evaluate the N_2O: NH_4^+ and N_2O: NO_3^- ratios, the dissolved N_2O concentrations were converted to units of µg N_2O-N L^{-1}.

The N_2O-N flux was estimated using floating chambers at drain sites 1, 3 and 5 according to the equation 3.12.

5.2.6 Inorganic –N analysis

Inorganic-N, (NH_4^+-N and NO_3^--N) analyses were performed on an Alpkem FS - 3000 twin channel Flow Injection Analyser (FIA) (Alpkem, College station, TX, USA). Ammonium was analysed using a gas diffusion technique and NO_3^- -N was determined using cadmium reduction to nitrite (NO_2^-)

followed by colorimetric determination (SolÓRzano, 1969). Detection limits of the FIA were 0.5 µg mL^{-1} for NH_4^+-N and 0.1 µg mL^{-1} for NO_3^--N. Therefore, low NH_4^+-N concentrations were reanalysed using a manual indo-phenol blue method. This reaction is based on there being NH_4^+ or NO_3^- in alkaline solution and when 'phenate' is introduced, an indo-phenol blue colour is produced in the presence of an oxidising agent, such as hypochlorite. This method detects both NH_4^+ and NO_3^- forms of N with a detection limit of 0.2 µg mL^{-1}.

5.2.7 Plants, biofilms and sediments

Aquatic plant samples were cut from available sites and brought to the laboratory where they were gently washed with de-ionized water. Then samples were dried at 40°C for 72 h. The plant samples were then finely ground (< 200 µm) and 4 mg of sample was then placed in a tin capsule for total N and ^{15}N enrichment determination using an IRMS (EA-CF/IRMS; Sercon™, Crew, UK).

Biofilms were scraped from 'planted' ceramic tiles that had been present for > 100 days before the experiment. The tiles were rinsed and scraped using a sterile spatula with the biofilms suspended in DI water in 30 mL plastic vials (Figure 5-1). Then the samples were filtered through glass filter papers and oven dried at 35°C for 48 hours. Dried bio-film material was carefully removed using a sterile spatula and placed in tin capsules for total N and ^{15}N enrichment determination using an IRMS.

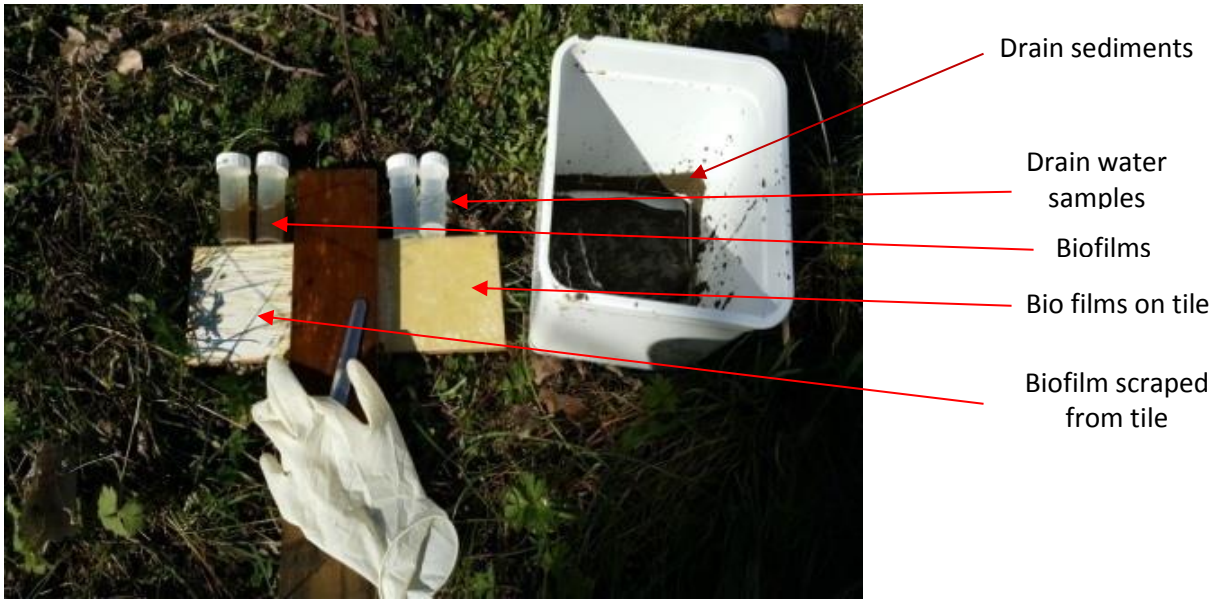

Figure 5-1 A photo of biofilm and soil sediment.

Sediment samples (0- 5 mm deep) were siphoned through plastic tube and transferred into plastic vials. The samples were then dried in an oven at 100°C for 24 hours. The dried sediment samples (50 mg) were placed in tin capsules and analysed for total N and ^{15}N enrichment using an IRMS.

5.2.8 Plants, biofilms, sediments and diffusions analysis in EA-CF IRMS

To determine ^{15}N enrichment of the solid samples in the tin capsules, they were placed into the auto-sampler of an elemental analyser (Sercon™ GSL, Crew, UK). Reference standards were also prepared in the same way and placed at a rate of one reference for every eight samples with further 'check' standards, to assess precision and accuracy. The samples were combusted in the presence of oxygen at 1000°C, converting the N to a mixture of N_2 and NO_x, which then passed through a packed copper reduction column at 600°C reducing any NO_x to N_2. Subsequently, the gas sample pulse flowed through CO_2 and moisture scrubbers and a GC column (0.5 m, Carbo-sieve G, 60-80 a mesh column). Finally, the gas passed into the IRMS (EA-CF/IRMS; Sercon™, Crew, UK) where masses 28, 29 and 30 were determined and subsequently used to calculate atom percent ^{15}N enrichment.

Figure 5-2 A photo of aquatic plant species; (a) *Ranunculus sp*. (b) Aquatic grass – *Carex sp.* (c) Duckweed – *Lemnoideae sp.*

5.2.9 Inorganic-N ^{15}N enrichment

The collected 1 L water samples were analysed for $^{15}N\text{-}NH_4^+$ and $^{15}N\text{-}NO_3^-$ using the diffusion methodology described by Brooks et al. (1989). This involved suspending 7 mm Whatman GF/D filter paper discs, on stainless steel wire, in the headspace of sealed jars. Prior to this an aliquot (10 µL) of 2.5 M $KHSO_4$ (potassium bisulphate) was pipetted on to the filter discs immediately. Analyses showed the majority of the water samples had NH_4^+-N concentrations < 1 µg mL^{-1}, thus to get a minimum of 50 µg N, a 150 mL water sample was placed in the jar, prior to it being sealed, along with 0.2 mg of furnace dried MgO (magnesium oxide) and a glass bead. The MgO raised the solution pH, causing the NH_4^+-N: NH_3-N equilibrium to shift in favour of NH_3-N whereupon volatilisation of NH_3 occurred, and the NH_3 was trapped on the acidified paper disc. The samples were left for six days. The filter papers were then removed and dried in desiccators for 24 hours. The filter papers were placed in tin capsules for $^{15}N\text{-}NH_4^+$ analysis. For $^{15}N\text{-}NO_3^-$ analysis, 50 mL of sample solution, with NH_4^+ already removed via diffusion was transferred to a clean 100 mL jar. Then, a new filter paper acidified with 10 µL of 2.5 M $KHSO_4$ was placed in the jar headspace before 0.4 Devarda's alloy and MgO were added. Devarda's alloy reduced the NO_3^--N to NH_4^+-N which then volatilised as before. Care was taken to prevent the alkaline solution from contacting the acidified filter paper and neutralising the acid. The jars were again left for another six days at 20°C. Then, filter papers were removed, dried and transferred into tin capsules for IRMS analysis as before.

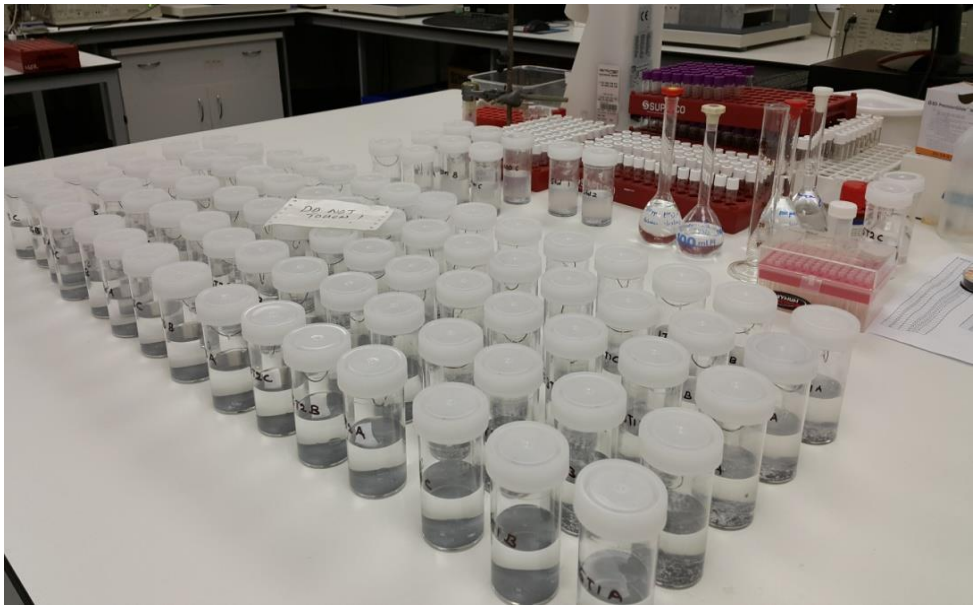

Figure 5-3 Samples undergoing ^{15}N diffusion to determine inorganic-N ^{15}N enrichment.

5.2.10 ^{15}N enrichment and recovery calculations

The absolute abundance of ^{15}N measurements are commonly reported in terms of atom percent. The atom % is determined as;

$$\text{Atom \% of } ^{15}N = [^{15}N / (^{15}N + ^{14}N)] * 100 \quad (5.1)$$

Compare to atmospheric ^{15}N abundance, the absolute ratio of ^{15}N enrichment in plant, soil sediment and gas samples was quite small and appeared on the third or fourth decimal place. Therefore, those samples' ^{15}N enrichment were transformed to parts per thousand and the values are reported as delta ^{15}N ($\delta^{15}N$). The $\delta^{15}N$ transformation was performed as;

$$\delta 15N = [(^{15}N / ^{14}N \text{ sample}) / (^{15}N / ^{14}N \text{ air}) - 1] * 1000 \quad (5.2)$$

where, $^{15}N/^{14}N$ air is 0.0036765.

The percentage ^{15}N recovery was calculated using the following equation (Cabrera & Kissel, 1988).

$$^{15}N \text{ recovered (\%)} = 100 \times \frac{p \times (c-b)}{f \times (a-b)} \quad (5.3)$$

where, p = the moles of N in the sample; f = the moles of N in the applied ^{15}N enriched $(NH_4)_2SO_4$; c = atom % of the recovered pool; a = atom % of the applied ^{15}N $(NH_4)_2SO_4$; and b = atom % ^{15}N abundance of control.

5.2.11 Statistical analysis

Statistical analyses were performed using Minitab® version 16 (Minitab Inc, PA, USA), Sigma Plot 12.3 and Microsoft Excel, 2010. Means, standard deviations and standard errors were calculated for different measurements where appropriate. Analysis of variance was employed to test if means of variables differed between sampling sites. When differences occurred, two-way Student tests were performed to determine the significance of differences between means and the levels of significance.

Both NH_4^+-N and NO_3^--N time series concentrations were fitted to a first order exponential function as follows (Lavagnini & Magno, 2007):

$$C_{(t)} = C_{(0)} e^{-kt} \quad (5.4)$$

where, *C* is the concentration of NH_4^+-N and NO_3^--N (mg L^{-1}) at time t (minutes), C_0 is the initial concentration at site 1, and *k* is the degradation constant (per minute). Values of the half-life ($t^{1/2}$) were calculated as;

$$t^{1/2} = Ln(0.5)/-k \quad 5.5$$

where, $t^{1/2}$ is the half-life (minutes), and *k* is the degradation constant (per minute).

5.3 Results

Complete mixing of tracer in the drain occurred 45 minutes after the tracer solution injection commenced (section 3.3.4). Therefore, the data used to assess drain water hydro-physical, biological and chemical transformations are taken from sampling times 3 (45 minutes), 4 (60 minutes) and 5 (75 minutes) only.

5.3.1 Dissolved oxygen (DO) and water temperature

Before the tracer solution injection, the average drain water dissolved oxygen (DO) concentration was relatively high 12.0 ± 0.1 (± stdev) mg L^{-1} which equated to 109.9 ± 0.7% saturation. However, following tracer solution addition, DO declined with increasing distance ($p < 0.05$). The DO averaged 12.4 ± 0.1 mg L^{-1} (108.9 ± 1.8%) at site 1 and gradually decreased to 10.1 ± 0.2 mg L^{-1} (94.97 ± 1.3%) at site 5 (Figure 4.4). In contrast, the average water temperature increased with distance ($p < 0.05$) averaging 11.0 ± 0.1°C at site 1 and increasing to 12.4 ± 0.1°C at site 5 (Figure 5-4).

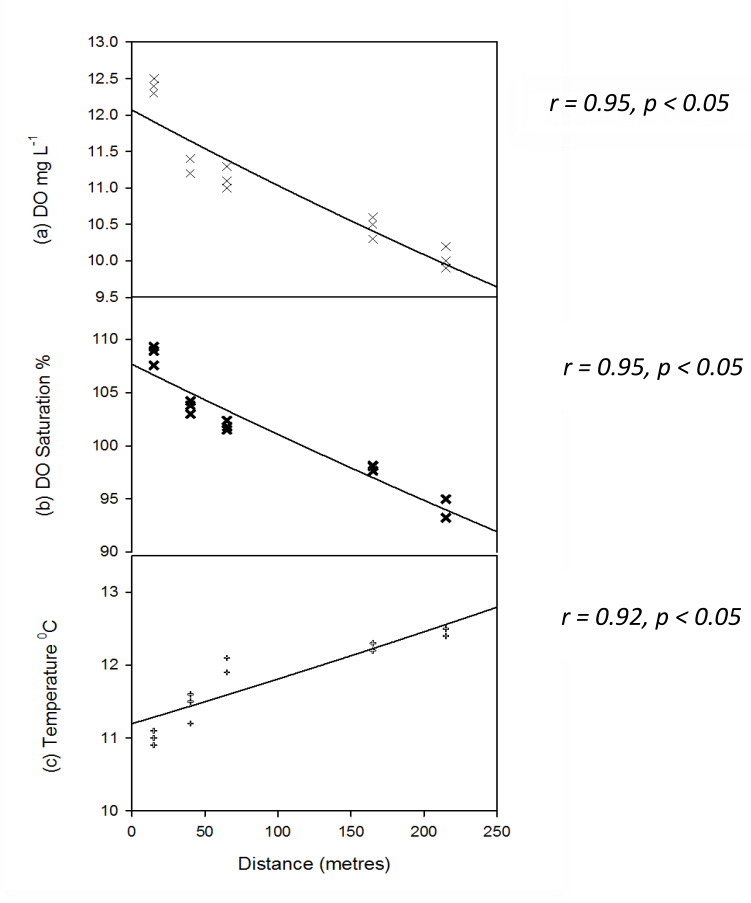

Figure 5-4 Change in (a) dissolved oxygen (DO) concentrations, (b) DO saturation and (c) water temperature over distance. Each data point denotes a single measurement at 10 cm depth (n = 15).

5.3.2 Drain water pH and electrical conductivity

There was a trend for pH to increase with distance following tracer injection, but this was not statistically significant ($p > 0.05$). The drain water pH averaged 6.99 ± 0.08 at site 1 and 7.07 ± 0.04 (± stdev) at site 5 when averaged across sample times 3 to 5 (Figure 5-5).

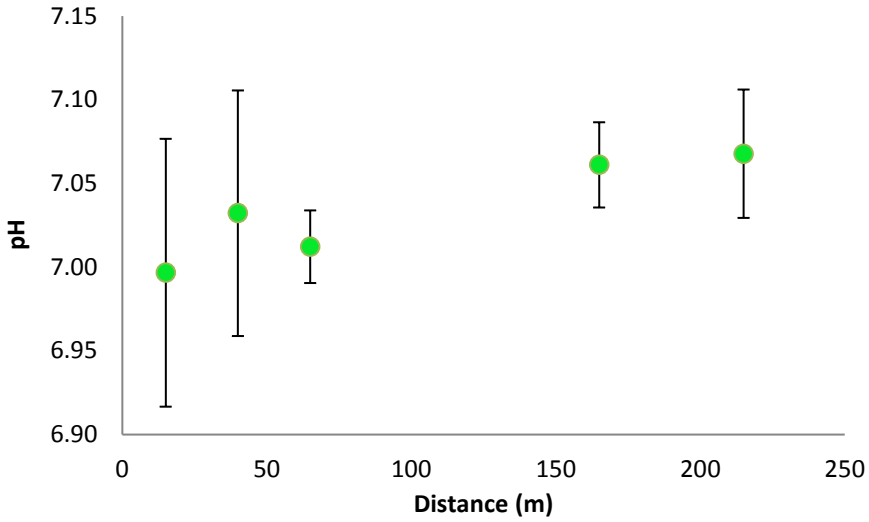

Figure 5-5 Change in water pH over distance. Data points are means, n= 9 (3 samples X 3 times) and error bars are ± Stdev.

There was a trend for electrical conductivity (EC) to decrease with distance after tracer solution injection, although this was not statistically significant ($p > 0.05$). The drain water EC averaged 321 ± 5 at site1 and 296 ± 21 (± stdev) at site 5, when averaged across sample times 3 to 5 (Figure 5-6).

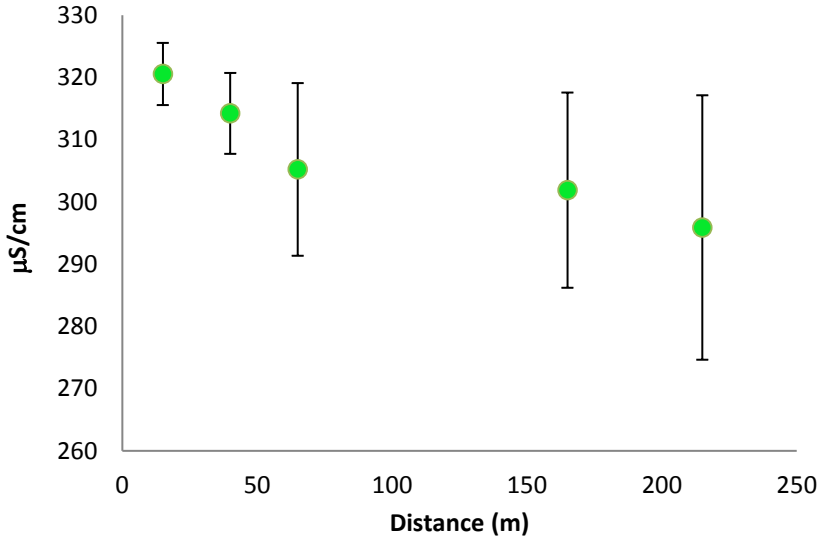

Figure 5-6 Drain water EC over distance. Data points are means, n=9 (3 samples X 3 sampling times) and error bars are ± Stdev.

5.3.3 Distribution of NH_4^+-N

Before the tracer solution was added, there was no detectable NH_4^+-N in the drain. Following tracer solution injection, the average drain water NH_4^+-N concentration immediately increased to an average of (± stdev) 1.36 ± 0.08 mg L^{-1} and then declined over distance and time to 0.54 ± 0.01 mg L^{-1} ($p < 0.01$).

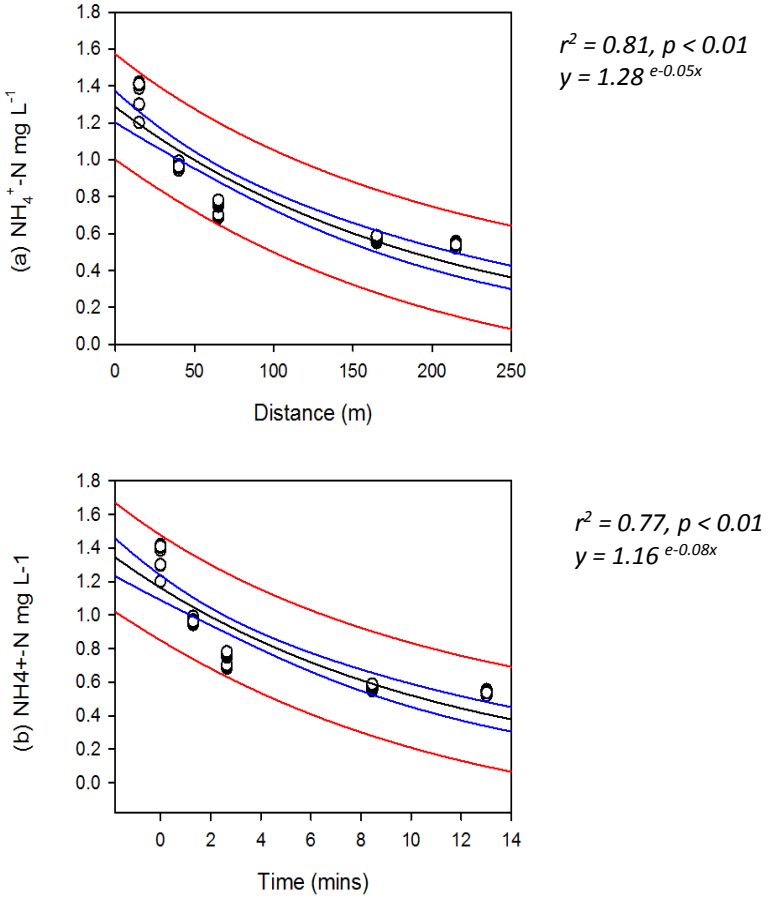

Figure 5-7 Drain water NH_4^+-N concentration versus distance (a) and time (b). The best-fit exponential regression lines are black, the 95% confidence intervals are between blue lines and predicted intervals are between red lines. Each data point denotes a single sample measurement (n = 45).

The mean NH_4^+-N concentrations were highest at site 1 (1.34 ± 0.07 mg L^{-1}; ± stdev) and lowest at site 5 (0.54 ± 0.01 mg L^{-1}). Ammonium -N concentrations decayed exponentially with both distance and time with regression analysis explaining 81 and 77% of the variations in NH_4^+-N concentration, respectively (Figure 5-7).

5.3.4 Half-life of NH_4^+-N

A fitted first order exponential decay function was fitted using Minitab, version 17 to determine the half-life of NH_4^+-N. Using equation 4.6 (section 4.2.11) and the degradation constant of the best-fit line (Figure 5-8), the half-life of NH_4^+-N was estimated to be 8.62 ± 0.26 (± stdev) minutes, equating to a distance of 141.9 ± 36.8 m based on the drain water velocity of 126.7 ± 3.6 L s^{-1} (Section 3.3.4).

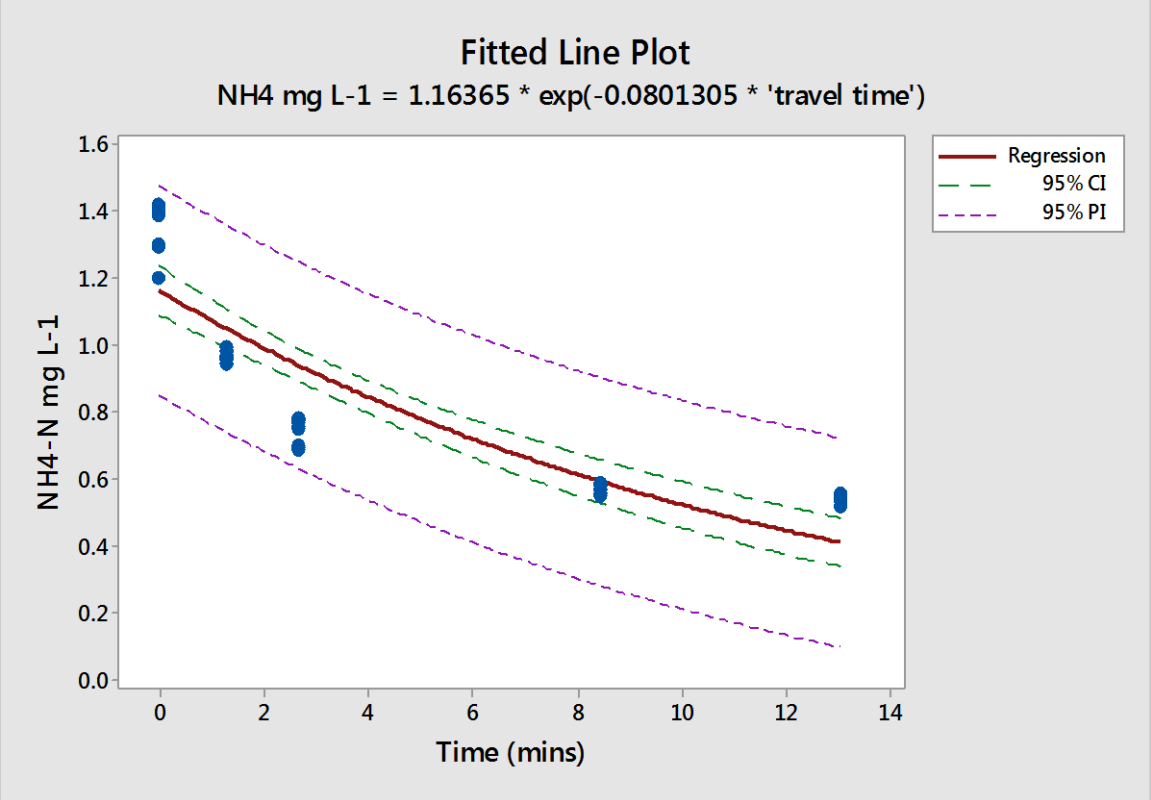

Figure 5-8 **Drain water NH_4^+-N concentration versus time. The brown line is the best-fit exponential curve (r^2 = 1.0). The brown line is the best-fit line (r^2 = 1), the area between the green lines represents the 95% confidence interval and the area between purple lines represents the prediction interval.**

5.3.5 $^{15}N\text{-}NH_4^+$ atom percentage

Linear regression analysis was performed on the $^{15}N\text{-}NH_4^+$ enrichment over distance and time (Figure 5-9). The variation in the ^{15}N enrichment of NH_4^+ was not significant ($p > 0.05$), and poorly explained by regression against distance or time, r^2 values of 0.04 and 0.03, respectively.

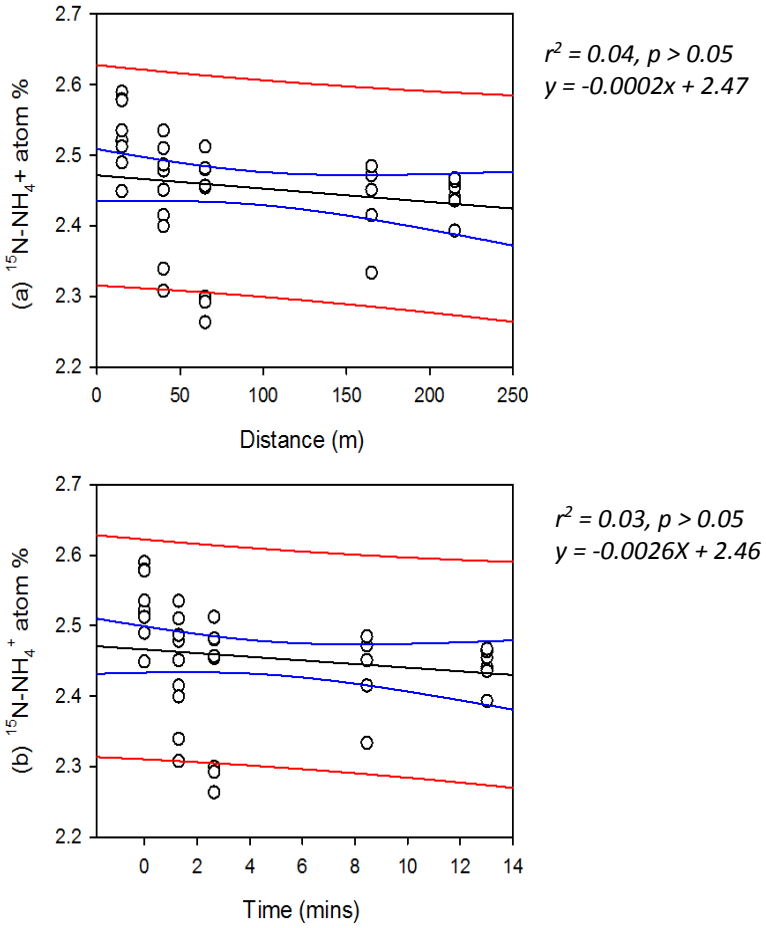

Figure 5-9 Drain water $^{15}N\text{-}NH_4^+$ atom % versus distance (a) and time (b). The black line is the best-fit regression curve, 95% confidence intervals are between blue lines and predicted intervals are between red lines. Each data point denotes a single sample measurement (n = 42).

5.3.6 NH_4^+-N concentration versus ^{15}N-NH_4^+ atom %

Linear regression analysis of NH_4^+-N concentration versus ^{15}N-NH_4^+ atom % (Figure 5-10) was poor with an r^2 values of 0.19.

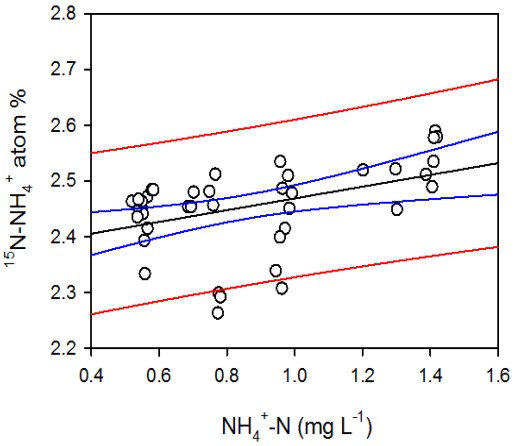

r^2 = 0.19, p < 0.01 (= 0.004)
y = 0.1055x + 2.39

Figure 5-10 Drain water NH_4^+-N concentration versus ^{15}N- NH_4^+ atom %. The black line is the best-fit regression curve, 95% confidence intervals are between blue lines and predicted intervals are between red lines. Each data point denotes a single sample measurement (n = 42).

5.3.7 $^{15}N\text{-}NH_4^+$ recovery

Recovery of ^{15}N injected as $^{15}N\text{-}NH_4^+$ declined exponentially over both distance and time. The $^{15}N\text{-}NH_4^+$ recovery averaged 86.3 ± 2.9% (± stdev) at site 1 and declined to 37.8 ± 4.1% at site 5. The variation in ^{15}N recovery as $^{15}N\text{-}NH_4^+$ was significant ($p < 0.01$), and well explained by changes in distance or time with r^2 values of 0.79 and 0.74, respectively (Figure 5-11).

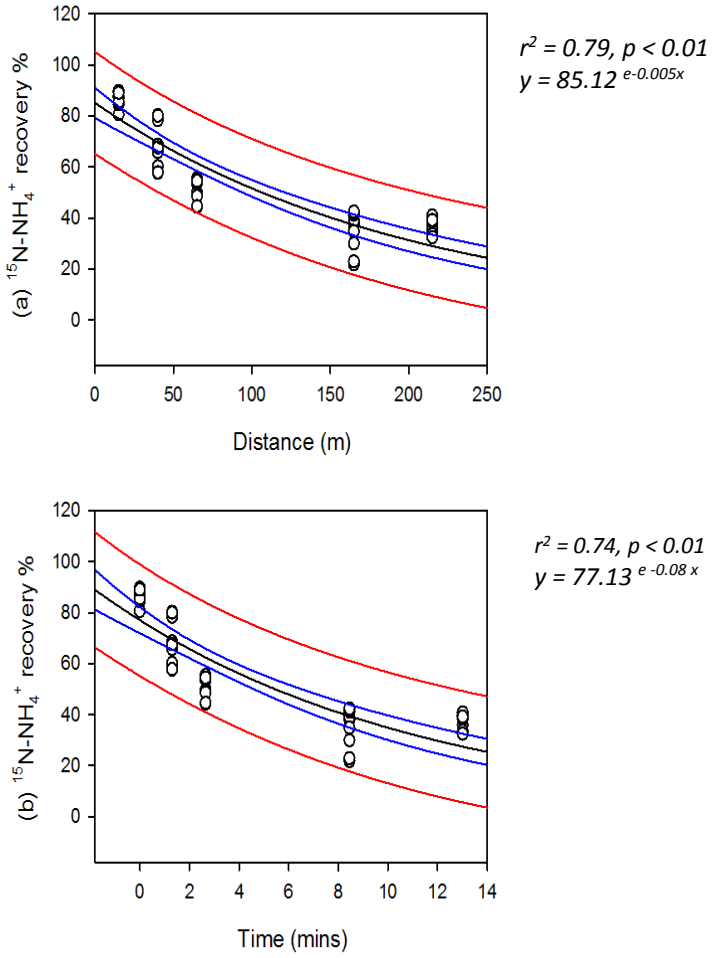

Figure 5-11 Drain water $^{15}N\text{-}NH_4^+$ recovery versus distance (a) and time (b). The black line is the best-fit regression curve, 95% confidence intervals are between blue lines and predicted intervals are between red lines. Each data point denotes a single sample measurement (n = 42).

5.3.8 Distribution of NO_3^--N

Before the tracer solution injection, the average drain water NO_3^--N concentration was 2.78 ± 0.12 mg L^{-1} at all sampling sites. After the tracer solution injection, NO_3^--N concentrations increased to 2.96 ± 0.01 mg L^{-1} (± stdev) at site 5.

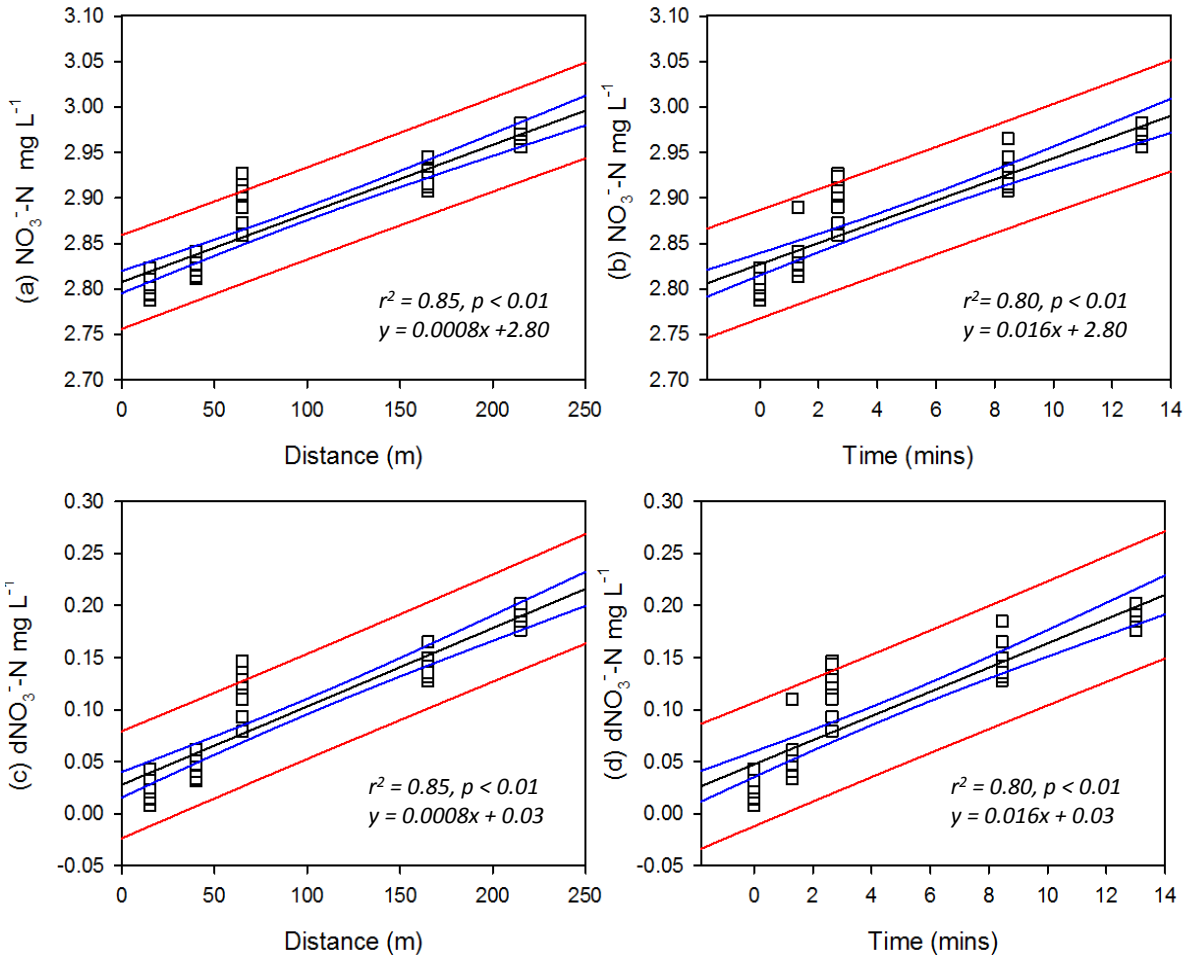

Figure 5-12 Drain water NO_3^--N concentration versus distance (a) and time (b) and the net change of NO_3^--N concentrations (dNO_3^--N) versus distance (c) and time (d). Black lines are the best-fit regression lines, the area between blue lines is 95% confidence interval and the area between red lines is predicted interval. Each data point denotes a single sample measurement (n = 45).

The increase in drain water NO_3^--N concentration was well explained by distance and time with r^2 values of 0.85 and 0.80, respectively. Changes in the difference between the pre-existing NO_3^--N concentration and the post equilibrium concentration (dNO_3^--N) were also well explained by distance and time with by r^2 values of 0.85 and 0.80, respectively (Figure 5-12).

5.3.9 NH_4^+-N concentration versus NO_3^--N concentration

The increase in dNO_3^--N was proportional to the dNH_4^+-N. A regression of 1/ dNH_4^+-N versus dNO_3^--N concentrations showed a strong linear relationship with an r^2 value of 0.90 (Figure 5-13).

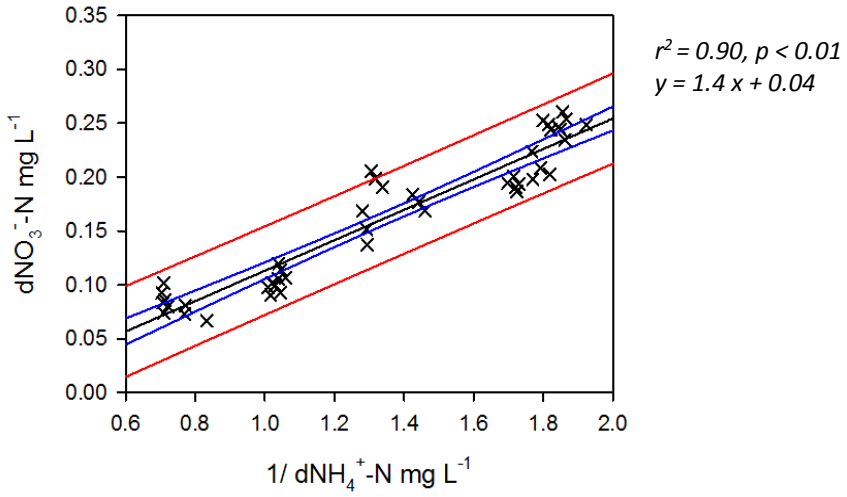

Figure 5-13 The $1/dNH_4^+$-N concentration versus the dNO_3^--N concentration (n = 45). The black line is the best-fit linear regression curve, the area between blue lines is 95% confidence intervals and the area between red lines is the predicted interval. Each data point denotes a single sample measurement (n = 42).

5.3.10 Doubling time of NO_3^--N

Minitab 17 was used to obtain the best-fit line for dNO_3^--N over time (Figure 5-14). A fitted first order exponential function was employed to measure the doubling time of dNO_3^--N. Using equation 4.6 (section 4.2.11) and the constant of the best-fit line (Figure 5.14) the doubling time of dNO_3^--N was estimated to be 12.63 ± 0.63 (± stdev) minutes equating to a distance of 192.8 ± 9.6 m based on drain water velocity.

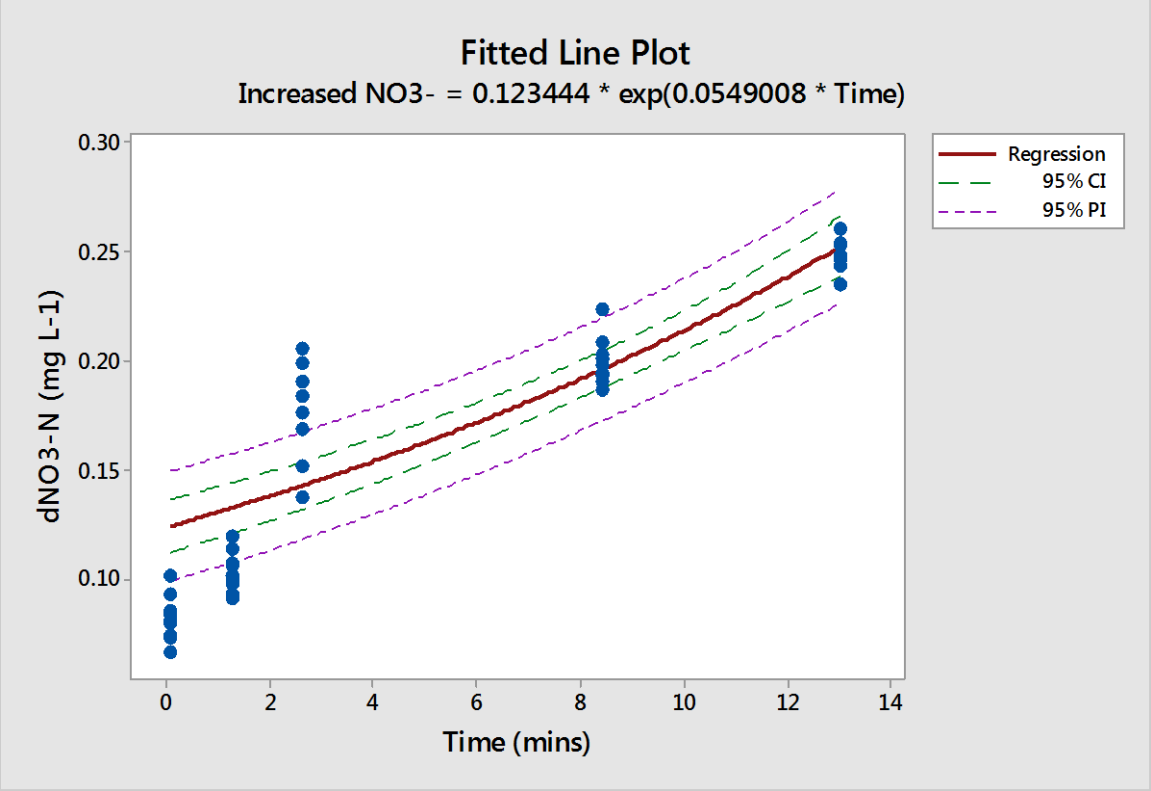

Figure 5-14 Drain water dNO_3^--N concentration versus time. The brown line is the best-fit exponential curve (r^2 = 1.0). The brown line is the best-fit line (r^2 = 1), the area between the green lines represents the 95% confidence interval and the area between purple lines represents the prediction interval.

5.3.11 $^{15}N\text{-}NO_3^-$ atom percentage.

Regression analysis of the ^{15}N enrichment of NO_3^- versus distance or time showed small increases in the ^{15}N enrichment of NO_3^- over distance or time (Figure 5-15) and the relative variation in ^{15}N enrichment of NO_3^- for distance or time were 13% and 15%, respectively.

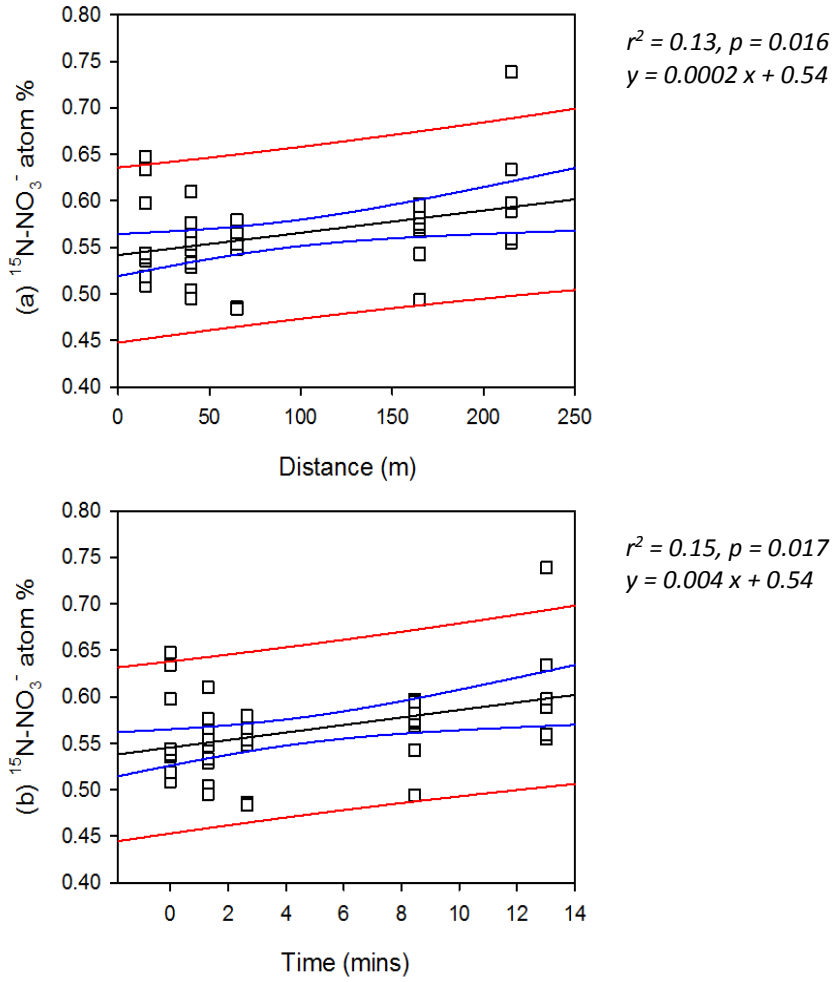

Figure 5-15 Drain water $^{15}N\text{-}NO_3^-$ atom % versus distance (a) and time (b). The black lines are the best-fit linear regression lines, the area between blue lines is 95% confidence interval and the area between red lines is the predicted interval. Each data point denotes a single sample measurement (n = 42).

5.3.12 NO_3^--N concentration versus ^{15}N-NO_3^--N atom %

Linear regression analysis of ^{15}N- NO_3^-atom % versus NO_3^--N concentration (Figure 5-16). The variation in the ^{15}N enrichment of NO_3^- was not significant ($r^2 = 0.07$).

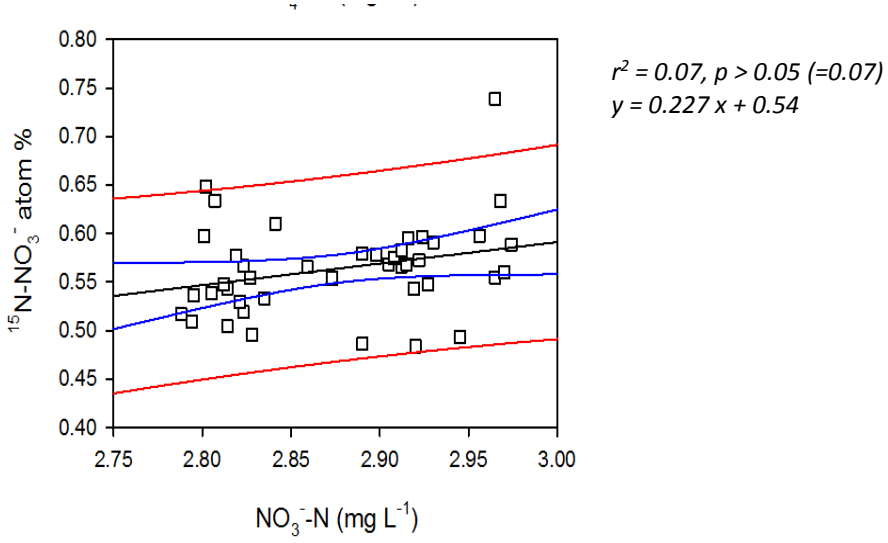

Figure 5-16 Drain water ^{15}N- NO_3^- atom % versus NO_3^--N concentration. The black lines are the best-fit linear regression lines, the area between blue lines is 95% confidence interval and the area between red lines is the predicted interval. Each data point denotes a single sample measurement (n = 42).

5.3.13 $^{15}N\text{-}NO_3^-$ recovery

In contrast to $^{15}N\text{-}NH_4^+$ recovery, the recovery of ^{15}N as NO_3^- increased with distance ($r^2 = 0.22$) and time ($r^2 = 0.25$). The average ^{15}N recovered as NO_3^- at site 1 was 13.9 ± 4.6% and this increased to 26.4 ± 10.4% (± stdev) at site 5.

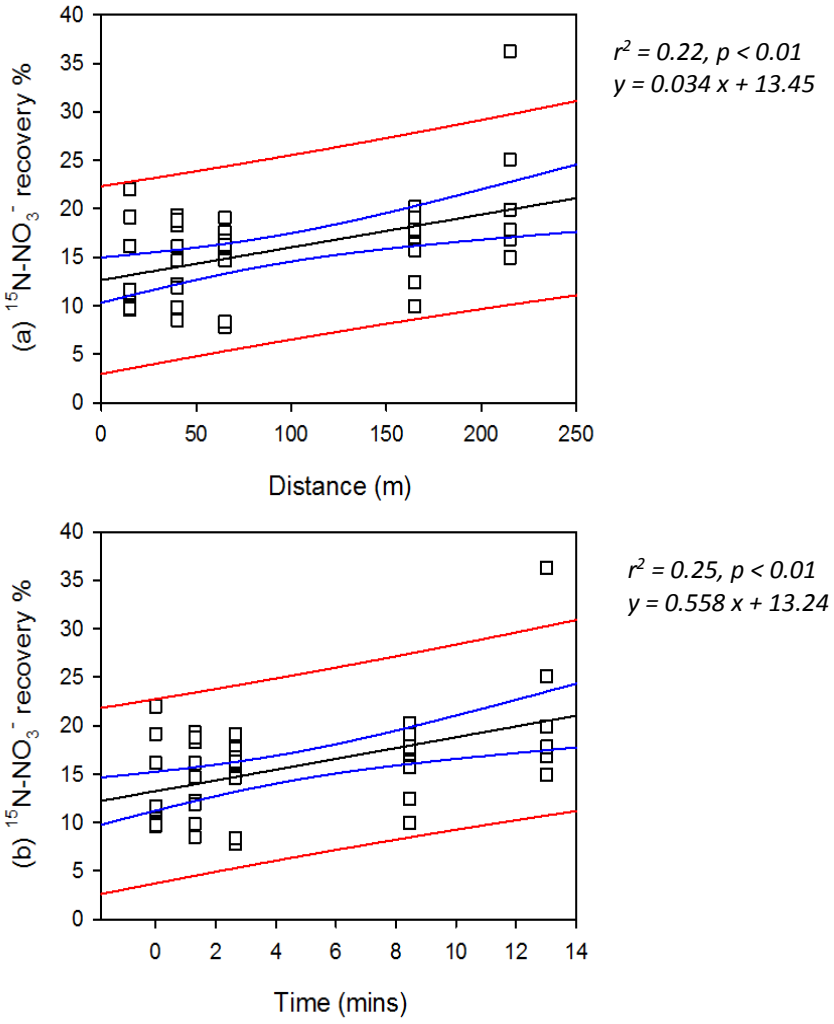

Figure 5-17 Drain water $^{15}N\text{- }NO_3^-$ recovery versus distance (a) and time (b). The black lines are the best-fit linear regression lines, the area between blue lines is 95% confidence interval and the area between red lines is the predicted interval. Each data point denotes a single sample measurement (n = 42).

5.3.14 Distribution of N_2O-N

Before the tracer solution injection, the drain water N_2O saturation ranged from 110 to 115% (0.35-0.37 µg N_2O-N L^{-1}; 12.4 -12.9 nmol L^{-1}) across all sampling sites. Following tracer solution addition, drain water N_2O saturation increased and averaged 129% (0.42 µg N_2O-N L^{-1}; 14.6 nmol L^{-1}) with the highest saturation equating to 156 % (0.51 µg N_2O-N L-1; 17.6 nmol L^{-1}).

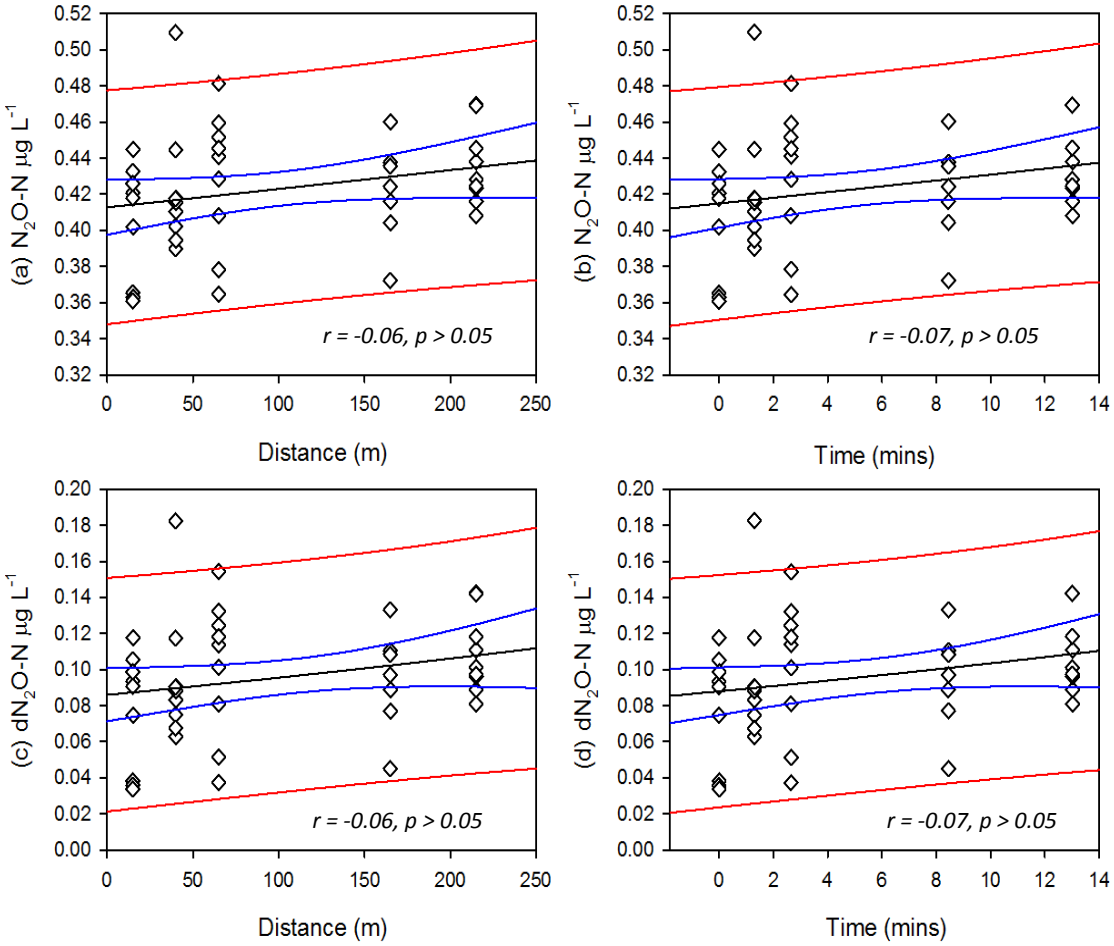

Figure 5-18 Drain water N_2O-N concentration versus distance (a) and time (b) and the net change of N_2O-N concentrations (dN_2O-N) versus distance (c) and time (d). The best-fit exponential regression lines are black, the area between blue lines is 95% confidence interval and the area between red lines is the predicted interval. Each data point denotes a single sample measurement (n = 39).

There was no statistically significant relationship ($p > 0.05$) between drain water N_2O-N concentrations and either distance or time with r^2 values of 0.06 and 0.07, respectively (Figure 5-18). When calculating the difference between pre-existing N_2O-N concentrations and the new equilibrium concentrations (dN_2O-N) across distance and time, no significant relationship was observed distance or time with r^2 values of 0.06 and 0.07, respectively.

5.3.15 Effect of DO, pH and temperature on N_2O production

Regression analyses were performed on drain water DO, pH and water temperature versus dissolved N_2O concentrations (Figure 5-19). The drain water N_2O concentrations showed a weak negative relationship with drain water DO ($r^2 = -0.3$, $p < 0.05$). There was no relationship between the dissolved N_2O concentration and water pH ($r^2 = 0.003$, $p > 0.05$). In contrast, drain water N_2O concentration showed a weak positive relationship with water temperature ($r^2 = 0.3$, $p < 0.05$).

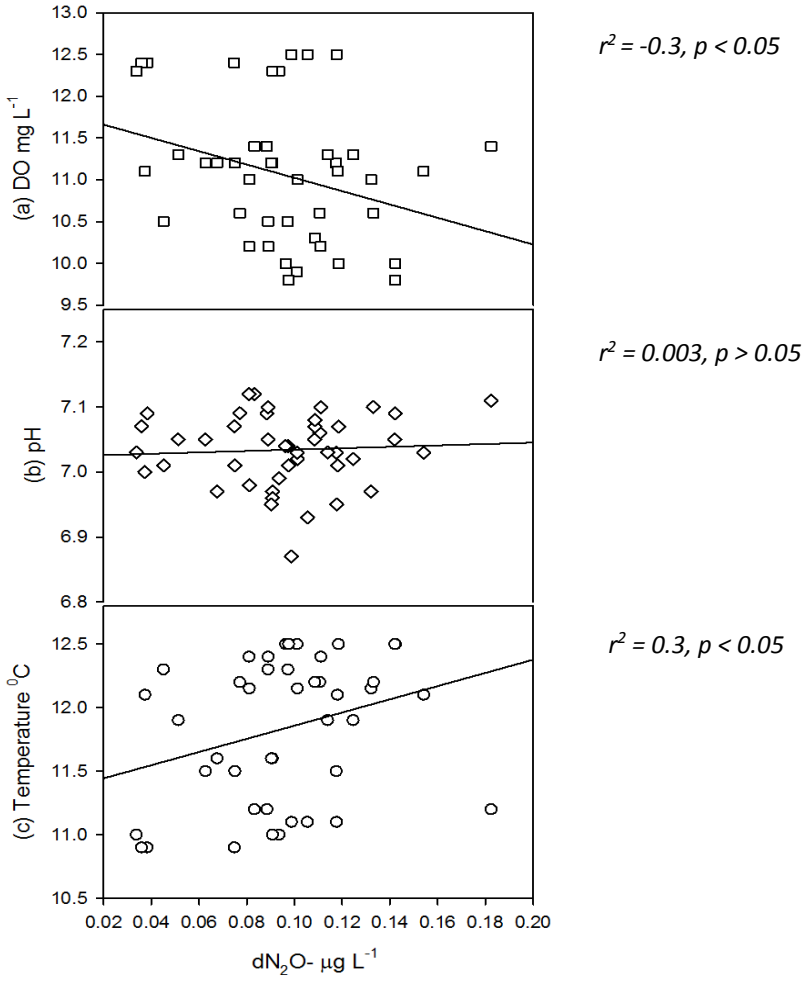

Figure 5-19 Change in N_2O-N concentrations versus (a) DO, (b) pH and (c) water temperature. The performed trend lines represent linear regressions (n = 45).

5.3.16 Inorganic-N (NH_4^+-N & NO_3^--N) versus N_2O production

Regression analysis was performed to assess the impact of dNH_4^+-N or dNO_3^--N on dN_2O-N (Figure, 5-20). The drain water dN_2O-N concentration had a weak, negative relationship to dNH_4^+-N concentration ($r^2 = 0.08$). In contrast, dN_2O-N concentration had a weak, but positive relationship with dNO_3^--N concentrations ($r^2 = 0.10$).

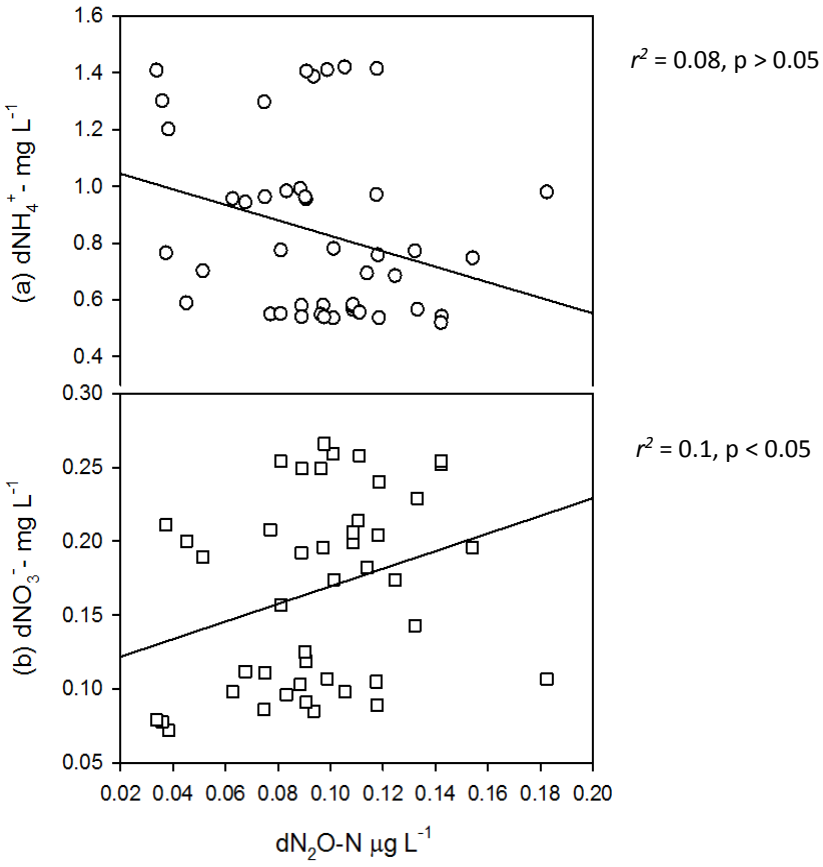

Figure 5-20 The drain water dN_2O-N changes versus (a) NH_4^+-N concentration and (b) dNO_3^--N concentrations. The trend lines are simple linear regressions (n = 45).

5.3.17 ^{15}N-N_2O atom %

The ^{15}N enrichment of the N_2O increased linearly over distance and time (Figure 5-21). The variation in N_2O atom percentage between sampling sites was significant ($p < 0.05$) and the variation in N_2O atom % was explained by distance or time, r^2 = 49% and 45%, respectively.

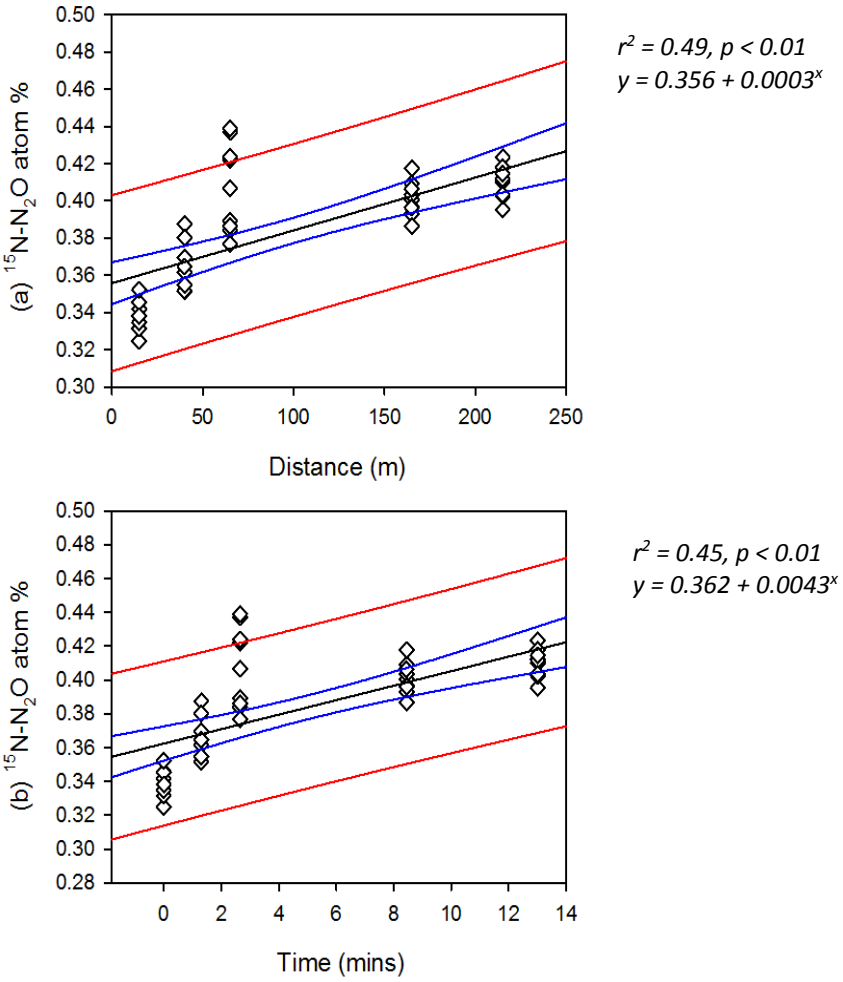

Figure 5-21 Drain water ^{15}N- N_2O atom % versus distance (a) and time (b). The black line are the best-fit regression lines, the area between blue lines are 95% confidence interval and the area between red lines are predicted interval. Each data point denotes a single sample measurement (n = 39).

5.3.18 NH_4^+-N & NO_3^--N atom % vs versus N_2O atom %

Regression analysis was performed to assess the relationships between ^{15}N enriched NH_4^+, NO_3^- and N_2O atom % (Figure 5-22). The drain water NH_4^+ atom % was not strongly related to NO_3^- atom % (r^2 = 0.34%; $p > 0.05$). However, N_2O atom % was lower when NH_4^+ atom % was higher (r^2 =29; $p < 0.05$).

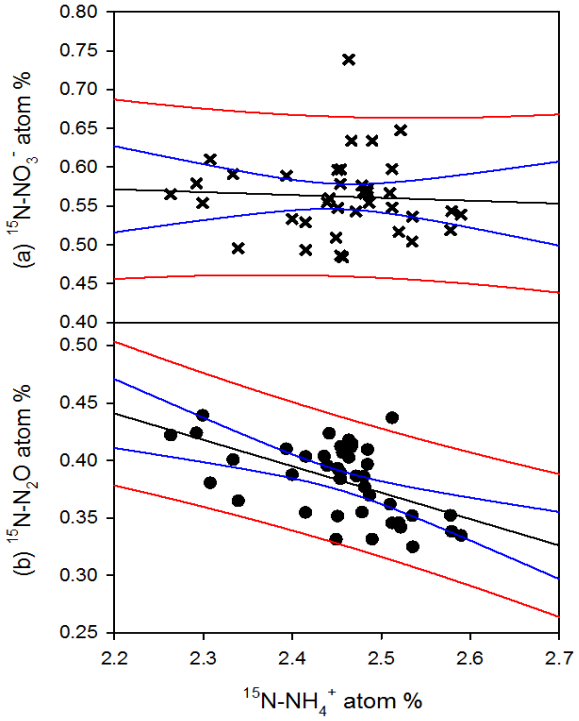

$r^2 = 0.0034$, $p > 0.05$
$y = -0.0368x + 0.653$

$r^2 = 0.2949$, $p < 0.05$
$y = -0.2295\ x + 0.946$

Figure 5-22 The drain water ^{15}N-NH_4^+ atom % versus ^{15}N-NO_3^- atom % (a) and ^{15}N-N_2O atom % (b).

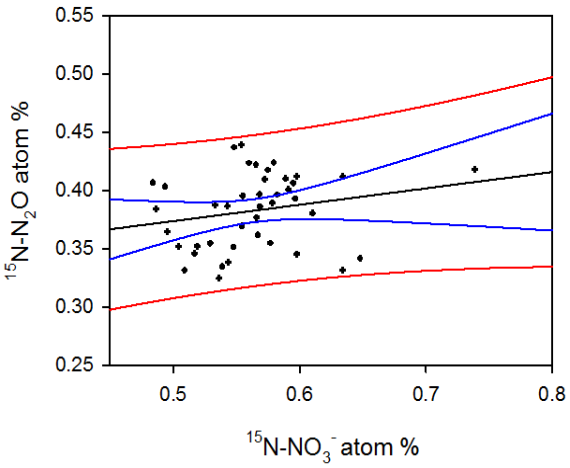

$r^2 = 0.0443$, $p > 0.05$
$y = 0.1403\ x + 0.303$

Figure 5-23 The drain water ^{15}N-NO_3^- atom % versus ^{15}N-N_2O atom %.

The NO_3^- atom % showed no relationship with N_2O atom % (r^2 = 4 %; $p > 0.05$).

5.3.19 ^{15}N-N_2O recovery

When compared to ^{15}N-NH_4^+ and ^{15}N-NO_3^- recoveries, ^{15}N-N_2O recovery was significantly lower, but increased over distance and time.

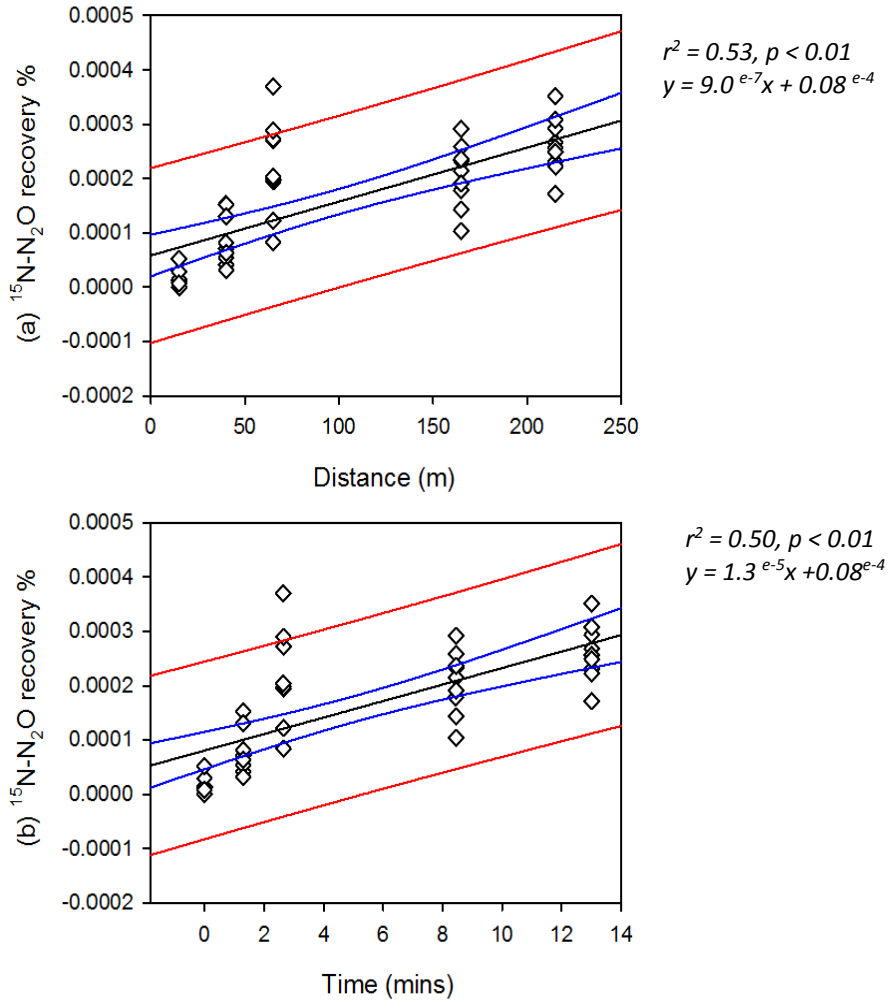

Figure 5-24 Drain water ^{15}N- N_2O recovery versus distance (a) and time (b). The best-fit regression lines are black, the 95% confidence intervals are between blue lines and the predicted intervals are between red lines. Each data point denotes a single sample measurement (n= 39).

5.3.20 Relationships of ^{15}N recoveries between $^{15}N\text{-}NH_4^+$ & $^{15}N\text{-}NO_3^-$ and $^{15}N\text{-}N_2O$

The drain water $^{15}N\text{-}NH_4^+$ recovery showed a weak and negative relationship with $^{15}N\text{-}NO_3^-$ recovery (r^2 = 8%). However, drain water $^{15}N\text{-}NH_4^+$ recovery showed a strong and negative correlation with $^{15}N\text{-}N_2O$ recovery (r^2 = 68%).

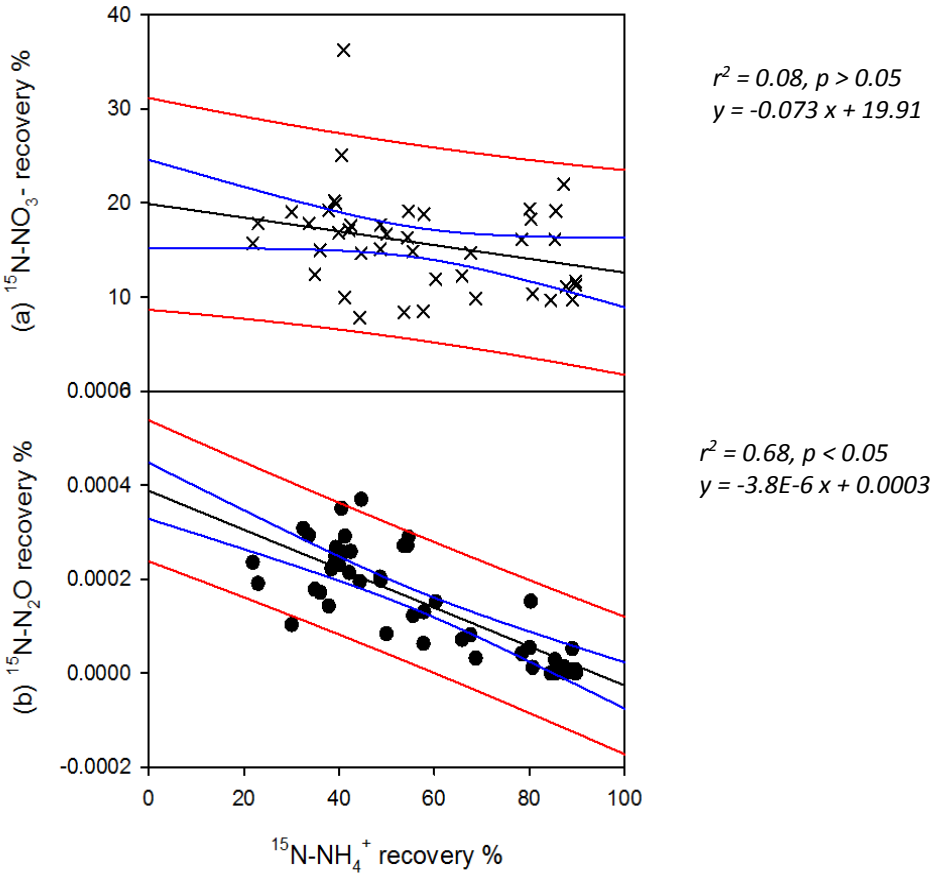

Figure 5-25 Interaction of the drain water $^{15}N\text{-}NH_4^+$ recovery % with $^{15}N\text{-}NO_3^-$ (a) and $^{15}N\text{-}N_2O$ recovery % (b); (n=39).

5.3.21 Surface N_2O and $^{15}N\text{-}N_2O$ flux measurements

The surface gas samples were collected to measure N_2O and $^{15}N\text{-}N_2O$ from floating chambers at site 1 (15 m), site 3 (65 m) and site 5 (215 m). The cumulative N_2O fluxes increased with distance reaching 15.37 ± 1.53 (± stdev) N_2O-N mg m^{-2} h^{-1} at site 1 to 43.99 ± 4.44 N_2O-N mg m^{-2} h^{-1} at site 5 (Figure 5-26).

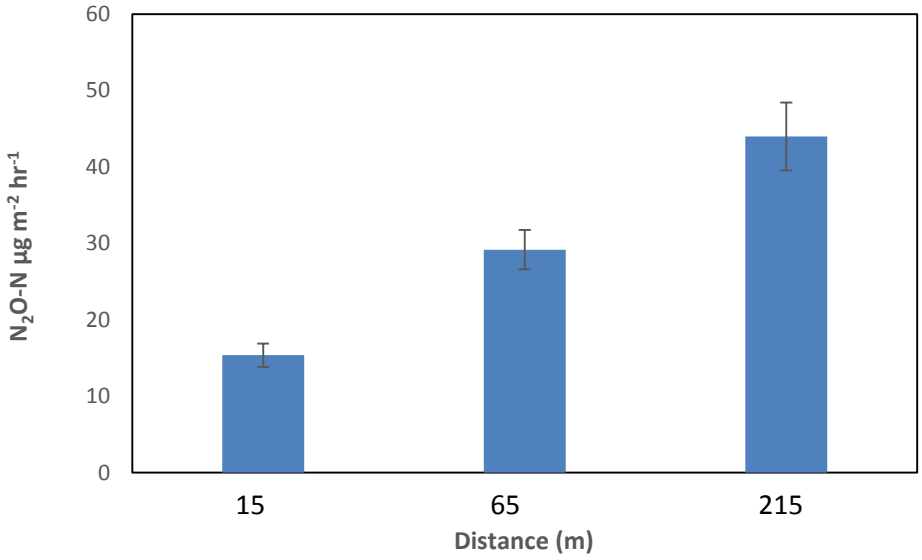

Figure 5-26 Hourly average N_2O flux at three sample sites (15 m, 65 m and 215 m; n = 3, error bars = ± stdev).

5.3.22 ^{15}N-N_2O atom% from floating chambers

Following the N_2O flux trend, the average ^{15}N-N_2O atom percentage also increased with tracer travel distance (Figure 5-27). The average ^{15}N-N_2O enrichment at site 1 was 0.41 ± 0.02 atom percentage. However, at site 3 and site 5, ^{15}N-N_2O enrichment increased to 0.67 ± 0.12 and 0.77 ± 0.23 (± stdev) respectively.

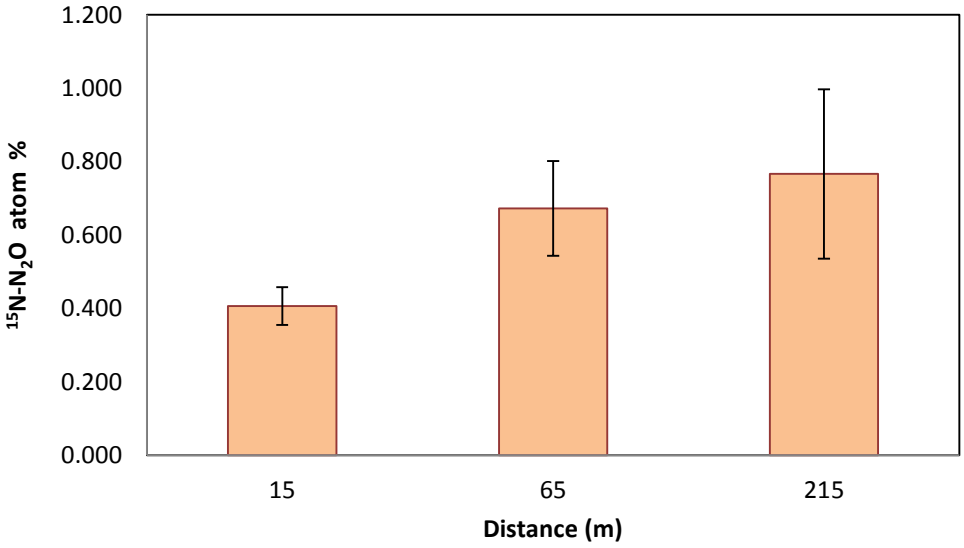

Figure 5-27 Average ^{15}N-N_2O atom percentage at three sample sites (15 m, 65 m and 215 m; n = 3, error bars = ± stdev).

5.3.23 ^{15}N-N_2O recovery from floating chambers

The average ^{15}N recovery as N_2O also increased with tracer travel distance (Figure 5-28). The average ^{15}N recovered as N_2O at site 1 was 2.6e-5 ± 2.0E-5 % and this increased to 2.6E-4 ± 2.9E-5% at site 5.

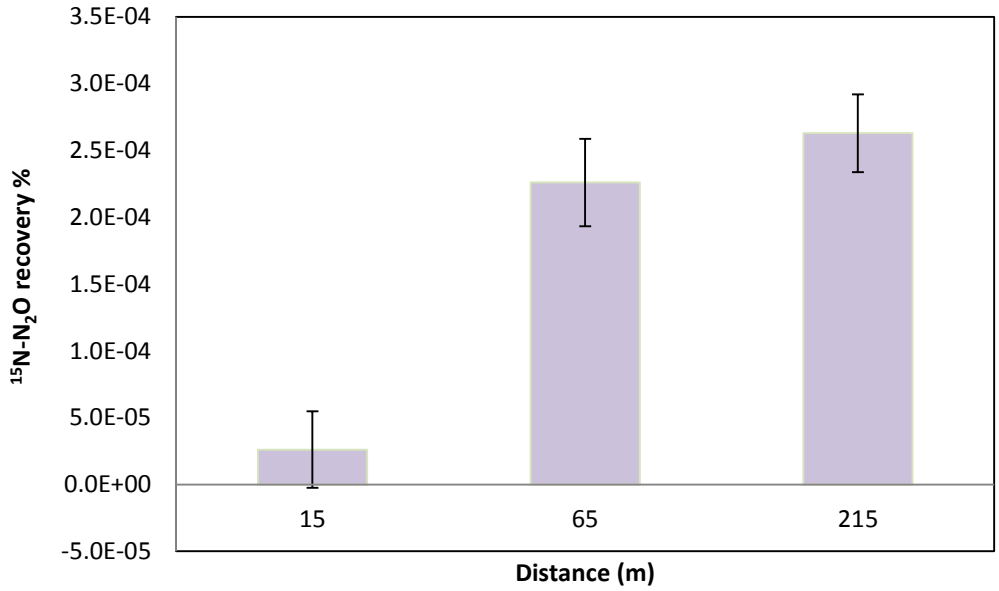

Figure 5-28 Average ^{15}N recovery as N_2O at three sample sites (15 m, 65 m and 215 m; n = 3, error bars = ± stdev).

5.3.24 Nitrogen uptake by river components

The ^{15}N enrichment of the drain water aquatic plants (*Ranunculus sp*., Aquatic grass – *Carex sp*. and Duckweed – *Lemnoideae sp*.), soil sediments and biofilms of the planted tiles were measured before the tracer solution addition, 24 hours after ^{15}N tracer addition and 10 days later. The pre tracer $\delta^{15}N$ of aquatic plants, soil sediments and biofilms were 6.53 ± 1.5, 4.31 ± 0.50 and 4.58 ± 0.81‰ N_2 air respectively. Twenty-four hours after ^{15}N tracer addition, the same components were enriched in ^{15}N with biofilms having the highest ^{15}N enrichment ($\delta^{15}N$ 96.81 ± 8.00‰). Ten days later, $\delta^{15}N$ had declined in all components to values comparable to those pre-trial, but the $\delta^{15}N$ of *Ranunculus sp.*, Aquatic grass and biofilms were still elevated 12.7 ± 0.05‰, 12.8 ± 1.2‰ and 7.95 ± 0.08‰ respectively (Figure 5-29).

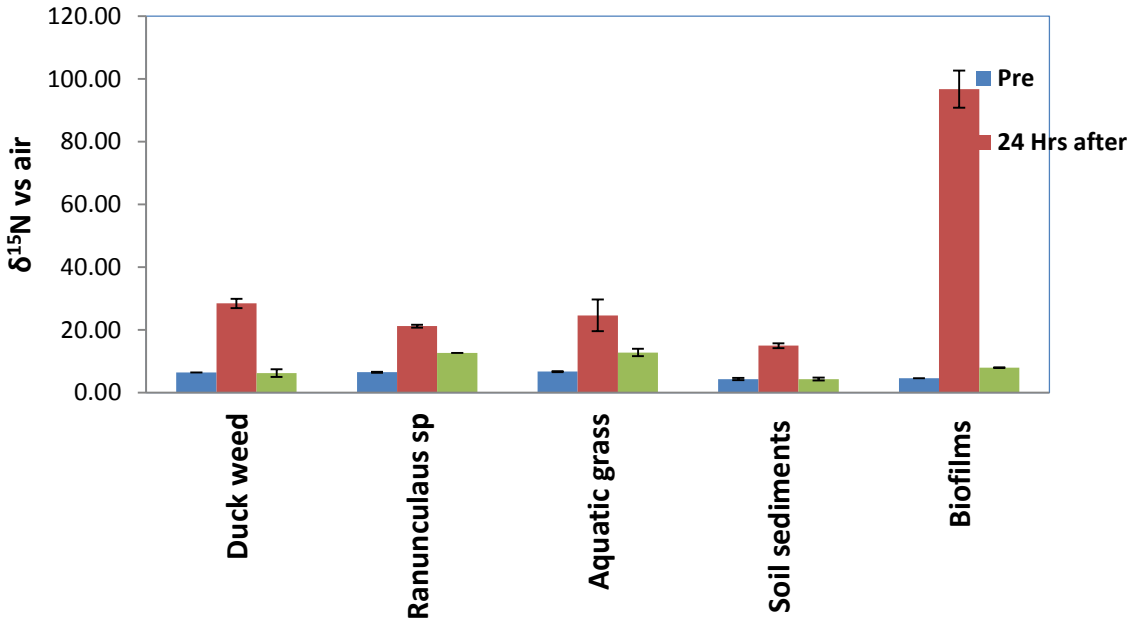

Figure 5-29 Temporal changes in $\delta^{15}N$ vs air (prior to tracer solution addition, 24 hrs after and 10 days later) in drain components (Biofilms n = 5, soil sediments n = 5, Duckweed n = 5, Aquatic grass n = 4 and *Ranunculus sp,* n = 2; Error bars = ± stdev).

The ^{15}N enrichment of the biotic drain water components were plotted over distance were plotted (Figure 5-30) but no spatial variances between sample sites occurred ($p > 0.05$).

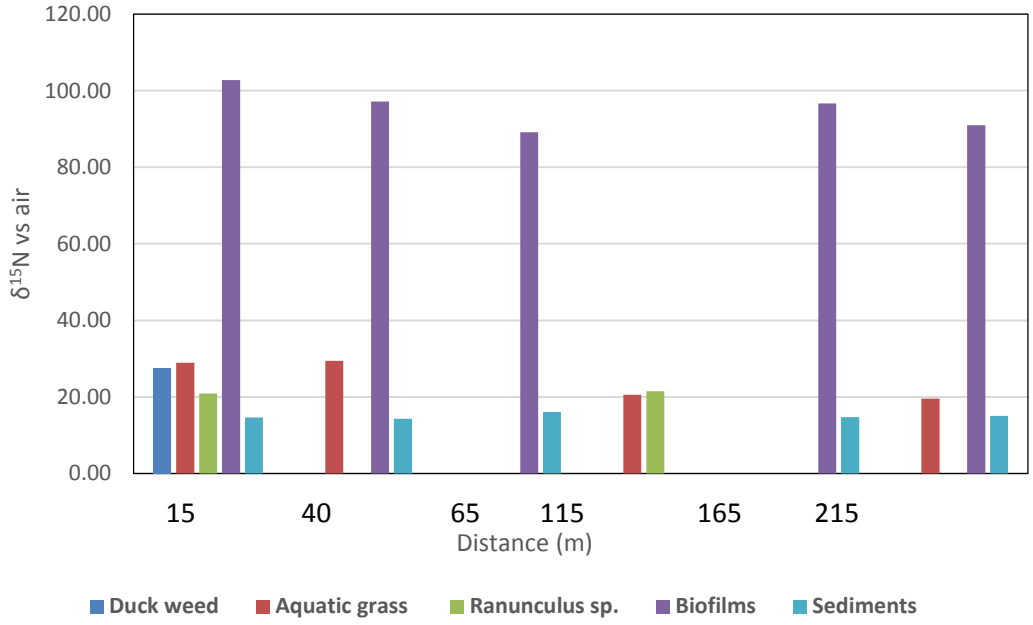

Figure 5-30 Spatial variances of $\delta^{15}N$ vs. air in drain components 24 hrs after tracer solution injection (n = 1).

Chapter 6

Drain water N dynamics and EF5-r measurements

The ^{15}N tracer addition study (Chapter 5) has provided new information on the fate of drain water NH_4^+-N and the effect of NH_4^+-N on drain N_2O-N and NO_3^--N. Variations in dissolved N_2O saturation between sampling sites may indeed be due to drain hydro physical variations and associated water chemistry. While chamber flux measurements (Figure 5-26) showed N_2O fluxes gradually increased with distance and time, it is difficult to prescribe the exact mechanism or mechanisms for the N_2O dynamics over time or distance. Even though, denitrification has been considered as a major river N_2O production process, the data also conclusively demonstrates nitrification occurring. Therefore, NH_4^+-N cannot be ruled out as a contributing source for dissolved N_2O.

6.1 NH_4^+-N versus NO_3^--N as a source of N_2O

Following the tracer solution addition, the drain water NH_4^+-N concentrations declined more rapidly than the rate of NO_3^--N production over distance and time (Figure 5-7). The drain NH_4^+-N concentration averaged 1.36 mg L^{-1} at sample site 1 and had reduced to 0.54 mg L^{-1} at site 5. The total NH_4^+-N loss which was estimated by concentration difference between sampling sites 1 and 5, was 0.82 mg L^{-1}. The drain water NO_3^--N concentration was 2.78 mg L^{-1} before the tracer addition, and increased to 3.03 mg L^{-1} after addition (Figure 5-12, a & b), and only increased by an averaged 0.25 mg L^{-1}. The half-life of NH_4^+-N concentration (8.62 minutes) was shorter than doubling life of NO_3^--N concentrations (12.63 minutes). Assuming the increase in NO_3^--N was all derived from the NH_4^+-N injected, it accounts for 30.5% of the NH_4^+-N lost, while 26.4% of the ^{15}N-NH_4^+ was recovered as NO_3^- (Figure 5-17).

Ammonium ^{15}N enrichment (atom %) did not change over distance or time (Figure 5-9) indicating NH_4^+-N inputs, other than the injected tracer, were not significant. Potentially, the increased N_2O flux could have been the result of demonstrated NH_4^+-N nitrification or the result of NO_3^--N denitrification. However, the N_2O-N atom %, ^{15}N enrichment increased over distance and time (Figure 5-21) indicating a ^{15}N source was the substrate for N_2O production.

There was no relationship between the NO_3^--N atom % ^{15}N enrichment and the ^{15}N enrichment of the N_2O evolved (Figure 5-23). However, there was a good relationship between NH_4^+-N atom % ^{15}N enrichment and the ^{15}N enrichment of the N_2O evolved (Figure 5-22, b) where NH_4^+-N atom %

declined as N_2O-N atom % increased. The ^{15}N enrichment of the N_2O-N was not equal to the ^{15}N-NH_4^+ enrichment indicating other natural abundance sources were also contributing to the drain N_2O-N flux. These could indicate antecedent N_2O, the less enriched NO_3^--N pool, or nitrification of NH_4^+-N being released as a result of mineralization.

Following ^{15}N tracer solution addition, biofilms, plants and soil sediments were highly enriched with ^{15}N tracer. The latter, this study was identified, as contributing to organic N turnover were, for example, biofilms and aquatic plants. The greater disappearance rate of NH_4^+-N in drain water thus also resulted from a high biological demand. However, not only added NH_4^+-N, but dissolved NO_3^- -N also present in the drain. Mulholland et al., 2004 stated that uptake of NH_4^+-N in river environments is favoured due to lower energy requirements for plant and biota assimilation. As a result, NH_4^+-N loss rates could be accounted for due to assimilation. Ten days after the tracer solution addition, ^{15}N enrichments of the drain biological components significantly reduced (Figure 5-29). Supporting of N mineralization was dominant in well oxygenated water, and benthic denitrification of NO_3^--N would not be expected to be a dominant source of N_2O. However, potentially water sediment denitrification could have been greater for drain *in-situ* N_2O flux.

6.2 N_2O-N flux estimations

In order to estimate the EF5-r, experiment #2 measured k_{N2O} values and the equilibrated dissolved N_2O concentrations in drain were substituted into equation 2.4 and the emitted N_2O-N fluxes were calculated. The estimated drain water N_2O-N saturation averaged 0.31 µg N_2O-N L^{-1}; 12.1 nmol L^{-1}. Following ^{15}N tracer addition, the drain water dissolved N_2O-N concentration averaged 0.42 µg N_2O-N L^{-1}; 14.6 nmol L^{-1}, where the net increase was 0.11 µg N_2O-N L^{-1}; 2.5 nmol L^{-1}. Therefore, the increase in the equilibrium N_2O-N concentration (dC N_2O-N) was 110 µg m^{-3}. Using this dissolved N_2O-N concentration and the k_{N2O} derived from four previously described methods (Sections 3.3.6 and 3.3.7), the N_2O-N flux was determined (Table 6.1).

Table 6.1 Nitrous oxide (N_2O-N) flux estimations from the measured k_{N2O} using different methods

Methods	k_{N2O} (m day^{-1})	dC N_2O-N (μg L^{-1})	dC N_2O-N (μg m^{-3})	Flux N_2O-N (μg m^{-2} day^{-1})
1. Headspace equilibrium	7.49	0.11	110	824
2. Floating chambers	6.98			769
3. Wilcock (1982) model; equation 2.10	8.65			952
4. Surface Flux (direct N_2O flux measurements)	6.06			667

From the data in Table 6.1, it can be seen that the N_2O-N flux ranged between 667 and 952 μg m^{-2} day^{-1}, depending on methods used.

6.3 EF5-r estimations

The current IPCC default emission factor EF5-r has a value of 0.0025 kg N_2O-N/ kg N leached. The IPCC methodology assumes nitrification rates exceed denitrification rates by two fold in rivers. Beaulieu et al., (2008) doubted N_2O emissions could exceed 12 mg N_2O-N m^{-2} day^{-1}. Clough and Kelliher (2012) measured N_2O-N fluxes from the Waikato River that were < 120 μg m^{-2} h^{-1} (< 2880 μg m^{-2} day^{-1}). According to the Waikato River 10 year median values for NO_3^- concentrations and flow rates, a calculated EF5-r value equated to 0.0005 kg (0.5 g) N_2O-N: kg N leached. Clough and Kelliher (2006, 2007 and 2011) estimated N_2O-N fluxes between 16 to 501 μg m^{-2} h^{-1} (384 to 12024 μg m^{-2} day^{-1}) that were based on the LII stream and low land spring fed streams and a braided river (Ashburton River) in the South Island, New Zealand. According to these studies and the study of Dong et al., (2004) is carried out in rivers of Wales and England, EF5-r for rivers has been estimated between 0.0003 and 0.0005 kg (0.3 and 0.5 g) N_2O-N/ kg N leached.

In order to measure the EF5-r in the current study, the following three methods were used.

1. The estimated N_2O-N fluxes in Table 6.1 are presented as a fraction of the drain NO_3^--N flux.

2. The measured N_2O-N flux using chambers at sampling sites 1, 3 and 5 are expressed as a fraction of the NO_3^--N flux.

3. The current IPCC, EF5-r default value (0.0025 kg N_2O-N: NO_3^--N kg) is used to measure the N_2O-N flux as a fraction of the NO_3^--N flux.

6.3.1 EF5-r measurements using the estimated N_2O-N fluxes and NO_3^--N flux

The measured flux (Table 6.1) using four different methods: the EF5-r is calculated as ratios of N_2O-N kg per NO_3^--N kg of N (Table 6.2).

Table 6.2 EF5-r estimations from the calculated N_2O-N flux using different k_{N2O}

Methods	Flux N_2O-N ($\mu g\ m^{-2}\ day^{-1}$)	N_2O-N from 314.4 ($m^2\ mg\ day^{-1}$)	NO_3^--N ($kg\ day^{-1}$)	EF5-r (N_2O-N kg: NO_3^--N kg)
1. Headspace equilibrium	824	259	31.6	8.21E-6 (8.2 mg/kg)
2. Floating chambers	769	242		7.66E-6 (7.66 mg/Kg)
3. Wilcock (1982) model	952	299		9.48E-6 (9.48 mg/Kg)
4. Surface N_2O flux	667	210		6.64E-6 (6.64 mg/Kg)

The calculated EF5-r (N_2O-N kg / NO_3^--N Kg) ranged between 6.64E-6 (6.64 mg kg^{-1}) to 9.48E-6 (9.48 mg kg^{-1}) which is significantly less than the IPCC predicted EF5-r value of 0.025 N_2O-N kg: NO_3^--N Kg. It is also smaller than the Dong et al., (2004) and Clough et al., (2012) EF5-r estimations of 0.0003 N_2O-N kg (0.3 g) and 0.0005 N_2O-N kg (0.5 g): NO_3^--N Kg, respectively. The Wilcock (1982) model produced higher EF5-r than all the other three methods due to a high k_{N2O} value. In contrast, the lowest EF5-r was estimated using the direct N_2O fluxes from floating chambers.

6.3.2 EF5-r measurements from N_2O-N flux and dissolved NO_3^--N

In experiment 2, the deployed chambers at sites 1, 3 and 5 directly measured the N_2O-N flux. The amount of NO_3^--N flowing through each site was estimated using the NO_3^--N concentration, drain water velocity and discharge rate (2.80 - 2.96 mg L^{-1} *126.7 L s^{-1} * 3600 s hr^{-1}). Following the IPCC method, the EF5-r is calculated using the ratios of emitted N_2O-N kg hr^{-1} to NO_3^--N kg hr^{-1} flux (Table 6.3)

Table 6.3 EF5-r estimations from the chamber N_2O-N flux measurements at sites 1, 3 and 5.

Site	N_2O-N ($\mu g\ m^{-2}\ hr^{-1}$)	Area (m^2)	N_2O-N ($\mu g\ hr^{-1}$)	NO_3^--N ($kg\ hr^{-1}$)	EF5-r (N_2O-N kg hr^{-1}/ NO_3^--N kg hr^{-1})
1	15.37	1.43	21.98	1.28	1.72E-11 (0.00002 mg/kg)
3	29.18	1.64	47.85	1.32	3.62E-11 (0.00004 mg/kg)
5	43.99	1.98	87.10	1.35	6.43E-11 (0.00006 mg/kg)

The chamber estimated EF5-r values (Table 6.3) were significantly lower than those derived using k_{N2O} (Table 6.2). The reason for lower EF5-r values could be, uneven water flow occurs in the drain due to bed friction which may have lowered the actual NO_3^--N flow beneath the chambers than estimated. Similarly, deploying many chambers at a single sample site may have broken the drain water flow, causing release of N_2O-N to air before accumulating within chamber headspace. As a result the measured surface N_2O flux may have been underestimated.

6.3.3 Comparison of total N_2O-N flux from EF5-r values

The drain water average NO_3^--N concentration was 2.883 mg L^{-1} and the drain discharge rate was 126.7 L s^{-1}. If the drain continuously discharges at the same rate with the same NO_3^--N concentration throughout a year, the annual total NO_3^--N mass would be 11519 kg (2.883 mg L^{-1} *126.7*3600 s hr^{-1} *24 hrs day^{-1} * 365 days yr^{-1}). Then, using the calculated EF5-r values and the IPCC EF5-r default value, the possible annual total N_2O-N emissions from Raineys Road drain were estimated. The possible annual N_2O-N emissions from four different k_{N2O} calculated EF5-r values (Table 6.2) ranged between 7.65E-2 and 9.46E-2 kg N_2O-N yr^{-1}: NO_3^--N kg yr^{-1}. However, EF5-r derived from chamber N_2O-N flux measurement (Table 6.3) was 4.5E-4 kg N_2O-N yr^{-1}: NO_3^--N kg yr^{-1}. Using the current IPCC EF5-r default value, the annual loss of N_2O-N was 28.8 kg N_2O-N yr^{-1}: NO_3^-- N kg yr^{-1} (0.0025 kg N_2O-N * 11519 kg NO_3^--N).

6.4 Summary and suggestions for future research

According to the above analysis, the IPCC suggested EF5-r default value significantly overestimates the N_2O emissions from rivers and drainages. The EF5-r estimates using measured k_{N2O} values were in general agreement. The k_{N2O} derived from the Wilcock (1982) model and the dissolved N_2O concentrations produced higher EF5-r values due to the measured higher value of k_{N2O}. In contrast, the chamber methodology underestimated the N_2O flux to NO_3^--N ratio and consequently produced lower EF5-r values and appears to be an inadequate for gas flux measurements on flowing water surfaces. However, it should be noted, the chamber data were collected from a single sample collection time at the end of experiment. Therefore, N_2O flux measurements should be repeated using chambers.

The method used and detailed involving N isotope additions, have to be repeated to validate the measurements of dissolved N_2O-N, N_2O fluxes and NO_3^--N concentrations in drains. After the ^{15}N tracer addition, the increased ^{15}N enrichment within biotic components reduced to background levels, demonstrated mineralization occurred. More ^{15}N studies are required using both NH_4^+-N and NO_3^- -N moieties separately, under the same experimental conditions to verify the relative effect of nitrification and denitrification on drain N_2O flux.

Appendix A

Abbreviations

A	Area
ANOVA	Analysis of variances
Br^-	Bromide ions
CO_2	Carbon dioxide
CH_4	Methane
C_3H_8	Propane
$CHCl_3$	Tri-Chloro methane
dC	Concentration difference
dt	Temperature difference
EF5	Emission factor for indirect nitrous oxide emissions
EF5-g	Nitrous oxide emission factor for ground water and surface drainage
EF5-r	Nitrous oxide emission factor for rivers and flowing waters
EF5-e	Nitrous oxide emission factor for estuaries
F	Gas flux
FRACLEACH	Fraction of nitrogen leached
GHG	Greenhouse gas
h	water depth
hr	hour
KBr	Potassium bromide
k'	Gas transfer coefficient
k	gas transfer velocity
K	Temperature in Kelvin
k_H	Henry's coefficient
$KHSO_4$	Potassium bisulphate
MgO	Magnesium oxide
N_2	Di nitrogen
N_2O	Nitrous oxide
NH_4^+	Ammonium ions
NO_3^-	Nitrate ions
NO_2^-	Nitrite ions
NH_3	Ammonia (gas)

^{15}N	^{15}N labelled nitrogen
$(NH4)_2SO_4$	Ammonium sulphate
NLEACH	Nitrogen leaching and runoff
NFERT	Nitrogen input as fertilizer
NEX	Amount of nitrogen leached as excreta
n	number of moles
O_2	Oxygen
P	Pressure
Q	Water discharge rate
R	Universal gas constant
RR	Tracer solution release rate
Sc	Schmidt number
T	Temperature
t	time
U	water velocity
V	Volume
$X_{(aq)}$	Dissolved gas concentration in a aqueous phase
$X_{(g)}$	Equilibrium gas concentration in gas phase
$\eta 2$	Sum of squares between groups divided by the total sum of squares

Appendix B

Equations

k'_{N2O}	=	$k'_{Tracer\ gas} * (Sc_{N2O} / Sc_{Tracer\ gas})^{-n}$	2.1
F_{N2O}	=	$h * k'_{N2O} (X_{aq} - X_g)$	2.2
k_{N2O}	=	$h * k'_{N2O}$	2.3
F_{N2O}	=	$k_{N2O} * (X_{aq} - X_g)$	2.4
k_{N2O}	=	$F_{N2O} / (X_{aq} - X_g)$	2.5
K_H	=	$P_{X(g)} / X_{(aq)}$	2.6
$X_{(aq)}$	=	$F_{(g)} / K_H$	2.7
$X_{(aq)}$	=	F / k	2.8
k_{water}	=	$(D*U/h)^{0.5}$	2.9
k	=	$k_{(20)} * [1.0241]^{T-20} * 3.74 * [U^{0.5}/h^{1.5}]$	2.10
$NLEACH$	=	$[NFERT+NEX]*FRACLEACH$	2.11
$N_2O\ (L)$	=	$NLEACH* EF5$	2.12
Q	=	Solution $[Br^-]$ X RR / Site $[Br^-]$	3.1
D	=	$Q / U*W$	3.2
M	=	$Cg\ X\ [V_g + (V_l\ x\ \theta)$	3.3
n	=	PV / RT	3.4
dC / dt	=	$k' (C_t - C_0)$	3.5
C_t	=	$C_0 - k' (t_1 - t_0)$	3.6
$ln\ C_t / C_0$	=	$-k' (t_1 - t_0)$	3.7

$Sc_{(C3H8)}$	=	$1911.1 - 118.11*T + 3.4527*T2 - 0.04132*T3$	3.8
$Sc_{(N2O)}$	=	$2055.6 - 137.11*T + 4.3173*T2 - 0.05435*T3$	3.9
k'_{N2O}	=	$(Sc_{N2O} / Sc_{C3H8})^{-n} * k'_{C3H8}$	3.10
$k'_{2(N2O)}$	=	$k'_{N2O} (600 / Sc_{N2O(T)})^{-n}$	3.11
F	=	$(dC/dt) *(V/A) * (P/RT)$	3.12
k_{C3H8}	=	$F_{C3H8} / (X_{aq} - X_g)$	3.13
k_{N2O}	=	$(Sc_{N2O} / Sc_{C3H8})^{-n} * k_{C3H8})$	3.14
$k_{(N2O)}$	=	$k_{N2O} (600 / Sc_{N2O(T)})^{-n}$	3.15
k_{N2O}	=	$(Sc_{N2O} / Sc_{O2})^{-n} * k_{O2}$	3.16
Atom % of ^{15}N	=	$[^{15}N / (^{15}N + ^{14}N)] * 100$	5.1
$\delta^{15}N$	=	$[(^{15}N / ^{14}N \text{ sample}) / (^{15}N / ^{14}N \text{ air}) - 1] *1000$	5.2
^{15}N recovered (%)	$=100 \times \frac{p \times (c-b)}{f \times (a-b)}$		5.3
$C_{(t)}$	=	$C_{(0)} e^{-kt}$	5.4
$t^{1/2}$	=	$Ln(0.5) / -k$	5.5

References

Alin, S. R., Rasera, M. d. F. F. L., Salimon, C. I., Richey, J. E., Holtgrieve, G. W., Krusche, A. V., & Snidvongs, A. (2011). Physical controls on carbon dioxide transfer velocity and flux in low-gradient river systems and implications for regional carbon budgets. *Journal of Geophysical Research, 116*, 148-227. doi:10.1029/2010JG001398

An, S., & Joye, S. B. (2001). Enhancement of coupled nitrification-denitrification by benthic photosynthesis in shallow estuarine sediments. *Limnology and Oceanography, 46*, 62-74.

Baulch, H. M., Schiff, S. L., Maranger, R., & Dillon, P. J. (2011). Nitrogen enrichment and the emission of nitrous oxide from streams. *Global Biogeochemical Cycles, 25*(4), 1-15.

Beaulieu, J. J., Arango, C. P., Hamilton, S. K., & Tank, J. L. (2008). The production and emission of nitrous oxide from headwater streams in the Midwestern United States. *Global Change Biology, 14*, 878-894. doi:10.1111/j.1365-2486.2007.01485.x

Beaulieu, J. J., et al. (2010). Nitrous oxide emission from denitrification in stream and river networks *Proc. Natl. Acad. Sci. U. S. A., 108*, 214-219. doi:10.1073/pnas.1011464108

Beaulieu, J. J., Golden, H. E., & Knightes, C. D. (2015). Urban stream burial increases watershed-scale nitrate export. *Public Library of Science, 10*, 1-14.

Beaulieu, J. J., Tank, J. L., Hamilton, S. K., Wollheim, W. M., Hall, J. R. O., Mulholland, P. J., . . . Galloway, J. (2011). Nitrous oxide emission from denitrification in stream and river networks. *PNAS, 108*(1), 214-219.

Borges, A. V., Vanderborght, J. P., Schiettecatte, L. S., Gazeau, F., Smith, S. F., Delille, B., & Frankignoulle, M. (2004). Variability of the Gas Transfer Velocity of CO_2 in a Macrotidal Estuary (the Scheldt). *Estuaries, 27*(4), 593-603.

Boumansour, B. E., & Vasel, J. L. (1998). A new tracer gas method to measure oxygen transfer and enhancement factor on RBC (Rotating Biological Contractors). *Water Research, 32*(4), 1049-1058. doi:10.1016/S0043-1354(97)00324-2

Bremner, J. M. (1997). Sources of nitrous oxide in soils. *Nutrient Cycling in Agroecosystems, 49*, 7-16.

Brooks, P. D., Stark, J. M., McInteer, B. B., & Preston, T. (1989). Diffusion method to prepare soil extracts for automated nitrogen-15 analysis. *Soil Science Society of America Journal, 53*, 1707-1711.

Cabrera, M. L., & Kissel, D. E. (1988). Review and simplification of calculations in ^{15}N tracer studies. *Fertilizer Research, 20*(1), 11-15. doi:10.1007/BF01055396

Cameron, K. C., Di, H. J., & Moir, J. L. (2013). Nitrogen losses from the soil/plant system: a review. *Annals of Applied Biology, 162*(2), 145-173. doi:10.1111/aab.12014

Caplow, T., & Schlosser, P. (2004). Tracer study of mixing and transport in the upper Hudson River with multiple dams. *Journal of Environmental Engineering, 130*, 1498 – 1506. doi:10.1061/(ASCE)0733-9372(2004)130:12(1498)

Chapra, S. C., & Wilcock, R. J. (2000). Transient storage and gas transfer in lowland streams. *Journal of Environmental Engineering, 126*(8), 708-712.

Churchill, M. A., Elmore, H. L., & Buckingham, R. A. (1962). The prediction of stream reaeration rates. *Journal of the Sanitary Engineering Division, ASCE 88*(SA4), 1-46.

Ciais, P., Sabine, C., Bala, G., Bopp, L., Brovkin, V. J., Canadell, J., . . . Thornton, P. (2013). *Carbon and Other Biogeochemical Cycles.* Retrieved from Cambridge, United Kingdom and New York USA. p465-570.

Clark, J. F., Wanninkhof, R., Schlosser, P., & Simpson, H. J. (1994). Gas exchange rates in the tidal Hudson river using a dual tracer technique. *Tellus, Series B, Chemical and physical Metrology, 46*(4), 274-285. doi:10.1034/j.1600-0889.1994.t01-2-00003.x

Clough, T. J., Bertram, J. E., Sherlock, R. R., Leonard, R.L. & Nowicki, B. L. (2006). Comparison of measured and EF5-r-derived fluxes from a spring-fed river. *Global Change Biology, 12*, 352-363.

Clough, T. J., Buckthought, L. E., Casciotti, K. L., Kelliher, F. M., & Jones, P. K. (2011). Nitrous Oxide Dynamics in a Braided River System, New Zealand. *Journal of Environment Quality, 40*, 1532-1541.

Clough, T. J., Buckthought, L. E., Kelliher, F. M., & Sherlock, R. R. (2007). Diurnal fluctuations in dissolved N_2O concentrations in a spring-fed temperate river: Implications for measuring N_2O fluxes and IPCC methodology. *Global Change Biology, 13*, 1016-1027.

Clough, T. J., & Kelliher, F. M. (2012). *Nitrous oxide emissions from waterways*. Ministry for Primary Industries. MPI Sustainable land management mitigation and adaptation to climate change research programme, MPI Technical paper, NO: 2013/05: ISBN No: 978-0-478-40581-1 (online).

Cole, J. I., & Caraco, N. F. (1998). Atmospheric exchange of carbon dioxide in a low-wind oligotrophic lake measured by the addition of SF_6. *Limnology and Oceanography, 43(4)* 647-656. doi:10.4319/lo.1998.43.4.0647

Cole, J. I., & Caraco, N. F. (2001). Emissions of nitrous oxide (N_2O) from a tidal, freshwater river, the Hudson River, New York. *Environment Science and Technology, 35*(6), 991-996.

Crutzen, P. J. (1981). *Atmospheric chemical process of the oxides of nitrogen including nitrous oxide. In Denitrification, Nitrification and Atmospheric Nitrous Oxide*. New York: John Wiley and Sons.

Davidson, E. A., & Firestone, M. K. (1988). Measurement of nitrous oxide dissolved in soil solution. *Soil Science Society of America Journal, 52*, 1201-1203.

de Klein, C. A. M. (2006). *A review of the N_2O emission factor for excreta deposited by grazing animals. Paper prepared as part of the 2006 Revised Guidelines for Greenhouse Gas Inventories of the Intergovernmental Panel on Climate Change*.

de Klein, C. A. M., Sherlock, R. R., Cameron, K. C., & van der Weerden, T. J. (2001). Nitrous oxide emissions from agricultural soils in New Zealand— a review of current knowledge and directions for future research. *Journal of The Royal Society of New Zealand, 31*, 543-574.

Delwiche, C. C. (1981). *Denitrification, Nitrification and Atmospheric Nitrous Oxide*: John Wiley & Sons, Inc., Toronto.

Di, H. J., & Cameron, K. C. (2002b). Nitrate leaching and pasture production from different nitrogen sources on a shallow stony soil under flood irrigated dairy pasture. *Australian journal of soil Research, 40*, 317-334.

Dong, l. F., Nedwell, D. B., Colbeck, I., & Finch, J. (2004). Nitrous oxide emission from some English and Welsh Rivers and estuaries. *Water Air Soil Pollution, 4*, 127-134.

Elmore, H. L., & West, W. F. (1961). Effect of water temperature on stream reaeration. *Journal of the Sanitary Engineering Division, ASCE 87*(SA6), 59-71.

Frankignoulle, M. (1988). Field measurements of air-sea CO_2 exchange. *Limnology and Oceanography, 33*(3), 313-322. doi:10.4319/lo.1988.33.3.0313

Grant, R. S., & Skavroneck, S. (1980). *Comparison of tracer methods and predictive equations for determination of stream-reaeration coefficients on three small streams in Wisconsin, USA.*

Hall, R. O., & Tank, J. L. (2003). cosystem metabolism controls nitrogen uptake in streams in Grand Teton National Park, Wyoming. *Limnology and Oceanography, 48*, 1120-1128.

Harrison, J., & Matson, P. (2003). Patterns and controls of nitrous oxide emissions from waters draining a subtropical agricultural valley. *Global Biogeochemical Cycles, 17*(3), 6-1 to 6-13. doi:10.1029/2002gb001991

Harrison, J. A., Matson, P. A., & Fendorf, S. E. (2005). Effects of a diel oxygen cycle on nitrogen transformations and greenhouse gas emissions in a eutrophied subtropical stream. *Aquatic Science, 67*, 308-315. doi: 10.1007/s00027-005-0776-3

Hemond, H. F., & Duran, A. P. (1989). Fluxes of N_2O at the sediment-water and water-atmosphere boundaries of a nitrogen-rich river. *Water Resources Research, 25*(5), 839-846. doi:10.1029/WR025i005p00839

Hinshaw, S. E., & Dahlgren, R. A. (2013). Dissolved Nitrous Oxide Concentrations and Fluxes from the Eutrophic San Joaquin River, California. *Environment Science and Technology, 47*(3), 1313-1322.

Hiscock, K. M., Bateman, A. S., Muhlherr, I. J., Fukada, T., & Dennis, P. F. (2003). Indirect Emissions of Nitrous Oxide from Regional Aquifers in the United Kingdom. *Environment Science and Technology, 37*, 3507-3512.

Hutchinson, G. L., & Mosier, R. (1981). Improved Soil Cover Method for Field Measurement of Nitrous Oxide Fluxes *Soil Science Society of America Journal, 45*(2), 311-316. doi:10.2136/sssaj1981.03615995004500020017x

Hwa-Seong, J., David, S. W., James, B. R., & George W, K. (2012). Mixed Tracer Injection Method to Measure Reaeration Coefficients in Small Streams. *Water, Air, & Soil Pollution, 223*(8), 5297-5306. doi:10.1007/s11270-012-1280-8

IPCC Guidelines for National Greenhouse Gas Inventories, Reporting Guidance and Tables; Eggleston H.S., Buendia L., Miwa K., Ngara T. and Tanabe K, (2006).

IPCC. (2007). *Climate change Synthesis Report 2007* Paper presented at the IPCC 4th Assessment, Geneva, Switzerland.

Isaacs, W. P., & Guady, A. F. (1968). Atmospheric oxygenation in a simulated stream. *Journal of Sanitary Engineering Division, ASCE 94*(SA2), 319-344.

Ivens, W. P. M. F., Tysmans, D. J. J., Kroeze, C., Löhr, A. J., & van Wijnen, J. (2011). Modeling global N_2O emissions from aquatic systems. *Current Opinion in Environmental Sustainability, 3*(5), 350-358.

Jähne, B., Münnich, K. O., Bösinger, R., Dutzi, A., Huber, W., & Libner, P. (1987). On the parameters influencing air-water gas exchange. *Journal of Geophysical Research, Volume 92* (Issue C2), 1937–1949 doi:10.1029/JC092iC02p01937

Jones Jr, J. B., & Mulholland, P. (1998). Methane input and evasion in a hardwood forest stream: Effects of subsurface flow from shallow and deep pathways *Limnology and Oceanography, 43*(6), 1243-1250.

Kelliher, F. M., Sherlock, R. R., Clough, T. J., Premaratne, M., Laughlin, R. J., McGeough, K. L., . . . Saggar, S. (2015). Air sample collection, storage and analysis (Chapter 4). In C. A. M. de Klein & M. Harvey (Eds.), *Nitrous Oxide Chamber Methodology Guidelines* (Vol. 1.1, pp. 596-572): Ministry for Primary Industries.

Knowles, R. (1982). Denitrification. *Microbiological Reviews, 46*, 43-70.

Lal, S., & Patra, P. K. (1998). Variabilities in the fluxes and annual emissions of nitrous oxide from the Arabian Sea. *Global Biogeochemical Cycles, 12*, 321-327.

Langbein, W. B., & Durum, W. H. (1967). *The reaeration capacity of streams U.S Geological Survey, Circular*, 542, p6.

Lavagnini, I., & Magno, F. (2007). A statistical overview on univariate calibration, inverse regression, and detection limits: Application to gas chromatography/mass spectrometry technique. *Mass Spectrometry Reviews, 26*, 1-18.

Liang, W. S., & Richardson, E. W. (1971). *Water Management Research in Arid and Sub-Humid Lands of the Less Developed Countries. Technical report 3. E*ngineering research centre, Colarado State university, p9.

Maartje, A. H. J. v. K., Speth, D. R., Albertsen, M., Nielsen, P. H., Camp, H. J. M. O. d., Kartal, B., . . . Lücker, S. (2015). Complete nitrification by a single microorganism. *Nature*, 1-17. doi:10.1038/nature16459

MacIntyre, S. W., Eugster, W., & Kling, G. W. (2001). The critical importance of buoyancy flux for gas flux across the air-water interface. In: M. A. Donelan, W. M. Drennan, E. S. Saltzman, & R. Wanninkhof (Eds.), *Gas Transfer at Water Surfaces*.

Mackay, D., Shiu, W. Y., & Sutherland, R. P. (1979). Determination of Air-Water Henry's Law Constants for Hydrophobic Pollutants *Environment Science and Technology, 13*(3), 333-337. doi:10.1021/es60151a012

Marzolf, E. R., Mulholland, P. J., & Steinman, A. D. (1994). Improvements to the Diurnal Upstream–Downstream Dissolved Oxygen Change Technique for Determining Whole-Stream Metabolism in Small Streams. *Canadian Journal of Fisheries and Aquatic Sciences, 51*(7), 1591-1599. doi:10.1139/f94-158

Melching, C. S., & Flores, H. E. (2007). Reaeration equations derived from U.S. Geological Survey Database. *Journal of Environmental Engineering, 125(5)*, 407-414. doi: ISSN 0733-9372/99/0005-0407–0414

Mosier, A. R., Kroeze, C., Nevison, C., Oenema, O., Seitzinger, S., & van Cleemput, O. (1998). Closing the global N_2O budget: nitrous oxide emissions through the agricultural nitrogen cycle. OECD/IPCC/IEA phase II development of IPCC guidelines for national greenhouse gas inventory methodology *Nutrient Cycling in Agroecosystems, 52*, 225-248.

Mulholland, P. J., Valett, H. M., Webster, J. R., Thomas, S. A., Cooper, I. N., Hamilton, S. K., & Peterson, B. J. (2004). Stream denitrification and total nitrate uptake rates measured using a field ^{15}N isotope tracer approach. *Limnology and Oceanography, 49*, 809-820.

Muller, C., & Sherlock, R. R. (2004). Nitrous oxide emissions from temperate grassland ecosystems in the Northern and Southern Hemispheres. *Global Biogeochemical Cycles, 18*. doi:0886-6236/04/2003GB002175

Murphy, J. L. (2003). The use of Krypton as a tracer to quantify reaeration in surface waters. PhD Thesis, Queen's university, Belfast, UK. p.241.

Nevison, C. (2000). Review of the IPCC methodology for estimating nitrous oxide emissions associated with agricultural leaching and runoff. *Chemosphere - Global Change Science, 2*(3-4), 493-500. doi:10.1016/S1465-9972(00)00013-1

O'Connor, D. J., & Dobbins, W. E. (1958). Mechanisms of reaeration in natural streams *Transactions of the American Society of Civil Engineers, 123*, 641-684.

Owens, M., Edwards, R. W., & Gibbs, J. W. (1964). Some reaeration studies in streams. *International Journal of Air and Water Pollution, 8*, 469-486.

Parfitt, R. L., Stevenson, B. A., Dymond, J. R., Schipper, L. A., Baisden, W. T., & Ballantine, D. J. (2012). Nitrogen inputs and outputs for New Zealand from 1990 to 2010 at national and regional scales. *New Zealand Journal of Agricultural Research, 55*(3), 241-262. doi:10.1080/00288233.2012.676991

Peterson, B. J., Wollheim, W. M., Mulholland, P. J., Webster, J. R., Meyer, J. L., Tank, J. L., . . . Morrall, D. D. (2001). Control of nitrogen export from watersheds by headwater streams. *Science, 292*, 86-90.

Rasera, M. F. F. L., Ballester, M. V. R., Krusche, A. V., Salimon, C., Montebelo, L. A., Alin, S. R., . . . Richey, J. E. (2008). Estimating the surface area of small rivers in the southwestern Amazon and their role in CO_2 outgassing. *Earth Interact, 12*, 1-16.

Raymond, P. A., Zappa, C. J., Butman, D., Bott, T. L., Potter, J., Mulholland, P., . . . Newbold, D. (2012). Scaling the gas transfer velocity and hydraulic geometry in streams and small rivers. *Limnology and Oceanography; Fluids and Environments, 2*, 41-53. doi:10.1215/21573689-1597669

Reay, D. S., Edwards, A. C., & Smith, K. A. (2008). Importance of indirect nitrous oxide emissions at the field, farm and catchment scale. *Agriculture Ecosystems & Environment, 133*(3-4), 163-169.

Reay, D. S., Smith, K. A., & Edwards, A. C. (2003). Nitrous oxide emission from agricultural drainage waters. *Global Change Biology, 9*, 195-203.

Riley, W. J., Ortiz-Monasterio, I., & Matson, P. A. (2001). Nitrogen leaching and soil nitrate, nitrite, and ammonium levels under irrigated wheat in Northern Mexico. *Nutrient Cycling in Agroecosystems, 61*, 223-236.

Roberts, B. J., Mulholland, P.J. and Walter, R.H. (2007). Multiple scales of temporal variability in ecosystem metabolism rates: results from 2 years of continuous monitoring in a forested headwater water stream. *Ecosystems, 10*, 588-606.

Rosamond, M. S., Thuss, S. J., & Schiff, S. L. (2012). Dependence of riverine nitrous oxide emissions on dissolved oxygen levels. *Nature Geoscience, 5*, 715-718. doi:10.1038/ngeo1556

Seitzinger, S., Harrison, J. A., Bohlke, J. K., Bouwman, A. F., Lowrance, R., Peterson, B., & Van drecht, G. (2006). Denitrification across landscapes and waterscapes: A synthesis. *Ecological Applications, 16*(6), 2064-2090.

Seitzinger, S. P., & Kroeze, C. (1998). Global distribution of nitrous oxide production and N inputs in freshwater and coastal marine ecosystems. *Global Biogeochemical Cycles, 12*(1), 93-113. doi:10.1029/97GB03657

SolÓRzano, L. (1969). Determination of ammonia in natural waters by phenol hypochlorite method. *Limnology and Oceanography, 14*, 799-801.

Stolk, P. C., Jacobs, C. M. J., Moors, E. J., Hensen, A., Velthof, G. L., & Kabat, P. (2009). Significant non-linearity in nitrous oxide chamber data and its effect on calculated annual emissions. *Biogeosciences Discussions, 6*, 115-141.

Sutton, M. A., Bleeker, A., Dragosits, U., Hicks, W. K., Bealey, W. J., & Hallsworth, S. (2011). Current and future policy options for tackling nitrogen deposition impacts on Natura 2000 sites In: Hicks, W.K., Whitfield, C.P., Bealey, W.J. and Sutton, M.A., eds. (2011a): *Science and Practice in DeterminingEnvironmental Impacts COST, pp.221-242.*.

The European Nitrogen Assessment: Sources, E. a. P. P., & by, e. (2011). *The European Nitrogen Assessment: Sources, Effects and Policy Perspectives*: Cambridge University Press.

Thomas, S. M., Ledgard, S. F., & Francis, G. S. (2005). Improving estimates of nitrate leaching for quantifying New Zealand's indirect nitrous oxide emissions. *Nutrient Cycling in Agroecosystems, 73*, 213-226.

Tiedje, J. M. (1983). Denitrification. In: Methods of Soil Analysis. *Agronomy, 9*, 1011-1026.

Tsivoglou, E. C. (1967). Tracer measurements of stream reaeration; Report to the Federal Water Pollution Administration. *Journal of Water Pollution Control Fedn., 48(12), 2669–2689*.

Turner, P. A., Griffisa, T. J., Lee, X., Baker, J. M., Venterea, R. T., & Wooda, J. D. (2015). Indirect nitrous oxide emissions from streams within the US Corn Belt scale with stream order. *PNAS, 112* (32), 9839–9843. doi:10.1073/pnas.1503598112

Venkiteswaran, J. J., Rosamond, M. S., & Schiff, S. L. (2014). Nonlinear Response of Riverine N_2O Fluxes to Oxygen and Temperature. *Environment Science and Technology, 48*(3), 1566-1573.

Wanninkhof, R. (1992). Relationship between wind speed and gas exchange over the ocean. *Journal of Geophysical Research, 97*(C5), 7373–7382 doi:10.1029/92JC00188

Wanninkhof, R., Mulholland, P. J., & Elwood, J. W. (1990). Gas exchange rates for a first-order stream determined with deliberate and natural tracers. *Water Resources Research, 26*(7), 1621-1630. doi:10.1029/WR026i007p01621

Ward, M. (1998). The Kyoto Protocol - an overview. Proceedings of the Workshop on the Science of Atmospheric Tracer Gasses. *NIWA Technical Report: 15, p 11-12.*

Watson, C. J., Jordan, C., & Allen, M. D. B. (1994). Relationships between Denitrifying Enzyme Activity and Soil Properties. *Biology and Environment:, 94B*(3), 237-244.

Webster, E. A., & Hopkins, D. W. (1996). Contributions from different microbial processes to N_2O emission from soil under different moisture regimes. *Biology and Fertility of Soils, 22*, 331-335.

Weiss, R. F. (1974). Carbon dioxide in water and seawater; the solubility of a non-ideal gas. *Mar. Chem, 2*, 203-215.

Wilcock, R. J. (1984). Methyl chloride as a gas-tracer for measuring steam reaeration coefficients-I. Laboratory studies. *Water Research, 18*, 47-52.

Wilcock, R. J. (1982). Simple predictive equations for calculating stream reaeration rate coefficients. *New Zealand Journal of Science, 25*, 53-56.

Wilcock, R. J. (1984). Methyl chloride as a gas-tracer for measuring stream reaeration coefficients-II, stream studies. *Water Research, 18*, 53-57.

Wilcock, R. J., & Chapra, S. C. (2005). Diel changes of inorganic chemistry in a macrophyte-dominated, softwater stream. *Marine and Freshwater Research, 56*(8), 1165-1174. doi:http://dx.doi.org/10.1071/MF05049

Wilcock, R. J., & Sorrell, B. K. (2008). Emissions of Greenhouse Gases CH_4 and N_2O from Low-gradient Streams in Agriculturally Developed Catchments. *Water, Air, and Soil Pollution, 188*(1-4), 155-170. doi:10.1007/s11270-007-9532-8

Wise, D. L., & Houghton, G. (1968). Diffusion coefficients of neon, krypton, xenon, carbon monoxide and nitric oxide in water at 10–60°C. *Chemical Engineering Science, 23*(10), 1211-1216. doi:10.1016/0009-2509(68)89029-3

Wrage, N., Velthof, G. L., van Beusichem, M. L., & Oenema, O. (2001). Role of nitrifier denitrification in the production of nitrous oxide. *Soil Biology and Biochemistry, 33*, 1723-1732.

Young, R. G., & Huryn, A. D. (1999). Effects of land use on stream metabolism and organic matter turnover. *Ecological Applications, 9*(4), 1359-1376. doi:10.1890/1051-0761

Yu, Z., Deng, H., Wang, D., Ye, M., Tan, Y., Li, Y., . . . Xu, S. (2013). Nitrous oxide emissions in the Shanghai river network: implications for the effects of urban sewage and IPCC methodology. *Global Change Biology, 19*, 2999-3010. doi:10.1111/gcb.12290

Zappa, C. J., McGillis, W. R., Raymond, P. A., Edson, J. B., Hintsa, E. J., Zemmelink, H. J., . . . Ho, D. T. (2007). Environmental turbulent mixing controls on air-water gas exchange in marine and aquatic systems. *Geophysical Research Letters, 34*(10). doi:10.1029/2006gl028790

Zhu, X., Burger, M., Doane, T. A. D., & Horwath, H. W. (2013). Ammonia oxidation pathways and nitrifier denitrification are significant sources of N_2O and NO under low oxygen availability. *PNAS, 110*(16), 6328-6333.